DNA double strand break repair and cell cycle control of murine stem cells after exposure to ionizing radiation

TECHNISCHE UNIVERSITÄT DARMSTADT

Vom Fachbereich Biologie der Technischen Universität Darmstadt
zur Erlangung des akademischen Grades eines
Doctor rerum naturalism (Dr. rer. nat.)
genehmigte Dissertation von

M.Sc. Amir Mofidi
aus Teheran (Iran)

Referent: Prof. Dr. Markus Löbrich
Koreferentin: Prof. Dr. Ulrike Nuber

Tag der Einreichung: 05.10.2017
Tag der mündlichen Prüfung: 14.11.2017

Darmstadt 2017
D17

For my Mother,
without her none of my success would be possible.

Ehrenwörtliche Erklärung

Ich erkläre hiermit ehrenwörtlich, dass ich die vorliegende Arbeit entsprechend den Regeln guter wissenschaftlicher Praxis selbstständig und ohne unzulässige Hilfe Dritter angefertigt habe.

Sämtliche aus fremden Quellen direkt oder indirekt übernommenen Gedanken sowie sämtliche von Anderen direkt oder indirekt übernommenen Daten, Techniken und Materialien sind als solche kenntlich gemacht. Die Arbeit wurde bisher bei keiner anderen Hochschule zu Prüfungszwecken eingereicht.

Darmstadt, 05.10.2017 .....

Amir Mofidi

Table of content

Abbreviations

53BP1	P53 binding protein 1
Ab	Antibody
alt-NHEJ	Alternative non-homologous end-joining
APS	Ammonium persulfate
ATM	Ataxia telangiectasia mutated
bFGF	Basic fibroblast growth factor
BME	Beta-mercaptoethanol
bp	Base pair
BrdU	5-bromo-2'-deoxymuridine
BSA	Bovine serum albumin
c-NHEJ	Classical non-homologous end-joining
CDKs	Cycline-dependent kinases
Chk1	Checkpoint kinase 1
Chk2	Checkpoint kinase 2
CtIP	C-terminal binding protein-interacting protein
D-loop	Displacement/DNA loop
DAPI	4', 6-diamidino-2-phenylindole
DDR	DNA damage response
DMEM	Dulbecco's Modified Eagle Medium
DMSO	Dimethyl sulfoxide
DNA	Deoxyribonucleic acid
DNA-PK	DNA-dependent protein kinase
DNA-PKcs	DNA-dependent protein kinase catalytic subunit
DRB	5,6-dichloro-1-b-D-ribofuranosyl benzemidazol
DSB	Double-strand break
dsDSB	Double stranded DSB
EDTA	Ethylenediaminetertraacetic acid
EdU	5-ethynyl-2'-deoxyuridine
EGF	Epidermal growth factor
ESC	Embryonic stem cells
Exo1	Exonuclease1
FA	Formaldehyde
FACS	Fluorescence activated cell scanning
FCS	Fetal calf serum

GAPDH	Glyceraldehyd-3-Phosphat-Hehydrogenase
GFP	Green fluorescent protein
Gy	Gray
h	Hour
H2AX	Histon 2AX
H_2O_2	Hydrogen peroxide
HR	Homologous recombination
HRP	Horseradish peroxidase
i	Inhibitor
IF	Immunflurorescence
IR	Ionizing radiation
IRIF	Irradiation induced foci
kDa	Kilo Dalton
kV	Kilo volt
LIF	Leukemia inhibitory factor
Lig1	Ligase I
Lig3	Ligase III
Lig4	Ligase IV
mA	Milli Ampere
MEF	Mouse embryonic fibroblasts
MiliQ water	Purified water
min	Minutes
Mre11	Meiotic recombination 11
MRN	Mre11-Rad50-Nbs1
Nbs1	Nijmegen breakage syndrome 1
NEAA	Non-essential amino acids
NHEJ	Non-homologous end-joining
nt	Nucleotide
OH	Hydroxyl
P	Phosphate
PAGE	Polyacrylamide gel electrophoresis
PAR	Poly(ADP-ribose)
PARP1	Poly(ADP-ribose) polymerase-1
PBS	Phosphate buffer saline
PI	Propidium iodide

Plk3	Poli-like kinase 3
PVDF	Polyvinyldifluorid
Rad51	Rdiation repair protein 51
R-loop	Displacement/RNA loop
RNA	Ribonucleic acid
RNase	Ribonuclease
RNA pol II	RNA polymerase II
RPA	Replication protein A
RPM	Rotation per minute
RT	Room temperature
SDS	Sodium dodecyl sulfate
siRNA	Small interfering RNA
SSB	Single-strand break
ssDNA	Single stranded DNA
TBS	Tris buffered saline
V	Volt
WB	Western blot
WT	Wild type
XLF	XRCC4-like factor
XRCC1	X-ray cross complementing protein 1
XRCC4	X-ray cross complementing protein 4

Figures

Tables

1 Summary

Ionizing radiation (IR) induces a variety of DNA lesions among which DNA double strand breaks (DSBs) are biologically most significant. In somatic cells, several cellular DNA damage response (DDR) mechanisms such as cell cycle checkpoints and DSB repair pathways work in concern to handle these threats. In response to DNA damage, G1/S and G2/M checkpoints activities prevent the progression of the cells to the next cell cycle phase. This mechanism prohibits replication and division of the cells containing DSBs and provides them time for repair. In parallel to this event, DNA repair machinery repairs the DSBs. The majority of IR-induced DSBs are repaired fast via canonical non-homologous end-joining (c-NHEJ) in which DNA-PKcs is one of the core enzymes. In contrast, a sub-fraction of breaks is repaired with slow kinetics in an ATM-dependent manner. This repair pathway represents homologous recombination (HR) in G2 and resection-dependent c-NHEJ in G1 phase. In stem cells, although it is appreciated that DDR regulation is distinct from that in somatic cells, the key factors and their functional mechanisms still remain unknown.

The main aim of this thesis was to understand the mechanism/s by which stem cells retain their genomic integrity. Moreover, the level of repair capacity in pluripotent and multipotent stem cells has been compared. To achieve these aims, the DDR mechanism has been characterized in mouse embryonic stem cells (ESCs) and ESC-derived neural stem cell (NSCs).

Cell cycle checkpoint analysis after 2 Gy X-rays demonstrated an ineffective G1/S checkpoint arrest in NSCs, whereas, ESCs failed to prevent cell cycle progression into S phase. In both cell types, cell cycle was completely arrested by G2/M checkpoint. However, ESCs showed a prolonged G2/M arrest compared to NSCs.

Analyzing DSB repair in NSCs after exposure to 10 mGy and 100 mGy X-rays revealed that the repair capacity is reduced by decreasing the radiation dose. After 10 mGy IR, the value of the IR-induced DSBs was remained constant until 4 h post IR. This is evident that the DSB repair machinery cannot be fully activated by low doses of IR.

Investigation of DSB repair capacity after 2 Gy X-rays showed that wild type (WT) ESCs and NSCs have similar repair kinetics and almost all IR-induced DSBs were repaired within 6 h post IR. Inhibition of ATM impaired the slow component of DSB repair in both cell types, whereas, the fast component was not affected. Interestingly, DNA-PKcs inhibitor induced a temporary repair defect followed by an efficient repair to the background DSB levels in ESCs. In contrast, in NSCs, DSB repair was almost stalled after inhibition of DNA-PKcs. Moreover, inhibition of Rad51 impaired the DSB repair in G2-phase NSCs, whereas in ESCs, the repair kinetic was not impaired. Therefore, we asked if an alternative repair pathway provides a backup repair mechanism in DNA-PKcs- and Rad51-deficient ESCs.

To address the aforementioned question, we investigated the role of alt-NHEJ pathway in ESCs and NSCs by inhibiting PARP1. Importantly, PARP1-inhibition did not influence DSB repair kinetics in WT or ATM-inhibited cells. However, inhibition of PARP1 induced an additional significant repair defect in DNA-PKcs- and Rad51-inhibited ESCs, not in NSCs. These data demonstrated that PARP1-dependent alt-NHEJ functions as a backup repair pathway for impaired c-NHEJ or HR in ESCs.

It is well know that PARP1-dependent alt-NHEJ is a resection dependent pathway. Analyzing resection in G2 phase by scoring Rad51 foci displayed a higher foci level in ESCs than in NSCs. In addition, investigation of resection in G1 phase uncovered that ESCs form pRPA foci, not NSCs. Furthermore, inhibition of the proteins regulating resection in G1 phase, like PLK3, not only diminished the formation of pRPA foci but also impaired DSB repair in ESCs. Whereas, in non-pluripotent cells (NSCs or HeLa cells), no repair defect was observed after inhibition of resection in G1 phase. These observations revealed that ESCs perform more resection than NSCs, suggesting that resection dependent-NHEJ is a prominent DSB repair pathways in G1-phase ESCs. All together, the data implies that, ESCs can perform long-range resection of DSB ends and, therefore, in case of impaired classical repair pathways, can readily switch to PARP1-dependent alt-NHEJ.

Previously, it was shown that nascent RNAs mediate an error-free c-NHEJ by serving as templates to faithfully restore the lost genomic information at the break site. Moreover, it was demonstrated that RNA transcription machinery functions as a molecular motor to promote excessive DNA resection. These evidences led to the curiosity to understand if RNA mediates the long range resection in G1-phase ESCs.

The detection of RNA-DNA hybrids at the DSB sites, as well as, reduction in pRPA foci level after inhibition of transcription verified our hypothesis that RNA transcription machinery might mediate long-range resection in G1 phase ESCs. Furthermore, destabilization of the RNA-DNA hybrids by overexpression of RNaseH1 enzyme, induced a significant repair defect in G1 phase ESCs. This effect was identical to the repair defect which was observed after inhibition of PLK3. These observations confirmed the role of RNA in mediating resection in G1-phase ESCs. These findings suggest that, the involvement of RNA as a template during DSB repair might be mediating an error-free repair and thus play an important role in maintaining the genomic integrity of pluripotent stem cells.

Zusammenfassung

Ionisierende Strahlung (IR) verursacht verschiedene Formen der DNA-Schädigung, unter denen der DNA-Doppelstrangbrüch (DSB) der biologisch schwerwiegendste ist. In somatischen Zellen gibt es eine Vielzahl an zellulären Schadensantworten (DNA damage response, DDR), wie die Zellzykluskontrolle oder DSB-Reparaturmechanismen. Eine koordinierte Zusammenarbeit dieser Prozesse sorgt so für den Schutz vor langfristigen DNA-Schäden. Der G1/S- und G2/M-Checkpoint verhindert die Progression der Zellen in die nächste Zellzyklusphase. Durch diesen Mechanismus wird die Replikation und Teilung der Zellen verhindert, wodurch Zellen, die DSBs enthalten, genügend Zeit für die Reparatur erhalten. Die Mehrheit der IR-induzierten DSBs wird schnell über die kanonische nicht-homologe Endverknüpfung (c-NHEJ) repariert, in der DNA-PKcs eines der Kernenzyme darstellt. Im Gegensatz dazu, wird eine Subfraktion von Schäden mit langsamer Kinetik in einer ATM-abhängigen Weise repariert. Dieser Reparaturweg repräsentiert die homologe Rekombination (HR) in der G2-Phase und das resektionsabhängige c-NHEJ in der G1-Phase. In Stammzellen, bei welchen sich die DDR-Regulation von denen in somatischen Zellen unterscheidet, sind die Schlüsselfaktoren und ihre Funktionsmechanismen noch unbekannt.

Das Hauptziel dieser Arbeit war es, den Mechanismus zu verstehen, durch den Stammzellen ihre genomische Integrität bewahren. Darüber hinaus wurde der Umfang der Reparaturkapazität und die Genauigkeit in pluripotenten und multipotenten Stammzellen verglichen. Um diese Ziele zu erreichen, wurde der DDR-Mechanismus in embryonalen Mausstammzellen (ESCs) und ESC-abgeleiteten neuronalen Stammzellen (NSCs) charakterisiert.

Die Zellzykluskontrollanalyse nach 2 Gy-Röntgenstrahlung zeigte einen ineffektiven G1/S-Zellzyklusarrest in NSCs, während ESCs die Zellzyklusprogression in die S-Phase nicht verhindern konnten. In beiden Zelltypen wurde der Zellzyklus vollständig durch den G2/M-Checkpoint angehalten. ESCs zeigten jedoch einen längeren Zellzyklusarrest im Vergleich zu NSCs.

Die Anzahl der DBS, die durch 10 mGy und 100 mGy Röntgenstrahlung in NSCs induziert wurden, ergab, dass die Reparaturkapazität durch Verringerung der Strahlendosis reduziert wurde. Nach 10 mGy IR blieb das Niveau der DSBs konstant, bis 4 h nach der Bestrahlung. Dies könnte auf eine mangelnde Aktivierung der DNA-Reparatur zurückzuführen sein. Außerdem haben wir gezeigt, dass unter diesen Bedingungen DNA-PK nicht ausreichend aktiviert wird, um H2AX in Abwesenheit von ATM zu phosphorylieren.

Die Untersuchung der DSB-Reparaturkapazität nach 2 Gy-Röntgenstrahlung ergab, dass Wildtyp (WT) ESCs und NSCs ähnliche Reparaturkinetiken aufweisen und die IR-induzierten DSBs innerhalb von 6 h nach IR fast komplett repariert werden. Die ATM-Inhibition in ESCs und NSCs hatte keinen Einfluss auf die schnelle DSB-Reparaturkomponente, während die langsame Komponente beeinträchtigt war. Interessanterweise induziert die DNA-PKcs-Inhibition einen temporären Reparaturdefekt in ESCs,

gefolgt von einer effizienten Reparatur auf Kontroll-Niveau. Im Gegensatz dazu, wurde die DSB-Reparatur in NSCs nach der DNA-PKcs-Inhibition fast komplett gestoppt. Die Inhibierung von Rad51 verhindert die DSB-Reparatur in G2-Phasen-NSCs, während die Reparaturkapazität in ESCs nicht betroffen war. Daraus ergab sich die Frage, ob die DSBs in DNA-PKcs- und Rad51-defizienten ESCs über einen alternativen Reparaturweg repariert werden.

Um die oben genannte Frage zu beantworten, untersuchten wir die Rolle des alt-NHEJ-Reparaturweges in ESCs und NSCs durch die Inhibition von PARP1. Die PARP1-Inhibition hat dabei weder die DSB-Reparaturkinetik in WT- oder ATM-inhibierten ESCs, noch in NSCs beeinflusst. Allerdings induzierte es einen zusätzlichen, signifikanten Reparaturdefekt in DNA-PKcs- und Rad51-inhibierten ESCs, nicht jedoch in NSCs. Diese Daten zeigten, dass das PARP1-abhängige alt-NHEJ als Backup-Reparaturweg für c-NHEJ und HR in ESCs fungiert.

Es ist bereits bekannt, dass PARP1-abhängiges alt-NHEJ ein resektionsabhängiger Reparaturweg ist. Untersuchungen der Resektion in der G2-Phase zeigten ein höheres Level an Rad51-Foci in ESCs, als in NSCs. Zusätzlich konnte eine Untersuchung der Resektion in der G1-Phase die Bildung von pRPA-Foci in ESCs, nicht jedoch in NSCs, bestätigt werden. Darüber hinaus verringerte die Inhibierung der Proteine, die die Resektion in der G1-Phase regulieren, wie PLK3, nicht nur die Bildung von pRPA-Foci, sondern auch die DSB-Reparatur in ESCs. Während in nicht pluripotenten Zellen (NSCs oder HeLa-Zellen) kein Reparaturdefekt nach Inhibierung der Resektion in der G1-Phase beobachtet wurde. Diese Ergebnisse zeigten, dass ESCs mehr Resektion als NSCs durchführen. Resektionsabhängiges NHEJ stellt demnach einen prominenten DSB-Reparaturweg in G1-Phase-ESCs dar. Die gesammelten Daten implizieren, dass ESCs eine weitreichende Resektion von DSB-Enden durchführen können und daher im Falle von beeinträchtigten klassischen Reparaturpfaden leicht zu PARP1-abhängigem alt-NHEJ wechseln können.

In einer Studie konnte die Beteiligung von naszierenden RNAs an einer fehlerfreien c-NHEJgezeigt werden, indem sie als Vorlagen für die genomische Information an den Bruchstellen dient. Darüber hinaus wurde gezeigt, dass die RNA-Transkriptions-Maschinerie als molekularer Motor fungiert, um eine exzessive DNA-Resektion zu fördern. Diese Beweise führten zu der Frage, ob RNA die Resektion in G1-Phase-ESCs vermittelt.

Der Nachweis von RNA-DNA-Hybriden an den DSB-Stellen, sowie die Reduktion der pRPA-Foci nach Hemmung der Transkription, bestätigten unsere Hypothese, dass die RNA-Transkription eine weitreichende Resektion in G1-Phase-ESCs vermitteln könnte. Darüber hinaus induzierte die Destabilisierung der RNA-DNA-Hybride durch Überexpression des RNaseH1 Enzyms einen signifikanten Reparaturdefekt in G1-Phase-ESCs. Dieser Effekt war identisch mit dem Reparaturdefekt, der nach der Hemmung von PLK3 beobachtet wurde. Diese Beobachtungen bestätigten die Rolle der RNA bei der Vermittlung der Resektion in G1-Phase-ESCs. Diese Ergebnisse deuten darauf hin, dass die Beteiligung von RNA als Vorlage während der DSB-Reparatur eine fehlerfreie Reparatur vermittelt und

somit eine wichtige Rolle bei der Aufrechterhaltung der genomischen Integrität von pluripotenten Stammzellen spielen könnte.

2 Introduction

2.1 Stem cells

Stem cells are a specific type of cell that have distinct abilities in the body. Regardless of their source, all stem cells have three unique properties: they are unspecialized, they can self-renew for long periods of time and they have the ability to give rise to specialized cell types (Marrison, et al., 1997). Stem cells are classified into two main groups: embryonic stem cells (ESCs) and adult stem cells (also known as non-embryonic stem cells). ESCs, as their name suggests, are involved in the course of embryogenesis and postnatal development. They are derived from the cells of the inner cell mass at the blastocyts. These cells are pluripotent and have the capability to differentiate into all three germ layers of the embryo (Thomson JA, 1998). The pluripotency of ESCs is regulated by the interaction between different factors (Rodda, et al., 2005). Octamer-binding transcription factor 4 (Oct-4) is promoting the expression of the genes which are involved in regulation of pluripotency in ESCs (Boiani, et al., 2005). Upon differentiation of ESCs, the expression of Oct-4 is down-regulated (Cauffman, et al., 2005). Sex determining region Y-box 2 (Sox-2) is another factor essential for maintaining the pluripotency of ESCs (Adachi, et al., 2010).

In contrast to ESCs, non-embryonic stem cells are multipotent and are present not only in embryo but also in adult tissues. The differentiation capability is restricted in this type of stem cells and they are only able to differentiate into multiple specialized cell types present in a specific tissue, e.g. hematopoietic stem cells (HSCs) and neural stem cells (NSCs) (Lee, et al., 2006). NSCs are progenitor cells in the central nervous system (CNS) and they have a critical role in the embryogenesis and adult neurogenesis. They have the potential to give rise to neuron and glia (Gage, 2000). The stem cell properties of NSCs are controlled by different proteins. Nestin is a sort of intermediate filament proteins which regulates the self-renewal of NSCs (Park, et al., 2010). During life, most of the tissues undergo constant renewal to maintain homeostasis. Stem cells, by asymmetric cell division, generate and maintain the physiological tissue homeostasis in the body (Blanpain, et al., 2011). Using this particular cell division system, one half of the progeny are retained stem cell, while the second half commit to differentiation (Morrison, et al., 2006).

2.2 DNA damage

In all living cells, DNA is the repository of genetic information. The stability and integrity of DNA is essential for life. DNA is not inert and can be subjected to DNA damaging agents. It has been estimated that up to 1 million DNA damage may occur in a single cell per day (Lodish, et al., 2000). Multiple forms of DNA damage can be induced by damage agents including base damages and DNA backbone cleavages (Dianov, et al., 2007). Among different types of DNA lesions, double-stranded DNA breaks (DSBs) are the most serious forms. DSBs can be induced by endogenous or exogenous sources of DNA

damage agents (Khanna, et al., 2001). Endogenous DNA damage agents are byproducts of cellular metabolic processes, e.g. free radicals (ROS). Exogenous sources for DNA damage include various chemical agents, ultraviolet (UV) and ionizing radiation (IR).

IR describes all types of radiation that carry enough energy to emit an electron from the outer electron shell of an atom or molecule (ionize). The direct deposition of this energy and also indirect deposition, by ionization of water molecules and produce hydroxyl radicals, IR can damage the DNA. IR can be divided into neutrons, α- and β-particles, X- and γ-rays. Typical sources of IR that are of concern to human health are classified as natural sources, e.g. cosmic rays, and man-made sources, e.g. nuclear power. The dose of IR is measured in the unit Gray (Gy), which is the amount of radiation absorbed by 1 Kg of tissue (Dunne-Daly, 1999).

Between different types of IR, X-rays are routinely used in human life. X-rays are type of electromagnetic spectrum with a short wavelength, in fact it is 1000 times smaller than light wave. X-rays can easily penetrate low-density material, like flesh. Whereas, in high-density materials, like bone, they are reflected or absorbed. These properties make X-rays very useful for medical diagnosis and therapy. However, it is well known that X-rays, even low doses (between 1 mGy to 1 Gy), may induce DSBs and are potentially carcinogens (Rothkamm, et al., 2003).

2.3 Cell responses to the DNA damage

To minimize the harmful impact of DNA damage, cells have developed a DNA damage response (DDR) signaling cascade that controls cell cycle progression and DNA repair (van Gent, et al., 2001; Jackson, et al., 2009). The harmonious interaction of cell cycle control and DNA repair machinery is essential for maintaining cellular fidelity and avoiding the genome instability.

2.3.1 Cell cycle checkpoint

In eukaryotic cells, the cell cycle contains four phases: G1, S, G2 and M phase. During replication in S phase, DNA damage may lead to replication fork stalling or collapse which can induce further DSBs and chromosomal breaks. During cell division in M phase, unrepaired DSBs may cause genetic alterations in the daughter cells (Deckbar, et al., 2011). To avoid this, cell cycle checkpoints are present to ensure DNA is intact before S and M phases are initiated. In response to DNA damage, cell cycle progression is interrupted by G1/S and G2/M checkpoints. This ensures the cell has time to repair its DNA lesions.

The progression of cells from one cell cycle phase to another is regulated by specific protein complexes; within this two main protein groups are present: Cyclins and Cyclin-dependent kinases (Cdks). Inhibition of these protein complexes induces cell cycle arrest (Deckbar, et al., 2011). In somatic cells, G1/S checkpoint is regulated by CyclinD/Cdk4/6 and CyclinE/Cdk2 complexes (Yao, et al. 2008). Activation of signaling cascades inactivates these complexes and controls S phase entry

(Iliakis, et al., 2003; Lukas, et al., 2004). In these signaling cascades, following DSB induction, ATM up-regulates the expression of the p21 protein via phosphorylation of p53. p21 is a Cdk inhibitor and promotes G1/S checkpoint arrest by inactivating the CyclinD/Cdk4/6 and CyclinE/Cdk2 complexes.
The G2/M transition is regulated by the CyclinB1/Cdk1 protein complex (Fung, et al., 2005). The mechanism of G2/M checkpoint activation is very similar to the G1/S. In response to DNA damage, the ATM-dependent phosphorylation of Chk2 induces the cytoplasmic translocaction of Cdc25 proteins. Consequently, Cdc25 protein activates G2/M cell cycle arrest by inactivation of CyclinB1/Cdk1 complex.

2.3.2 DSB repair machinery

In somatic cells, IR-induced DSBs are repaired via biphasic kinetics which is comprised of a fast and a slow component (Löbrich, et al., 1995).

2.3.2.1 Fast component of DSB repair

Canonical non-homologous end-joining (c-NHEJ) represents the fast component of the DSB repair in somatic cells. c-NHEJ is the prominent DSB repair pathway in all cell cycle phases and the majority of IR-induced DSBs (80 %), in G1 and G2 phases, are repaired by this pathway (Rothkamm, et al., 2003; Beucher, et al., 2009).
c-NHEJ repair pathway contains several substantial proteins including: Ku70/80, DNA-dependent Protein Kinase catalytic subunit (DNA-PKcs), Artemis, X-rays Repair Cross Complementing protein 4 (XRCC4), XRCC4-Line Factor (XLF) and DNA-Ligase IV (Lig4) (Imamichi, et al., 2014).
The first event following the induction of DSB is the detection of the break site by Ku70/80 heterodimer. After Ku70/80 binding to the damaged DNA-ends, DNA-PKcs is recruited to form DNA-PK holoenzyme (Gottlieb, et al., 1993; Wang, et al., 2013). DNA-PKcs is capable of phosphorylating numerous downstream proteins required for ligation, like XRCC4 and Lig4 (Wang, et al., 2013; Imamichi, et al., 2014). XRCC4 is a scaffolding protein that facilitates the recruitment of other proteins to the DSB site. XRCC4 has two dimers thereby can interact with Lig4 and DNA-PK (Leber, et al., 1998). XRCC4 stabilizes Lig4 at the DSB site and stimulate its activity. At the final step, the XRCC4/Lig4 complex in association with XLF reseal the DNA-ends (Riballo, et al., 2004) (Figure 2.1). This form of repair may cause nucleotide deletion from either side of the DNA break and makes c-NHEJ potentially an error-prone repair pathway (Mahaney, et al., 2009).

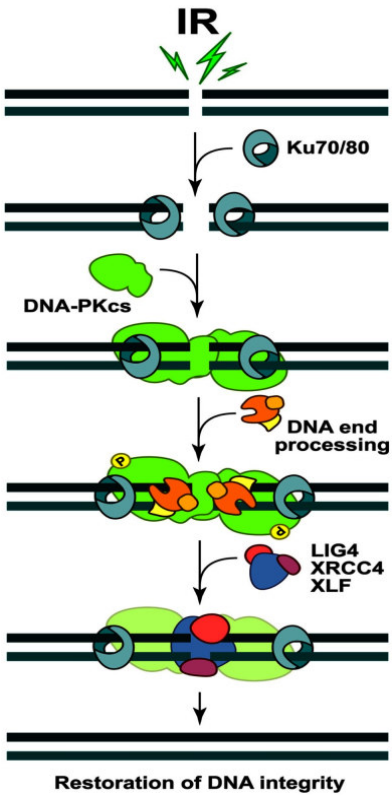

Figure 2.1. Model for c-NHEJ repair pathway. Ku70/80 detects the DSB site and binds to the DNA-ends immediately after damage induction. Then, DNA-PKcs is recruited by Ku to activate downstream proteins. Following a limited end-processing, the DNA-ends are resealed by employing Lig4, XRCC4 and XLF (Modified from Mladenov et al., 2013).

2.3.2.2 Slow component of DSB repair

If c-NHEJ fails to repair the DSBs, due to complexity or the location of the break in the chromatin, DSBs undergo the slow component of repair; which is resection dependent. In G2 phase, the Homologous Recombination repair pathway (HR) represents the slow component of repair. HR is one of the most important DSB repair pathways and it has been evolutionary conserved from bacteriophage to human (San Filipo, et al., 2008). Using the undamaged sister chromatin as a template to promote repair, HR minimizes the risk of genomic alteration during repair (Bell et al., 2016). Therefore, HR provides greater repair fidelity than c-NHEJ.

HR repair pathway begins with 5' to 3' nucleolytic degradation of the DNA-ends. This process, termed DNA-end resection, generates a long 3' single strand overhang. Resection process is initiated by MRN complex nuclease activity and CtIP-Brca1 proteins (Cannavo, et al., 2014). The initial resection is prolonged further by Exo1, BLM and DNA2 proteins (Gravel, et al., 2008; Mimitou, et al., 2009). Following resection, the Replication Protein A (RPA) immediately covers the 3' ss-DNA overhang, which subsequently replaced by the Radiation repair protein 51 (Rad51) (Trujillo, et al., 1998; San Filipo, et al., 2008). This process is regulated by Radiation repair protein 52 (Rad52) and Breast cancer type 2 substantial protein (Brca2). Rad51 is loaded to 3' ssDNA to form the pre-synaptic

nucleoprotein filament which is required for homology pairing at the sister chromatin (Sung, et al., 1995; Robertson, et al., 2009) (Figure 2.2). The invasion of the Rad51 nucleoprotein filament to the double-stranded donor DNA molecule yields a DNA joint called D-loop which is promoted by Radiation repair protein 54 (Rad54) (Mazón, et al., 2010; Goodarzi, et al., 2013). Using the homologous sequence as a template, DNA polymerase elongates the invaded DNA strand, yielding a double Holliday junction which can be dissolved by specialized nucleases. The orientation of the DNA incisions, determines whether a crossover or non-crossover recombinant is made (Figure 2.2).

a. b.

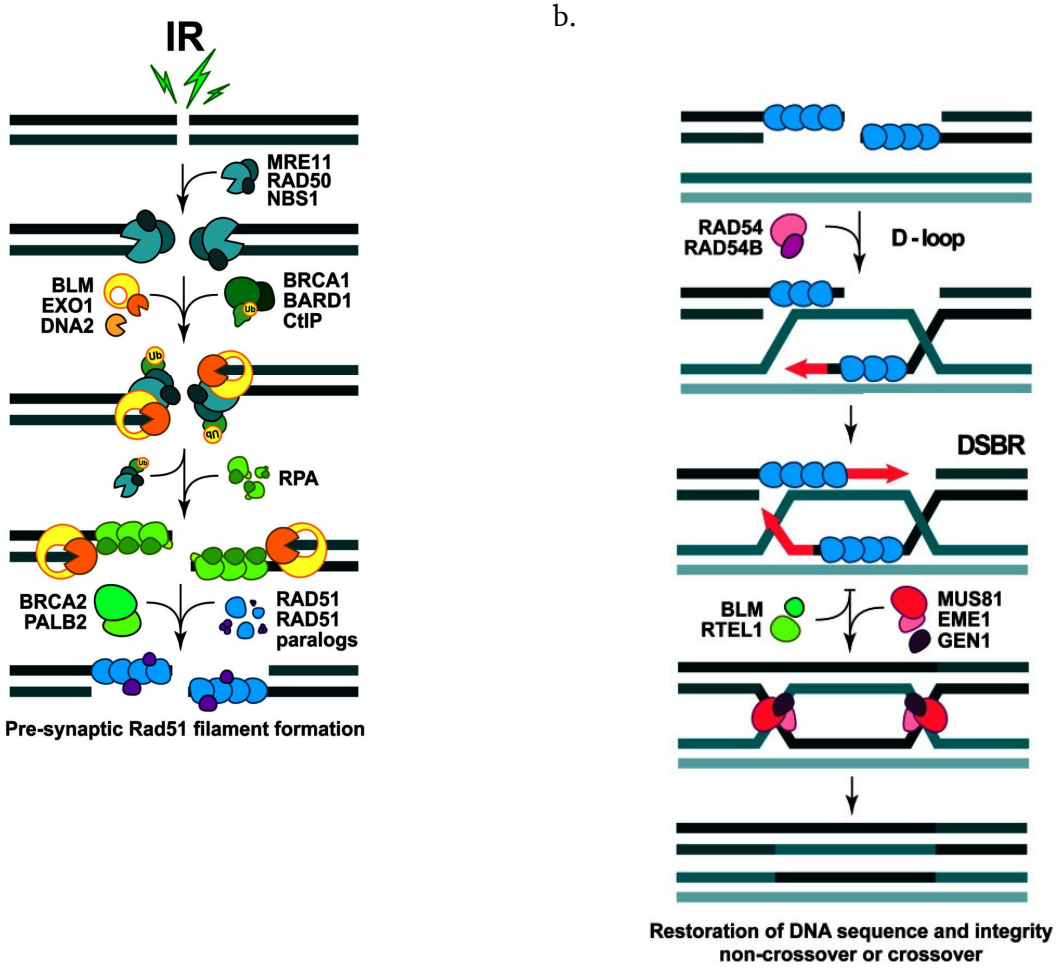

Figure 2.2. Model for HR repair pathway. a. Early steps of HR. DNA-ends resection initiates HR process. ssDNA overhang generated by nucleolytic degradation of DNA-ends is covered by RPA. Then, replacement of RPA with Rad51 forms pre-synaptic nucleoprotein filament (Modified from Mladenov et al., 2013). b. Late steps of HR. Rad51 nucleoprotein filament mediates homology search at the sister chromatid. Homologous pairing is followed by DNA elongation using homologous template (Modified from Mladenov et al., 2013).

In G1 phase, since there is no sister chromatin available, the slow component of DSB repair relies on resection-dependent c-NHEJ (Res-dep-NHEJ) (Biehs, et al., 2017). Similar to HR, Res-dep-NHEJ repair pathway begins by DNA-end resection. The factors regulating resection in this pathway are striking differenced to the HR. To initiate the process, Polo-Like Kinase-3 (PLK3) phosphorylates CtIP to interact with Brca1. The CtIP-Brca1 interaction promotes the initial step of resection (Barton, et al., 2014; Biehs, et al., 2017). Mre11, EXD2 and Exo1 then execute the resection with Artemis completing the process. In contrast to HR, following resection, the 3' ssDNA tail cannot be decorated by RPA, since resection in G1 phase is not as extensive as it is in G2 phase. However, induction of very complex DSBs, using high doses of X-rays or α-particle, induces long portion of resection covered by RPA in G1 phase (Barton, et al., 2014). The resection event is followed by the recruitment of c-NHEJ factors (Lig4, XRCC4 and XLF) essential for resealing the DNA-ends (Riballo, et al., 2004; Beucher, et al., 2009). Res-dep-NHEJ is an inaccurate repair pathway and is usually associated with chromosomal translocation (Barton, et al., 2014).

2.3.2.3 PARP1-dependent alternative-NHEJ

In the absence of c-NHEJ, alternative non-homologous end-joining (alt-NHEJ) serves as a backup repair pathway (Mansour, et al., 2013). alt-NHEJ is a resection dependent repair pathway and its function relays on CtIP and MRN complex nuclease activities (Lieber, et al., 2010). The mechanism of this pathway is independent of c-NHEJ core proteins including Ku70/80, XRCC4 and Lig4 (Deriano, et al., 2013). To repair DSBs, alt-NHEJ utilizes Poly (ADP-Ribose) Polymerase-1 (PARP1), DNA Ligase I and III (Lig1/3) and XRCC1 but not DNA-PKcs (Wang, et al., 2006; Lieber, et al., 2010).

Mechanistically, in the presence of a DSB, PARP1 recognizes the damaged site and catalyses the formation of Poly (ADP-Ribose) (PAR) on itself and other acceptor proteins including histones (Lindhal, et al., 1995). The scaffold created by PARP1 around the DSB site alters the chromatin structure, protects the DNA-ends and promotes the recruitment of other DNA repair factors involved in alt-NHEJ (Luijsterburg, et al., 2016). Finally, the coordination of PARP1 with Lig1/3 and XRCC1 complex promotes the ligation of DNA-ends (Iliakis, 2009) (Figure 2.3).

Compared to c-NHEJ, alt-NHEJ repair pathway is much less faithful and more critically dependent on micro-homology (Deriano, et al., 2013). This might cause a large nucleotide deletion which is highly mutagenic (up to 100 base pairs) (Mansour, et al., 2010)

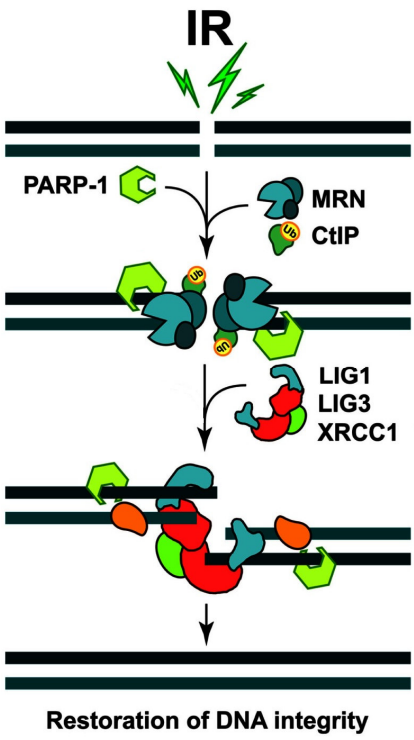

Figure 2.3. Model for alt-NHEJ repair pathway. PARP1 binds to the resected breaks generated by CtIP and MRN complex. Then, DNA repair was promoted by employing the Lig1/3 and XRCC1 (Modified from Mladenov et al., 2013).

2.4 DSB repair in stem cells

Stem cells, similar to the somatic cells in the body, are constantly exposed to DNA damaging factors. DNA damage and genetic alteration are the two major threats to the survival and function of stem cells (Blanpain, et al., 2011). The dysregulation of the genes controlling self-renewal and differentiation in stem cells might induce different catastrophic consequences which are particularly detrimental to the entire organism, e.g. cancer (Mimeault, et al., 2009; Behrens, et al., 2014). Furthermore, mutation in ESCs may enter the gremlin and soma which can affect subsequent generations.

ESCs exhibit an unusual cell cycle structure with a short G1 phase and a long S phase (White, et al., 2005). In contrast to somatic cells which have a large fraction of their cells in G1 phase (G1: 45 %, S: 29 % and G2: 26 %), ESCs have a large proportion of their cells in S phase (G1: 16 %, S: 56 % and G2: 28 %) (Fluckiger, et al., 2006). In spite of the short duration of G1 phase in ESCs, they fail to activate G1/S checkpoint and cells enter S phase with damaged DNA at a similar rate of undamaged cells (van der Laan, et al., 2013). p21 protein is one of the key factors promoting G1/S arrest by inactivating the CyclinD/Cdk4/6 and CyclinE/Cdk2 complexes (Deckbar, et al., 2011). The lack of p21 protein accumulation in response to DNA damage in ESCs, causes an inefficient G1/S cell cycle arrest (Dolezalova, et al., 2012; Suvorova, et al., 2016). In addition, the tumor suppressor protein retinoblastoma, which is essential for the activation of G1/S checkpoint is not active in ESCs (Savatier, et al., 1994).

ESCs have developed a robust non-mutagenic DSB repair capacity (Serrano, et al., 2011). DNA repair machinery has been evaluated with pronounced differences in repair capacities in ESCs compared to multipotent stem cell (e.g. NSCs) and differentiated cells (e.g. fibroblasts). These differences include the kinetics of the DNA repair and the preference for the use of HR over c-NHEJ. The amount of HR key proteins, e.g. Rad51, is 10 times higher in ESCs than in differentiated cells (Tichy, et al., 2010; Serrano, et al., 2011). This indicates that HR governs DSB repair in ESCs (Tichy, et al., 2010; Lan, et al., 2012). The HR protein level as well as DSB repair capacity has been decreased during the differentiation of stem cells (Adams, et al., 2010; Schneider, et al., 2012). This indicates that the DSB repair that occurs in ESCs is more efficient than in any other cell types (Figure 2.4).

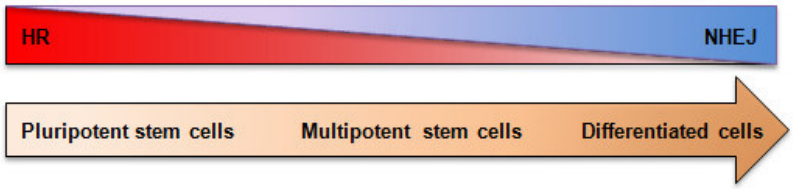

Figure 2.4. Contribution of HR and NHEJ during cell differentiation. DSB repair in pluripotent stem cells relays more on HR and less on NHEJ. During cell differentiation, there is a trend toward increase in NHEJ and decrease in HR**.**

2.5 Involvement of RNA in DSB repair

The detection of RNA in the vicinity of DSBs in different organisms (Lee, et al., 2009; Wei, et al., 2012; Francia, et al., 2015), raised the possibility that RNA may facilitate the DNA repair process. Since transcription occurs throughout the cell cycle, it is important to understand the mechanism whereby transcription promotes DSB repair in the cell. There are number of hypothesis and speculations that RNA can function as a template in DNA repair. Chakraborty et al. reported that the nascent RNA transcript can serve as the repair template for restoring the missing sequence at the DSB site. The authors suggested that the involvement of nascent RNA in c-NHEJ enhances repair efficiency and the c-NHEJ represents an error-free repair pathway in transcriptionally active cells (Chakraborty, et al., 2016). Furthermore, the involvement of RNA in HR has been previously suggested. In this novel model for HR, using the complementary RNA oligonucleotides as a template, instead of homologous sequence at sister chromatic, DNA polymerase alpha and delta syntheses the missing DNA sequences at the DSB site (Storici, et al., 2007; Keskin, et al., 2014; Keskin, et al., 2016).

The role of the transcription machinery, as a molecular motor to mediate the recruitment of repair proteins to the DSB site, has been described previously (McKay, et al., 2004; Lindsey-Boltz, et al., 2007). In yeast, Ohle et al., demonstrate that the activity of transcription machinery regulates excessive resection at DSB sites (Figure 2.5). In their model, the short ssDNA-ends at the DSB sites, generated by MRN complex, induce RNA polymerase II (Pol II) transcription activity. The translocation

of Pol II along DNA and the activity of chromatin remodelers open the DNA helix and facilitate additional resection by exonucleases. In the absence of non-template DNA strand, the nascent transcript would be more prone to re-hybridize with the ssDNA-template, directly competing with RPA. This results in the formation of RNA-DNA hybrid at the break site. In the final step, RNaseH1 enzyme removes the RNA from the hybrid and enhances the recruitment of RPA to the damage site (Figure 2.5).

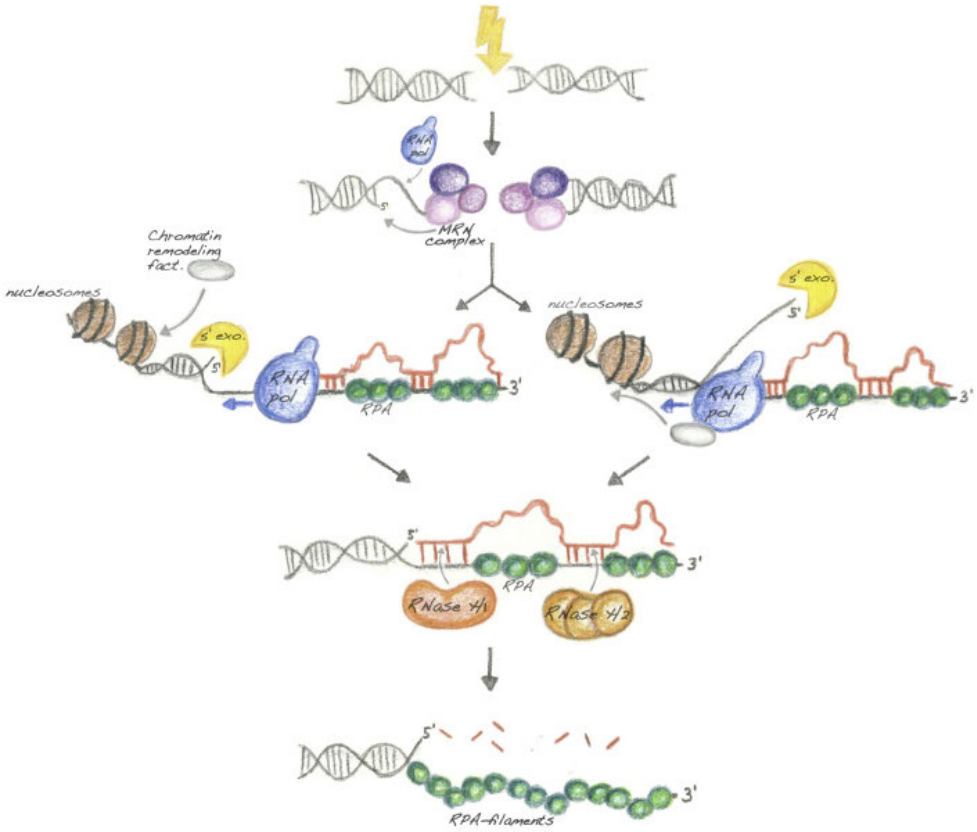

Figure 2.5. Model for the role of transcription machinery in long resection. Upon DSB induction, MRN starts resection at the break sites. The Pol II binds to the ssDNA segments and initiates transcription. Opening the DNA helix by chromatin remodelers and transcription factors facilitates the translocation of transcription machinery and subsequent long-range resection. Pol II can move ahead (left) or behind (right) the nuclease. In the absence of non-template DNA, RNA transcripts are prone to re-hybridize to their template-DNA. Finally, the RNA moiety is cleaved from RNA-DNA hybrid by RNaseH1 enzyme. The long-resected ssDNA will covered by RPA (Modified from Ohle et al., 2016).

R-Loop

RNA-DNA hybrids can also form through different biological process in the cells. During the elongation step of transcription, the nascent RNA can re-anneal to its DNA-template resulting in formation of RNA-DNA hybrid, termed to R-Loop structure (Figure 2.6). The formation of R-Loop can impair transcription and cause replication stress which may induce DNA damage (Aguilera, et al., 2012; Helmrich, et al., 2013). The mechanism of R-Loop formation, like what structure of DNA or RNA leads to re-association of transcript with its template, is still unclear. To prevent the formation of R-Loop, a co-transcription system has been evolved in eukaryotic cells. In this system, upon transcription, the nascent RNA transcripts are packaged into ribonucleoprotein particles (RNPs) and exported to the cytoplasm. Impairment of this system might lead to an increase in the level of R-Loop formation and genetic instability.

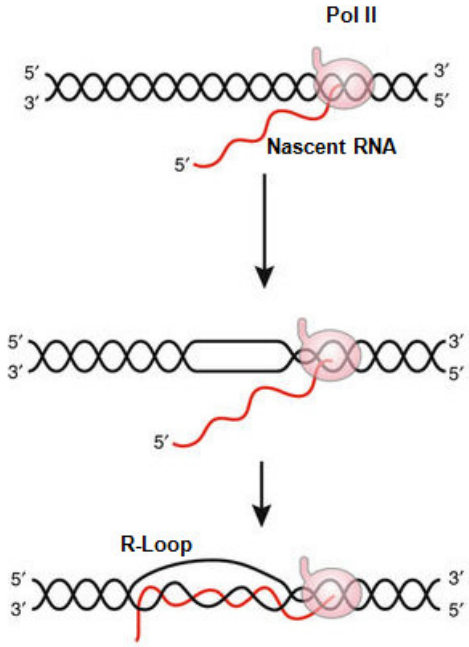

Figure 2.6. Model for the formation of R-Loop. While transcription elongation, nascent RNA re-hybridized with its cognate template DNA. The non-template DNA strand cannot bind to the second DNA strand and forms a loop structure called R-Loop (Modified from Aguilera and Gomez-Gonzales, 2017).

Degradation of RNA-DNA hybrids

RNA-DNA hybrids can be unwound by different factors. Ribonuclease H (RNaseH) enzymes family can remove RNA moiety from RNA-DNA hybrids. RNaseH is an endoribonuclease that degrades RNA-DNA hybrid by cleaving the RNA unit (Cerritelli, et al., 2009). Mechanistically, RNaseH cleaves the PO-3' bond of the RNA by a catalytic mechanism that contains Mg^{2+} and Mn^{2+} metal ions (Yang, et al., 2006). In eukaryotic cells, based on amino acid sequences, RNaseH enzymes are classified into two types, RNaseH1 (monomeric) and RNaseH2 (Heteromeric) (Tadokoro, et al., 2009).

DEAD box 1 (DDX1) is another factor involved in the degradation of RNA-DNA hybrids. DDX1 is

involved in the transport of RNA transcripts from the nucleus to the cytoplasm and also in the regulation of splicing (Chou, et al., 2013). But, it has been shown that DDX1 is recruited to DSBs containing RNA and mediates their repair by removing RNA from RNA-DNA hybrids (Li, et al., 2016). Together these studies provide remarkably consistent and unequivocal evidence that the transfer of genetic information from RNA to DNA is more general and might be utilized for DNA repair.

2.6 Aim of the study

In somatic cells, the interaction of cell cycle control and DNA repair is essential for the repair of DNA lesions and the maintenance of genome stability. The simple DSBs are re-ligated quickly via c-NHEJ in all cell cycle phases, whereas the complex DSBs are repaired with slow kinetics in a resection dependent manner (Beucher, et al., 2009). In S and G2 phase, DNA resection is followed by HR, which is an error-free pathway. In G1 phase, the resected DNA-ends are repaired by resection dependent c-NHEJ in an Artemis and CtIP dependent manner. This repair pathway is usually associated with chromosomal translocations and genome alterations (Biehs, el a., 2017).

ESCs exhibit an unusual cell cycle profile with a short G1 phase and lack the G1/S checkpoint (Fluckiger, et al., 2006; van der Laan, et al., 2013). To compensate this weakness and preserve the genomic content, ESCs have developed a robust DSB repair capacity. Several studies have reported that HR governs DSB repair in ESCs (Tichy, et al., 2010; Lan, et al., 2012). However, how ESCs deal with the complex DSBs in G1 phase, where HR is not active, remains unclear. Therefore, the main goal of this study was to characterize the mechanism/s by which ESCs retain their genomic integrity. As the resection dependent c-NHEJ is highly error-prone, we hypothesized that ESCs utilize a particular DSB repair process in G1 phase, distinct from that in somatic cells. In addition, to better understanding the DSB repair capacity at different levels of cellular differentiation, the DDR mechanisms in ESCs and ESC-derived NSCs have been distinctly characterized.

3 Materials and Methodes

3.1 Materials

3.1.1 Cell lines

ESC J1

Mouse embryonic stem cell line was derived from a male agouti 129S4/SvJae embryo, cultivated in DMEM supplemented with 1.5 % FCS, 0.1 % LIF, 1 % cell guard, 1 % Glutamine, 1 % NEAA, 1 % sodium pyruvate and 0.5 % ß-Mercaptoethanol. Cells were passaged three times a week (1:6). Cells were kindly provided by Prof. Dr. Leon Mullenders (Leiden university medical center, Netherlands).

NSC J1

Mouse neural stem cell line generated from ESC J1 in our lab, cultivated in Euromed-N supplemented with 1 % N-2 supplement, 1 % cell guard, 0.1 % EGF and 0.1 % bFGF. Cells were passaged three times a week (1:5 to 1:6).

ESC iB10

Mouse embryonic stem cell line was derived from a male 123/Ola background, cultivated in DMEM supplemented with 1.5 % FCS, 0.1 % LIF, 1 % cell guard, 1 % Glutamine, 1 % NEAA, 1 % sodium pyruvate and 0.5 % ß-Mercaptoethanol. Cells were passaged three times a week (1:6).
Cells were kindly provided by Prof. Dr. Leon Mullenders (Leiden university medical center, Netherlands).

HeLa-S3

Human cervical cancer cell line isolated from Henrietta Lacks in 1951, cultivated in DMEM supplemented with 10 % FCS and 1 % NEAA and passaged two times a week (1:10).

MEF

Mouse embryonic fibroblast cell line, cultivated in DMEM supplemented with 10 % FCS and 1 % NEAA. Cells were passaged two times a week (1:10).

MEF feeder layer

Cells were kindly provided by Prof. Dr. Leon Mullenders (Leiden university medical center, Netherlands).

3.1.2 Small molecule inhibitors

Table 3. 1. Inhibitors.

Inhibitor	Concentration	Company
ATM (Ku60019)	5 μM	Tocris Bioscience
ATR (VE-821)	5 μM	Selleckchem
DNA-PK (Ku7441)	10 μM	Tocris Bioscience
DRB	100 μM	Sigma
PARP1 (PJ34)	10 μM	Calbiochem
PLK1/3 (GW843682X)	0.5 μM	Tocris
Rad51 (B02)	50 μg/ml	Calbiochem

3.1.3 siRNA

Table 3. 2. siRNA.

siRNA	Sequence	Concentration (nM)	Company
Negative control	5' AATTCTCCGAACGTGTCACG 3'	25	Qiagen
Artemis (human)	5' AACTGAAGAGAGCTAGAACAG 3'	25	Qiagen
Artemis (mouse)	5' AAGGATCACATGAAAGGATTA 3'	50	Qiagen
CtIP (human)	5' TCCACAACATAATCCTAATTT 3'	50	Qiagen
DDX1 (human)	5'CAGGCUGAAUCUAUCCCAUUGAUCU 3'	10	Qiagen

3.1.4 DNA vectors

GFP pEGFP-C1, vector for GFP expression in mammalian cells, purchased from Clontech.

RNaseH1 pFRT-TODestGFP_RNAse, vector for RNaseH1 overexpression in mammalian cells, purchased from AddGene.

3.1.5 Transfection reagents

siRNA transfection reagents

Lipofectamine®RNAiMAX reagent Invitrogen

DNA transfection reagent

Lipofectamine® LTX with Plus reagent	ThermoFisher

Serum free medium

Opti-MEM® Medium	ThermoFisher

3.1.6 Kits

Venor®GeM Mycoplasma diagnosis kit	Sigma Aldrich
Click-iT™*EDU Imaging Kit*	Baseklick
BrdU FITC	BD
peqGOLD Xchange Plasmid maxi-EF kit	Peqlab
ZR Plasmid Miniprep™-Classic	ZYMO RESEARCH

3.1.7 Cell culture

Dulbecco's Modified Eagle's Medium (DMEM)	Sigma Aldrich
Euromed-N	Biozol
Non-essential amino acids (NEAA)	Biochrom
LIF (mouse)	ProSpec
Cell culture guard	BD
Fetal calf serum (FCS)	Biochrom
Sodium pyruvate	Applichem
L-Glutamine	Sigma Aldrich
N-2 supplement	Invitrogen
EGF (mouse)	ProSpec
bFGF (mouse)	ProSpec

3.1.8 Buffers and solutions

All pH analysis were measured by using HCl and NaOH.

Cell culture

PBS	137 mM NaCl	pH 7.4
	2.7 mM KCl	
	8 mM Na_2HPO_4	
	1.5 mM KH_2PO_4	

Trypsin/EDTA	0.5 M EDTA	pH 8
	2.5 % (v/v) Trypsin	in PBS

SDS-PAGE

Lysis buffer	20 mMTris/HCl	pH 8.2
	150 mMNaCl	
	1 % Triton	
	1x PhosStop	
	1x Complete	
RIPA buffer	50 mMTris-HCl	pH 8
	1 % Triton	
	0.5 % $C_{24}H_{39}NaO_4$	
Electrophoresis buffer	25 mMTris/HCl	pH 8.8
	0.2 M Glycine	
	(0.5 % /w/v) SDS	
5x Loading buffer (Laemmli)	60 nMTris/HCl	pH 6.8
	2 % (w/v) SDS	
	5 % (v/v) ß-Mercaptoethanol	
	10 % (v/v) Glycerin	
	0.01 % Bromophenol blue	
Stacking gel buffer	0.5 M Tris/HCl	
	1 % SDS	
Running gel buffer	1.5 M Tris/HCl	
	1 % SDS	

Western Blot

Transfer buffer	20 mM Tris/HCl	pH 8.3
	150 mM Glycine	
	20 % Methanol	
Washing buffer (TBS-T)	200 mMTris/HCl	pH 7.6
	1.4 M NaCl	
	0.1 % Tween20	
Blocking buffer	5 % nonfat milk in TBS-T	
Primary/Secondary antibody	1 % nonfat milk in TBS-T	

Immunofluorescence

Cell fixation	2.5 % Formaldehyde in PBS
Washing buffer	PBS
Permeabilization	0.2 % TritonX-100 in PBS
Blocking buffer	10 % Roti-Block in PBS
Primary/secondary antibodiy	10 % Roti-Block in PBS
DAPI	0.4 μM/ml DAPI in PBS

CytoSpin (ESC)

Cell fixation	4 % Formaldehyde
Permeabilization	0.5 % TritonX-100 in PBS

S9.6 stainig

Pre-wash	0.5 % Formaldehyde in CSK buffer
Cell fixation	Ice cold methanol
CSK buffer	10 mM PIPES
	100 mMNaCl
	300 mM sucrose
	3 mM $MgCl_2$
	0.7 % TritonX-100
	0.3 mg/ml RNase
Blocking buffer	2 % BSA, 0.5 % FCS in PBS
Hoechst	2 μg/μl

Cell viability assay

Crystal violet solution	0.1 % Crystal violet
	25 % Methanol
	In MiliQ

FACS

PI solution	0.1 mg/ml PI
	10 mg/ml RNaseA
	In PBS

Bacteria

Ampicillin	50 mg/ml in MiliQ water

LB Agar broth	10 g/l Tryptone
	2 % Yeast extract
	5 g/l NaCl
LB Agar plates	1.5 % Agar in LB broth

3.1.9 Antibodies

Table 3. 3. Primary antibodies.

Antibody	Species	Dilution	Company	Application
anti- H2AX	mouse	1:1000	Millipore	IF
anti- H2AX	rabbit	1:1000	Epotomics	IF
anti-53BP1	mouse	1:1000	Betyl	IF
anti-Artemis	rabbit	1:3000	GeneTex	WB
anti-CyclinB1	mouse	1:200	Thermofisher	IF
anti-pRPA (T21)	rabbit	1:10000	Abcam	IF
anti-Rad51	rabbit	1:10000	Abcam	IF
anti-GFP	mouse	1:500	Roche	IF
anti-DDX1	rabbit	1:1000	Batch 2923	IF
anti-S9.6	mouse	1:500	Kerafast	IF
anti-OCT4	rabbit	1:500	Abcam	IF
anti-SOX2	rabbit	1:500	Abcam	IF
anti-GFAP	mouse	1:300	Thermofisher	IF
anti-ß-IIITubulin	mouse	1:500	Thermofisher	IF
anti-Nestin	mouse	1:200	Abcam	IF
anti-GAPDH	rabbit	1:1000	Santa Cruz	WB

Table 3. 4. Secondary antibodies.

Antibody	Dilution	Company	Application
Goat anti-rabbit AlexaFluor 488	1:1000	Molecular Probes	IF
Goat anti-mouse AlexaFluor 488	1:1000	Molecular Probes	IF
Goat anti-rabbit AlexaFluor 594	1:1000	Molecular Probes	IF
Goat anti-mouse AlexaFluor 594	1:1000	Molecular Probes	IF
Donkey anti-rabbit Dylight	1:1000	Invitrogen	IF
Goat anti-mouse IgG-HRP	1:10000	Santa Cruz	WB
Goat anti-rabbit IgG-HRP	1:10000	Santa Cruz	WB

3.1.10 Protein standard

PageRuler™ Plus Prestained Protein (SM1811)	Fermentas

3.1.11 Laboratory consumables

Blotting paper, 703	VWR
Cell culture dishes (35x10 mm, 60x15 mm)	nunc ™ VWR
Cell culture flask (20 cm^2, 75 cm^2)	TPP
Cover slips, 15x15 mm	Roth
Centrifuge tubes (15 ml, 50 ml)	Greiner
FACS tubes	Beckman Coulter
Filter Cards, one hole	TharmacCellspin
Filter paper, Whatman	Schleicher &Schüll
Immersion oil	Zeiss
KimWipes	NeoLab
Kuvets, plastic	Roth
Micro tubes (Eppis)	Roth
Microscope slides, superfront	Roth
Parafilm	Bermis
Pasteur pipets, glas	Roth
Pasteur pipets, plastic	Roth
Pipet tips	Sarstedt
Pipet tips, filtered	Roth
Polysine® Slides	Thermo Scientific
PVDF membrane	Thermo Scientific
μ-slide VI	Ibidi
μ-slide IV	Ibidi

3.1.12 Chemicals

Accutase	Sigma-Aldrich
Agar	Roth
APS	Roth
Bromphenol blue	USB
BSA	AppliChem
BrdU (1 mM)	BD Bioscience
C_aCl_2	Roth
Crystal violet	Sigma-Aldrich
DAPI	Sigma-Aldrich
DMSO	Sigma-Aldrich
EDTA	Roth
EdU (10 mM)	Invitrogen
Ethanol, denatured	Roth
Formaldehyde (4 %)	AppliChem
Glycerin	Roth
Glycine	Roth
H_2O_2	Sigma-Aldrich
HCl	Roth
Isopropanol	Roth
KCl	Roth
KH_2PO_4	Roth
Methanol	Roth
$MgCl_2$	Roth
Mounting medium	Vectashield® Axxora Alexis
Nonfat-dried-milk	Reformhaus
Na_2HPO_4	Roth
NaCl	Roth
NaOH	Roth
PhosStop 10X	Roche
PIPES	Roth
Protease inhibitor 25x Compelete	Roche
RNase A	Sigma-Aldrich
Roti®-Block	Roth
SDS	Roth

Sodium deoxycholate	Roth
Sucrose	Roth
TEMED	Roth
Tris	Roth
TritonX-100	Roth
Trypsin	Roth
Tween®20	Roth
ß-Mercaptoethanol	Sigma-Adrich

3.1.13 Instruments

Camera system (microscope)	AxioCamMRm	Zeiss
Centrifuge	5451 R/5804 R	Eppendprf
Centrifuge	Biofugepico	Heraeus
Centrifuge	Cellspin I	THARMAC
Cell counting chamber	Neubauer improved	Marienfeld Superior
Chemiluminescence detection	Fusion FX	Viber Lourmat
Electrophorese system	SE260	Hoefer
Flow box	Herasafe	ThermoScientifid
Flow cytometer	Cytomics FC 500	Beckman Coulter
Incubator	Hera cell 240	Thermo Scientific
Microscope	Imager Z2	Zeiss
Microscope (cell culture)	Eclipse TS100	Nikon
Microscope (Live cell)	AXIOVERT200M	Zeiss
Microscope (confocal)	TCS SP5 II	Leica
Nanophotometer	P-Class	Implen
pH Metter	pMX2000	WTW
Power supply	PowerPac™HC	BIO-RAD
Scale	TE 1502S/TE 153S-DS	Sartorius
Shaker	3011	GFL
Thermomix	Comfort	Eppendorf
Vortex	Vortex genie2	Scientific Industries
Water bath	1083	GFL
Wester bloting system	Mini Trans-Blot®Cell	BIO-RAD
X-ray machine	X-RAD 320	PXi

3.1.14 Software

Flow cytomerty	CXP	Beckmann Coulter
Gele reader	ChemiCapt	Viber Lourmat
Fluoresent microscopy	Metafer4	Metasystems
Fluoresent microscopy	LAS AF Lite	Leica
Image analysis	Image J	Open Source

3.2 Methods

3.2.1 Cell biology

All cell lines were cultivated under sterile condition and they were regularly tested for mycoplasma contamination.

3.2.1.1 Differentiation of ESCs to NSCs

By following the protocol of Conti et al. (2005), the ESC J1 were differentiated *in vitro* into NSC J1. To this end, adherently growing colony-forming ESCs were seeded into serum-free differentiation medium lacking the cytokine LIF, which is needed for ESC propagation (Figure 3.1a). After approximately 5 days, newly differentiated and spherically growing neuronal precursor cells were re-seeded in NSC medium containing EGF and b-FGF. After an additional 3-5 days, adherent cells developed from the neurospheres and the procedure of re-seeding was repeated until a uniform, self-renewing monolayer of neural stem cells was established (Figure 3.1b).

a. b.

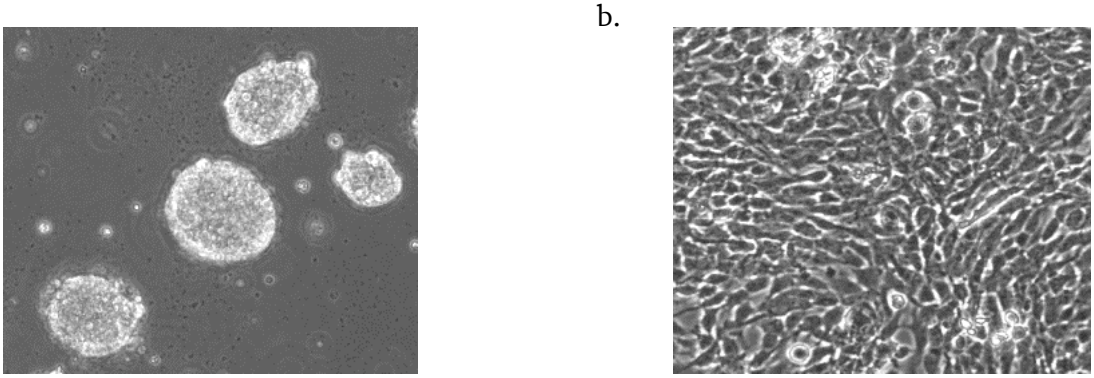

Figure 3.1. Morphology of ESC J1 and NSC J1. a. Transmission light microscopy images of ESC J1. b. Transmission light microscopy images of NSC J1.

To exclude that cells underwent transformation and developed chromosomal instability, chromosomal spreads were regularly tested by Mrs. Christel Braun for chromosomal aberrations (Figure 3.2.a). Cells were classified as genetically stable when 80 % of cells contained 39-41 chromosomes per cell (Figure 3.2.b). ESCs were chromosomally stable, whereas in NSCs occasional aberrations were observed at passage number >25. Thus, NSCs were only used between passage number 15 and 25 for the experiments.

a. b.

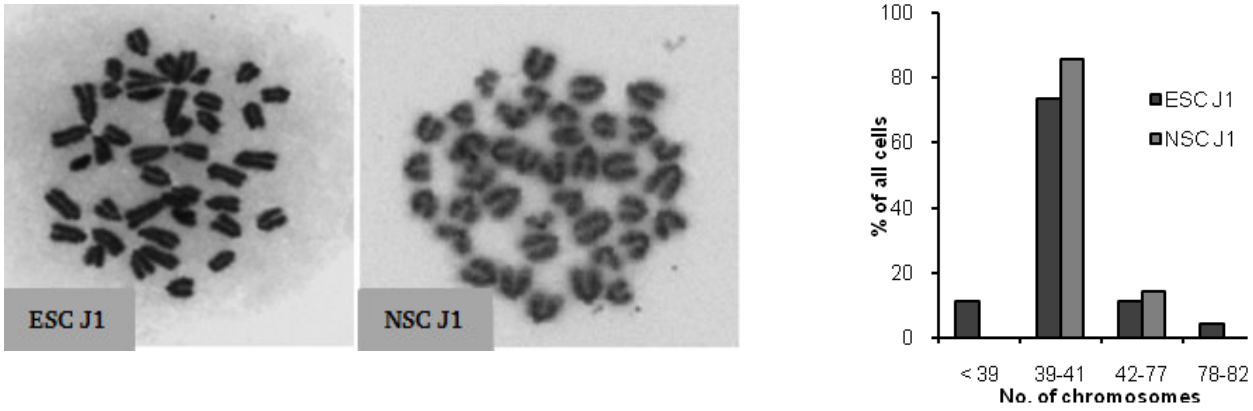

Figure 3.2. Karyotype testing of ESC J1 and NSC J1. a. Chromosomal spreads stained with Giemsa. b. Representative quantification of one karyotype testing.

3.2.1.2 Cell culture

To keep the cells healthy and growing, all cell lines were passaged when they reached 80-90 % confluency in culture flasks. To passage the cells, the old culture media was removed. Then, cells were washed once with 10 ml PBS and incubated with 3 ml Trypsin/EDTA (Accutase for NSCs) for 3-5 min at 37°C and 5 % CO_2. The trypsinization reaction was stopped by addition of 7 ml culture media. Then cell suspension was transferred in a 15 ml tube and centrifuged for 3 min at RT and 200 g. After resuspension of the cell pellet in 5-10 ml media, cells were passaged at a ratio of 1:5-1:10 in 75 cm^2 culture flasks depending on cell line and confluency. The information regarding to cell lines, passaging frequency as well as appropriate culture media is listed in chapter 3.1.1.

3.2.1.3 Cell seeding

Using a Neubauer counting chamber, the cell number was determined for cell seeding. To seed the cells on glass coverslips, autoclaved coverslips were placed in 35 mm culture dishes and 2 ml cell suspension containing 5 x 10^5 cells was added to each dish. For ESCs, cells were seeded on plastic surface without using cover slips. For siRNA or plasmid transfection, 3 x 10^5 cells were plated in 2 ml medium. In all conditions, after seeding, the cells were incubated at normal cell culture conditions.
To study DSB repair after low doses of X-rays, as well as laser micro-irradiation, cells were seeded in Ibidi slides 1 day prior to irradiation (Table 3.5).

Table 3. 5. Cell number and culture media volume for different culture dishes.

3.5 cm petri dish	10 cm petri dish	μ-slid (Ibidi IV)	μ-slide (Ibidi VI)
3-5 x 10^5 cell	5-8 x 10^5 cell	5 x 10^5 cell	3 x 10^5 cell
in 2 ml medium	in 5 ml medium	in 600 μl medium	in 200 μl medium

3.2.1.4 Inhibitor treatment

All small molecule inhibitors listed in Table 3.1 were mixed with fresh media containing 0.5 μM EdU and 100 ng/ml Nocodazole and added to the cells 30 min before irradiation. Inhibitors, EdU and Nocodazole remained in the culture medium during the entire incubation time after irradiation.

3.2.1.5 siRNA transfection

One day after cell seeding, cells were treated with siRNA (see Table 3.2). Transfection was performed following manufacturer's instructions. Briefly, siRNA was mixed with Lipofectamine RNAiMAX transfection reagent and Opti-MEM® serum free medium. After replacing the old media with 1ml Opti-MEM, the mixture was added dropwise to the cells under constant, slow rotation of the dish and incubated for 6 h at 37°C. Then the Opti-MEM containing siRNA was removed and fresh medium added to the cells and incubated at 37°C with 5 % CO_2. Irradiation of the cells was always performed 48 h after transfection.

3.2.1.6 Plasmid DNA transfection

Following the manufacturer's protocol, 3 μg/μl plasmid (section 3.2.1.6) was mixed with Lipofectamine® LTX with Plus reagent. Then the old medium was replaced by 1.5 ml Opti-MEM® serum free medium and the mixture was added dropwise to the cells under constant, slow rotation of the dish. After 6 h incubation at 37°C, the medium contains transfection reagent was removed and new media was added to the cells and incubated at 37°C with 5 % CO_2. Irradiation of the cells was always performed 24-48 h after transfection.

3.2.1.7 X-rays irradiation

To induce double stranded DNA breaks, cells were irradiated with high and low doses of X-rays. In all conditions, 30 min prior to irradiation, cells were treated with EdU (0.5 nM) and Nocodazole (100 μg/ml). EdU is a thymidine analoge and incorporated into the DNA structure while replication. Thus, cells in S phase during the time of irradiation and also the cells enter S phase during the repair incubation time are labelled. Nocodazole is an antimitotic agent, which causes cell cycle arrest at G2/M phase by disrupting microtubule polymerization. Using Nocodazole the contamination of G1 population with cells that were irradiated in G2 phase was prevented.
For irradiation, ESCs were seeded on plastic surface whereas other cell lines were seeded on sterile glass cover slips 24 h prior to irradiation (section 3.2.1.3). Cells were irradiated using X-RAD 320 X-rays machine. Different settings for high and low doses of X-rays irradiation were applied (Table 3.6). Irradiation for the cells growing on cover slips was performed under consideration of the glass factor effect 1.5 (Kegel, et al., 2007).

Table 3. 6. X-rays irradiation setting.

Gy	Filter	kV	mA	Distance	Time (sec)
2	1 (2 mm Aluminum)	250	10	50	52
1	2 (0.75 mm Copper, 0.25 mm Tin)	250	10	70	206
0.1	2 (0.75 mm Copper, 0.25 mm Tin)	250	10	70	21
0.01	2 (0.75 mm Copper, 0.25 mm Tin)	250	1	70	21

3.2.1.8 Laser micro-irradiation

For laser micro-irradiation, a Leica scanning confocal microscope (TCS SP5 II) and a 40x Leica objective were used. HeLa cells were grown in μ-Slide one day prior to irradiation (Table 3.5) and stained with Hoechst (2 μg/ml) for 10 min immediately before irradiation. To generate DNA damage, a preselected region of interest (ROI) within the nucleus of 1 μm thickness was micro-irradiated with the 405 nm laser set to 100 % at 200 Hz scanning speed. For standardisation, the FRAP wizard in the Leica software was used to set the irradiation parameters to 20 frames per ROI.

3.2.2 Immunostaining

To study the DSB repair behaviour in cell cycle specific manner, we combined the desired DSB markers with cell cycle specific markers (Figure 3.5).

3.2.2.1 Cell fixation, permeabilization and blocking

After irradiation and repair incubations, cells were washed once with BPS and fixed with 2.5 % formaldehyde for 15 min at RT. Then, cells were washed 3 times for 10 min with PBS. For permeabilization, cells were incubated with 0.2 % TritonX-100 for 10 min at RT. After permeabilization, cells were washed 3 times with 1x Roti block/MiliQ for 10min at RT (or overnight at 4°C) and incubated in the same buffer for 1 h at RT (or overnight at 4°C).

For ESCs, cells seeded on a plastic surface (section 3.2.1.7) were detached by Trypsin/EDTA (section 3.2.1.2). For fixation, the cell pellet was resuspended in 1ml 4 % TritonX-100 and incubated for 10 min at RT. Then, after centrifugation for 3 min at 4°C and 150 g, cells were resuspended in 1 ml PBS and spun down onto a glass slide by centrifuging for 1 min at RT and 10.000 RPM. The slides containing ESCs were incubated in permeabilization and blocking solutions as explained above.

For S9.6 staining, cells were washed once with PBS and pre-extracted with CSK buffer contains 0.5 % TritonX-100 for 5 min at RT. After washing 3 times for 1 min with PBS, cells were fixed with ice cold methanol for 10 min at -20°C. Then, cells were washed 3 times for 10 min with PBS and blocked with 2 % BSA, 0.5 % FCS/PBS for 1 h at RT (or overnight at 4°C).

3.2.2.2 Immunoflourescence staining

For foci staining, the primary antibodies listed in Table 3.3 were diluted in blocking solutions. Fixed cells on the glass coverslips or on the slides were incubated with 30 μl of primary antibodies for 4 h at RT (and overnight at 4°C for S9.6 foci staining). To provide humidity and prevent cells from drying while staining, the cells were incubated in wet chambers. After washing the cells 3 times for 10 min with 1x Roti block/MiliQ on the shaker, secondary antibodies (Table 3.4) diluted in blocking solution were added to the cells and incubated for 1 h at RT. Then, cells were washed again 3 times for 10 min with 1x Roti block/MiliQ on the shaker. To mark S-phase cells, cells were incubated with EdU-Click (Cy5) for 30 min at RT. After washing the cells three times for 10 min with 0.1 % Tween20/PBS, cells were incubated with 0.4 μg/ml DAPI for 5 min at RT to stain the nuclei. Finally, cells were washed once with PBS for 2 min. Then, the coverslips were transferred to the microscope slide with 2.5 μl of mounting medium and sealed with clear nail polish. The ESCs fixed on slide were covered by glass coverslips with 5 μl mounting medium.

3.2.2.3 Microscopy and data analysis

To specifically analyse of DNA repair in a particular cell cycle phase, cell cycle discrimination was conducted in a semi-automated way using Metafer software. Based on DNA content (DAPI signal) and EdU signal intensity, cells were scanned and distributed in a histogram depicting the different cell cycle phases (Figure 3.3a). Foci numbers were monitored in the EdU negative G1- and G2-phase cells. G1- and G2- phase cells were distinguished based on their DNA content (DAPI intensity). Additionally, G2-phase cells were identified by positive CyclinB1 staining. A minimum of 40 cells and 300 cells were analyzed respectively for high and low doses of X-rays (Figure 3.3.b).

a. b.

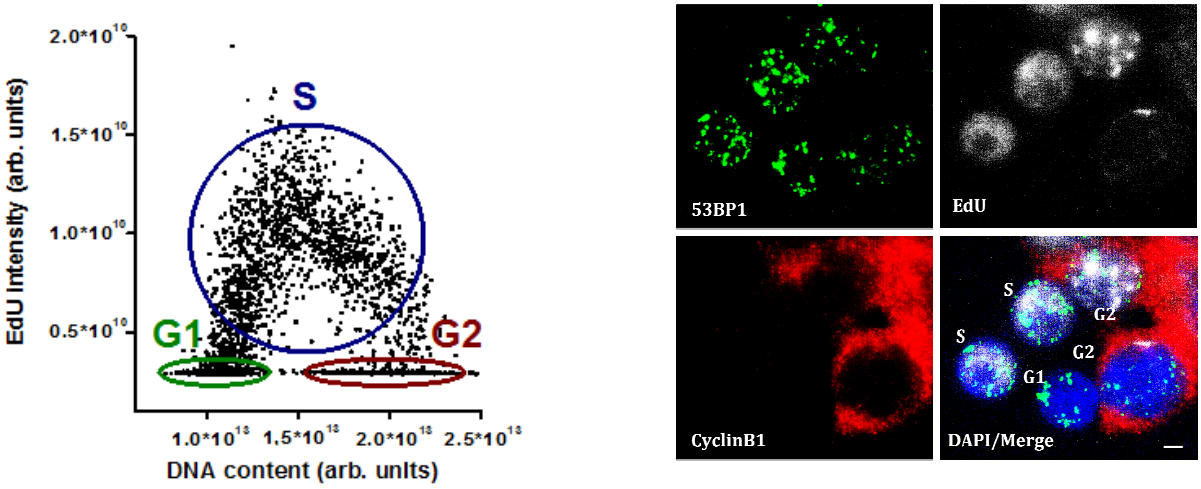

Figure 3.3. Specification of DNA repair in a particular cell cycle phase. a. Using a semi-automated system, cells were scanned for EdU and DAPI. Based on DNA content and EdU signal intensity, cells were distributed within G1-, S- and G2-phase of the cell cycle. b. Immunofluorescence staining of DNA damage marker 53BP1 and cell cycle specific markers, S-phase marker EdU and G2-phase marker CyclinB1. Scale bar represents 5 µM.

For S9.6 foci analysis, G1-phase cells were selected by DAPI signal intensity and images were taken using confocal microscopy. Using the ImageJ software, a quantitative analysis of S9.6 and γH2AX co-localization was performed.

All experiments were conducted at least in two to three independent repetitions. For all data points, the SEM was calculated between the mean values of all independent experiments. Furthermore, p-values were calculated using two sample t-test which compared the mean values of the all independent experiments (*=p≤ 0.05, **=p≤ 0.01, ***=p≤ 0.001, ****=p≤ 0.0001).

3.2.3 H_2O_2 treatment

To analyze the effect of oxidative stress on DSB repair capacity after irradiation with low doses of X-ray, cells were pre-treated with H_2O_2 3 h prior to irradiation. To this end, the media was removed and stored at 37°C. After washing once with PBS, cells were treated with 10 μM cold H_2O_2 and incubated for 30 min at 4°C. Then, H_2O_2 was replaced with the old media. 30 min prior irradiation, EdU, Nocodazole and inhibitors (ATM and DNA-PKcs) were added to the medium and cells were incubated at 37°C until irradiation was performed.

3.2.4 Amplification of DNA-plasmid

The bacteria contains RNAseH1 plasmid (Plasmid #65784) which purchased in an agar stab were cultured on an ampicillin contains agar. Three individual bacteria colonies were selected and inoculated for isolating the plasmids by miniprep kits. Next, using BamH1 restriction enzyme the plasmid size was measures based on restriction map. Finally, using peqGold xchange plasmid Maxi-EF kit and following the manufacturer's instructions, the isolated plasmids were purified for transfection.

3.2.5 Protein analysis

To check the protein depletion efficiencies after siRNA transfection, a western blot approach was used.

3.2.5.1 Sample preparation

Cells were seeded in 6 well plate (section 3.2.1.3) and transfected with siRNA (Table 3.2). 48 h after transfection, cells were washed with PBS and treated with 120 μl lysis buffer (RIPA buffer + protease inhibitor and phospho stop) and incubated for 5 min at 4°C. Then, the supernatant was transfered to a new micro tube and stored at -20°C.

3.2.5.2 Bradford assay

Using Bradford assay, the protein concentration in each sample was determined. To this end, Bradford reagent was diluted 1:5 into MilliQ water. For each sample, 1 μl of extract was mixed with 1 ml

diluted Bradford reagent, vortexed briefly and incubated 5 min at RT. Then the light absorption was measured at 590 nm by Nanophotometer.

3.2.5.3 SDS-Polyacrylamid-Gel Electrophorese (SDS-PAGE)

Samples with protein concentrations 20-50 $\mu g/\mu l$ were mixed with MilliQ water and loading buffer. After boiling for 10 min at 95°C, samples were loaded in a 10 % gel (Table 3.7). The gel was first run for 10 min at 90 V until the proteins entered the resolving gel, then the voltage was increased to 130 V. The total running time was varied between 1 to 2.5 h depending on the protein size.

Table 3. 7. Stacking and Resolving gel preparation.

	Stacking gel (5 % Acrylamid)	**Resolving gel (10 % Acrylamid)**
Stacking gel buffer	0.95 ml	
Resolving gel buffer		2.25 ml
Rotiphorese®Gel 30	550 μl	3 ml
H_2O	2.25 ml	3.5 ml
APS	25 μl	50 μl
TEMED	7 μl	5 μl

3.2.5.4 Western blot

After SDS-PAGE, the proteins were transferred from the resolving gel to a PVDF membrane. The PVDF membrane was activated by incubation in methanol for at least 1 min at RT. Then the membrane was washed briefly in the running buffer. The resolving gel was covered by membrane between multiple layers of Whatmann filter paper and a layer of sponge at each side. The air bubbles between gel and membrane were removed and the sandwich was placed inside the transfer chamber containing transfer buffer. To obtain better blotting, the transfer chamber was placed inside an ice bucket and a current of 300 mA was applied for 3 h. After completion of blotting, the membrane was immediately blocked with 5 % non-fat milk in TBS-T for 1 h at RT. Then, the membrane was incubated with primary antibody (Table 3.3) overnight on the shaker at 4°C. The next day, the membrane was washed 3 times with TBS-T for 10 min and incubated with HRP-conjugated secondary antibody (Table 3.4) for 1 h at RT. The membrane was washed 3 times for 10 min in TBS-T and incubated with HRP substrate for 1-2 min at RT. The chemiluminescent signal (protein band) was detected using a Fusion FX image acquisition system.

3.2.6 Cell viability assay

To check the cell viability after exposure to X-rays irradiation, colony forming assay was performed. To this end, cells were seeded in a 10 cm petri dish (50 ESCs, 500 MEFs). The next day, cells were irradiated with different X-rays doses (0.5-5 Gy) and incubated at normal growing condition (section 3.2.1.2). The culture media was changed two times a week until the colonies formed and were visible by eye. After approximately 7 days for ESCs and 10-14 days for MEFs, cells were washed with PBS and incubated with ice cold fixing solution (Acetic acid and methanol with ratio 1:3) for 20 min at 4°C. Then, the fixing solution was removed and 0.1 % crystal violet was added to the cells and incubated for 5 min at RT. After removing the dye and washing the cells with tap water, colonies were counted for each condition.

3.2.7 Flow cytometry

Cell cycle progression and cell cycle checkpoint activation after irradiation were analyzed using flow cytometry. To label the cells in S phase during irradiation, cells were treated with 10 μM BrdU 30 min prior to irradiation. BrdU is a thymidine analogue, which can be incorporated into the newly synthesized DNA of replicating cells during S phase. After irradiation and repair incubation, cells were trypsinized and washed in PBS. Then cells were centrifuged for 3 min at 200 g and resuspended in 2 ml ice cold ethanol (dropwise under permanent vortexing) and incubated at least 30 min at -20°C. Next, the ethanol was removed by centrifugation and cells were resuspended in 1 ml 2 M HCL/PBS and incubated for 2 min at RT. Cells were centrifuged, resuspended in 500 μl 0.1 M Sodium-Tetraborat (pH 8.5) and incubated for 2 min at RT. To detect the incorporated BrdU, cells were washed with 1 ml 1 % FCS/PBS and resuspended in 30 μl FITC-conjugated BrdU antibody, transferred to a flow cytometry tube and incubated for 30 min at RT. Finally, cells were resuspended in 500 μl PI solution (10 μg/ml propidium iodide, 0.5 mg/ml RNaseA/PBS) and measured by flow cytometry after 30 min.

3.2.8 Mycoplasma test

In order to test the mycoplasma contamination in our cell system, all cell lines were regularly tested using a PCR based technique. Since an anti-mycoplasma reagent was always used in our stem cell cultures, our cell system was mycoplasma negative. To test the cells, the manufacture's protocol was followed (Figure 3.4).

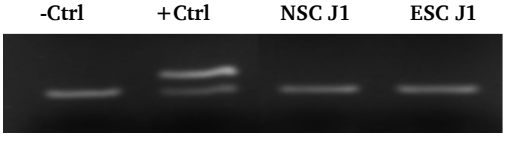

Figure 3.4. Mycoplasma test using PRC-based technique. 100 µl medium from cell culture flask was collected and analyzed for Mycoplasma contamination.

4 Results

4.1 Characterization of the cell system

4.1.1 Generation of NSC J1 from ESC J1

To better understand the mechanism of DSB repair in different stages of cell differentiation, which was one of the aims of this project, ESC J1 were differentiated to NSC J1. These ESC-derived NSCs have been identified using different stem cell markers.

Nestin, a well-known specific marker of NSCs (Lendahl, et al., 1990), showed a strong signal in newly derived NSCs (Figure 4.1). In contrast, the ESC specific marker Oct-4 (Pesce, et al., 2001) was not expressed in NSCs anymore. Sox-2, a marker for proliferative and undifferentiated cells (Fong, et al., 2008), was strongly expressed by ESCs, whereas in NSCs, the signal was weak (Figure 4.1). Furthermore, the lack of ß-III-Tubulin and GFAP signals indicated that the ESC-derived NSCs did not initiate neuron and glia differentiation (Data not shown).

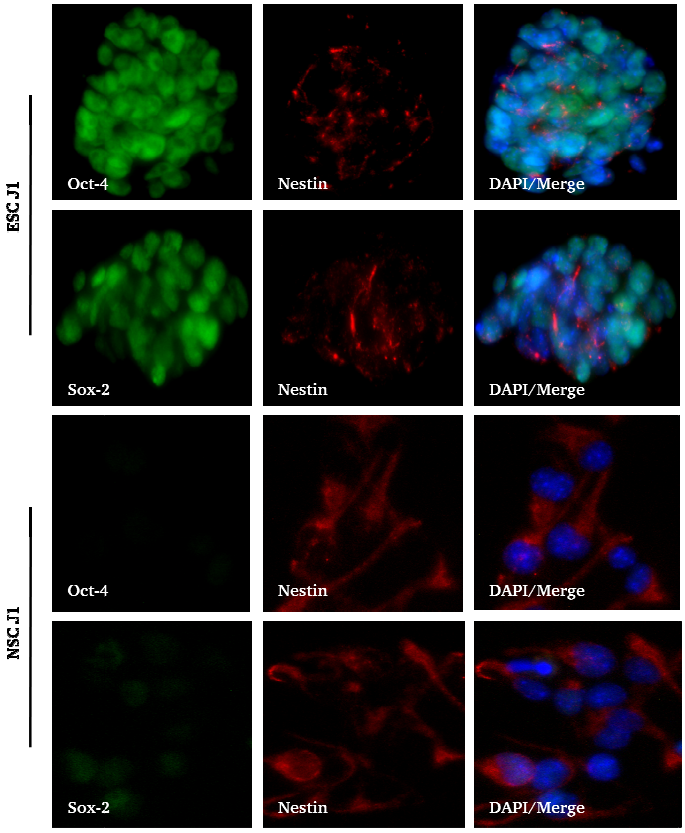

Figure 4.1. Characterization of ESC J1 and NSC J1. Immunofluorescence staining of stem cell markers in ECSs and ESC-derived NSCs. Cells were fixed and stained for ESC specific markers Oct-4 and Sox-2 as well as NSC specific marker, Nestin. ESCs showed a strong expression of Oct-4 and Sox-2 but only weak expression of Nestin. In contrast, NSCs were Oct-4 negative, expressed Sox2 weakly and displayed a strong expression of Nestin.

4.1.2 Cell viability

The colony forming assay is one the basic techniques in radiation biology to determine cell death after exposure to ionizing radiation or treatment with cytotoxic agents. This technique evaluates the ability of a single cell to proliferate into a large colony (50 cells or more) that can be identified with the naked eye. The number of the colonies formed in 1-2 week (s) post IR with the insult-producing agents are plotted, resulting in a cell survival curve. This describes a relationship between the proportion of the cells survived and the toxic agent.

To inspect the sensitivity of stem cells to irradiation in comparison with differentiated cells, ESCs and MEFs were exposed to X-rays in a dose variation from 0.5 to 5 Gy (section 3.2.6). As seen in Figure 4.2, both cell lines formed colonies after exposure to irradiation (Figure 4.2). However, the size of the colonies was bigger in ESCs compare to MEFs. Furthermore, the survival curve showed that the surviving rate of ESCs was higher than MEFs.

a. b.

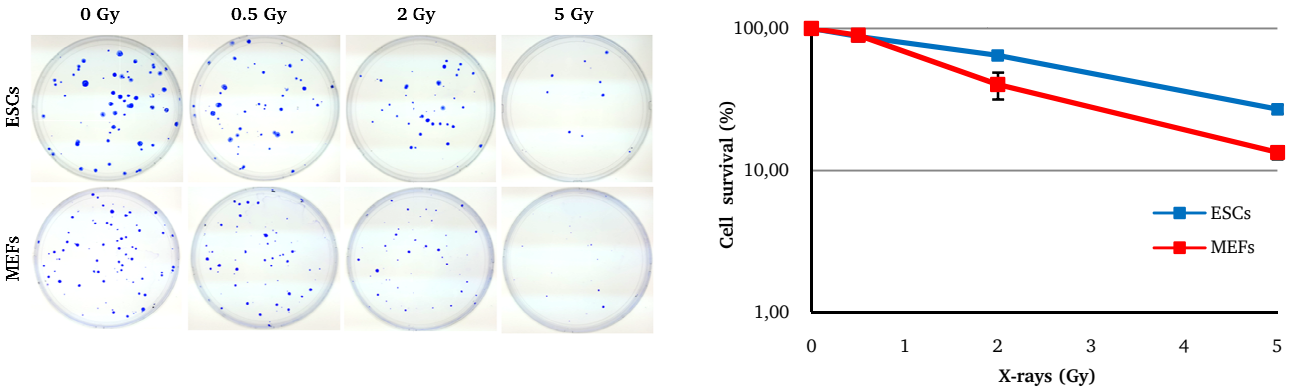

Figure 4.2. Colony forming assay after irradiation in ESCs and MEFs. Cells were seeded and incubated under normal cell culture conditions. After irradiation with variable doses of X-rays, cells were incubated for 1-2 weeks to form colonies. Then, the number of colonies was quantified to obtain a survival curve for each cell type. a. Digital image showing colony formation in ESCs and MEFs after IR. Since ESCs naturally grow in a colony form, colony formation is a fast process in this cell line. Furthermore, the size of the ESCs colonies was bigger than the colonies formed by MEFs. b. Survival curves of ESCs and MEFs plated one day prior to irradiation. Both cell types displayed similar survival rate after 0.5 Gy X-rays. However, ESCs are more radio-resistant than MEFs after exposure to 2 and 5 Gy.

4.1.3 Cell cycle checkpoints

Previously, it was shown that DNA damage induces cell cycle checkpoint activation which monitors the structural integrity of chromosomes before progression into the next cell cycle phase (Zhou, et al., 2000). The checkpoint arrest may occur at G1/S, intra-S and G2/M phases of the cell cycle (Lukas, et al., 2004; Terzoudi, et al., 2005). This mechanism enhances the opportunity to repair the damaged DNA before affecting the important events, like replication and mitosis (Terzoudi, et al., 2005).

G1/S checkpoint

It is known that ESCs lack the G1/S checkpoint (Hong, et al., 2004; Fluckiger, et al., 2006), whereas in NSCs, controversial data from *in vitro* and *in vivo* studies make the existence of G1/S checkpoint unclear (Roque, et al., 2012). To assess whether G1/S checkpoint becomes active after irradiation in ESCs and NSCs, a flow cytometry-based BrdU pulse labelling method was adjusted to the stem cell system. For this purpose, cells were pulse labeled with BrdU (section 3.2.7) and irradiated with 2 Gy X-rays. Following irradiation, the S-phase entry of G1-phase irradiated cells was monitored in BrdU-negative cells. Since BrdU-positive cells were in S phase during irradiation, they were excluded from the measurement. Flow cytometry analysis demonstrated that, neither in ESCs nor in NSCs, cell cycle progression was arrested by G1/S checkpoint immediately after irradiation and cells were able to enter into S phase. However, the S-phase entry at times >4 h post IR was slower in NSCs than in ESCs (Figure 4.3).

a. b.

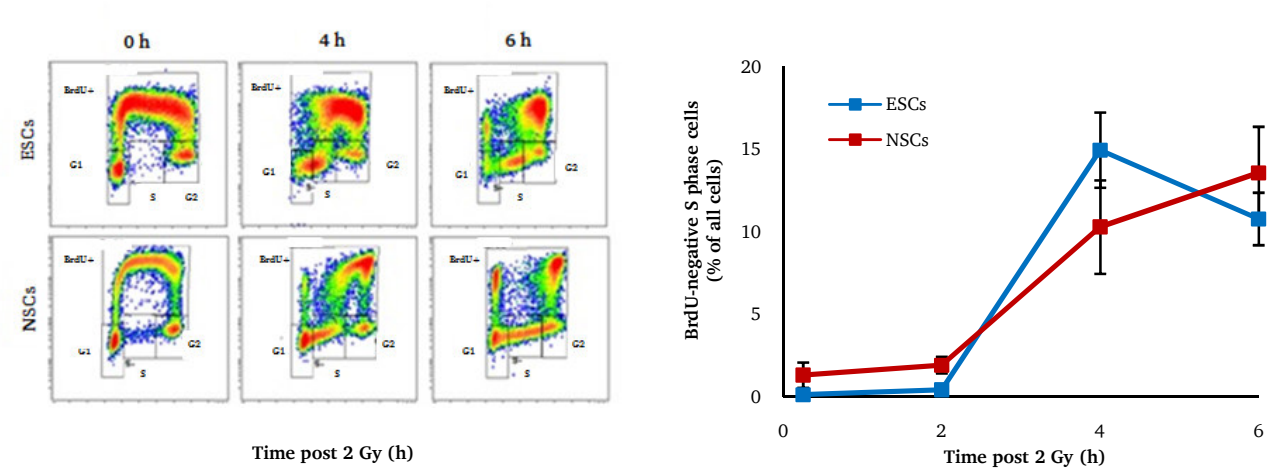

Figure 4.3. G1/S checkpoint in ESCs and NSCs using flow cytometry. Cells were pulse labeled with BrdU for 30 min prior to 2 Gy X-rays irradiation. At indicated time points, cells were fixed and stained for BrdU and PI. Since BrdU-labled cells were in S phase during irradiation, they were excluded from the evaluation and only BrdU-negative cells were quantified. a. Represent plot of flow cytometry analysis. The cell populations labeled with G1, S and G2 are BrdU-negative cells. b. Quantification of BrdU-negative S-phase cells. Error bars represent the SEM of three independent experiments**.**

G2/M checkpoint

The lack of G1/S checkpoint in ESCs and ineffectiveness G1/S checkpoint arrest in NSCs, enhances the importance of G2/M checkpoint for maintaining genomic integrity in these cells, particularly in ESCs. To investigate the efficiency of G2/M checkpoint activation after irradiation in ESCs and NSCs, BrdU pulse labeling was conducted to distinguish the S- and G2-phase cells. After exposure of the cells to 2 Gy X-rays, the cell cycle progression of BrdU-positive S-phase cells was monitored using flow cytometry. The results revealed a complete cell cycle arrest in both cell types (Figure 4.4). However,

between 4-6 h post IR, NSCs started to leave the G2/M checkpoint, whereas, ESCs were still stuck in the checkpoint (Figure 4.4).

a. b.

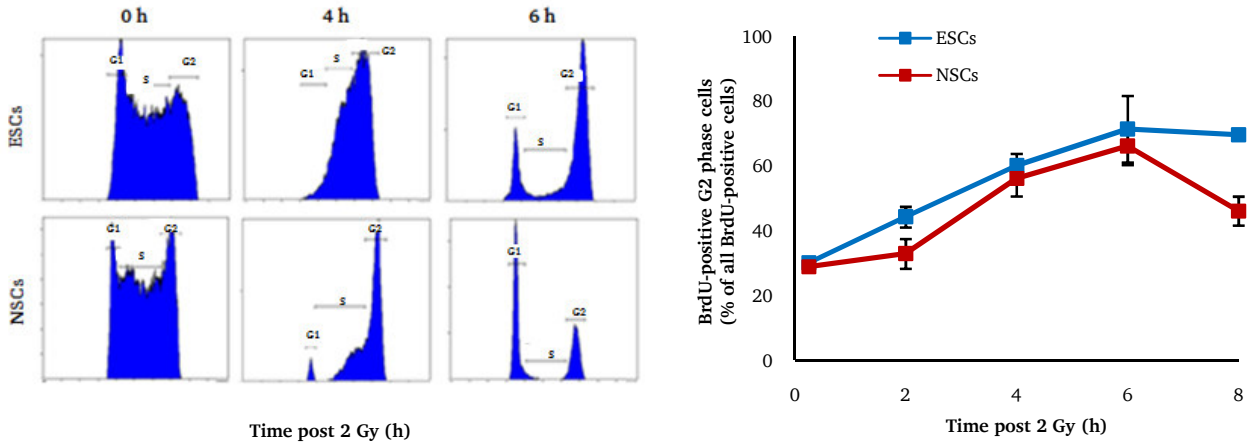

Figure 4.4. G2/M checkpoint in ESCs and NSCs using flow cytometry. Cells were pulse labeled with BrdU for 30 min prior to 2 Gy X-rays irradiation. Then, cells were fixed and stained for BrdU and PI at the indicated time points. The BrdU-negative cells were excluded from the evaluation, as they were in G1 and G2 phases during irradiation. The BrdU-positive cells represent the fraction of cells entered in G2 phase after irradiation. a. Representative plot of BrdU-positive flow cytometry. b. Quantification of BrdU-positive G2 phase cells. Error bars represent the SEM of three independent experiments.

4.2 DNA repair in G1 and G2 phase

As previously mentioned, the main objective of this project was to investigate the DSB repair mechanisms in a cell cycle specific manner in ESCs and NSCs. To this end, DSB and cell cycle specific markers were combined (section 3.2.2.1) and DSB repair was analyzed in G1 and G2 phase cells using Metafer software (Figure 3.6).

4.2.1 DSB repair after low X-rays doses

4.2.1.1 DSB repair capacity

It has been reported that, in human fibroblasts, an efficient DSB repair becomes active only after irradiation with doses above 20 mGy (Rothkamm, et al., 2003; Grudzenski, et al., 2010). Thus, to investigate whether this is also the case in stem cells, ESCs and NSCs were irradiated with 10 mGy, 100 mGy and 1 Gy X-rays (section 3.2.1.7), and the repair capacity was assessed in G1- and G2- phase cells using 53BP1 as a DSB marker.

A preliminary analysis of DSB repair in ESCs after 100 mGy revealed an efficient repair with 35-45 % reduction in DSB level within 4 h post IR (Figure 4.5). In ESCs, since the G2/M checkpoint cannot be induced by low doses of IR and also the lack of G1 checkpoint (Figure 4.3), the majority of the cells are in S phase. The small population of the cells in G1- and G2-phase was a big limitation to study DSB

repair after low doses of IR in ESCs. Thus, ESCs were excluded for further study of DSB repair capacity after IR with doses <100 mGy.

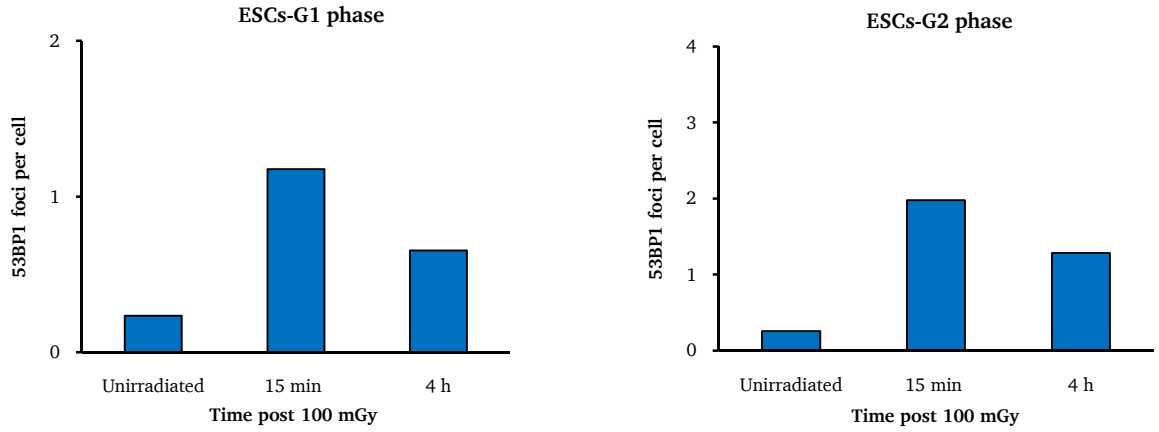

Figure 4.5. DSB repair after low dose irradiation in G1- and G2-phase ESCs. Cells were plated and incubated for one day under normal cell culture condition. Then, cells were irradiated with 100 mGy X-rays. At the indicated time points, cells were spun down on glass slide, fixed and stained with 53BP1 and CyclinB1 antibodies. Repair incubation took place in the presence of EdU and Nocodazole. 53BP1 foci were quantified in G1- (EdU-negative, CyclinB1-negative) and G2- (EdU-negative, CyclinB1-positive) phase cells. This experiment was only performed once.

In NSCs, a similar efficiency of DSB repair with respect to ESCs has been observed in both G1 and G2 phase after 100 mGy X-rays (Figure 4.6). In contrast, a massive impairment in DSB repair was observed in G1-phase NSCs after 10 mGy. While in G2 phase almost 50 % of DSBs were repaired, in G1 phase nearly no repair could be detected (Figure 4.6).

a.

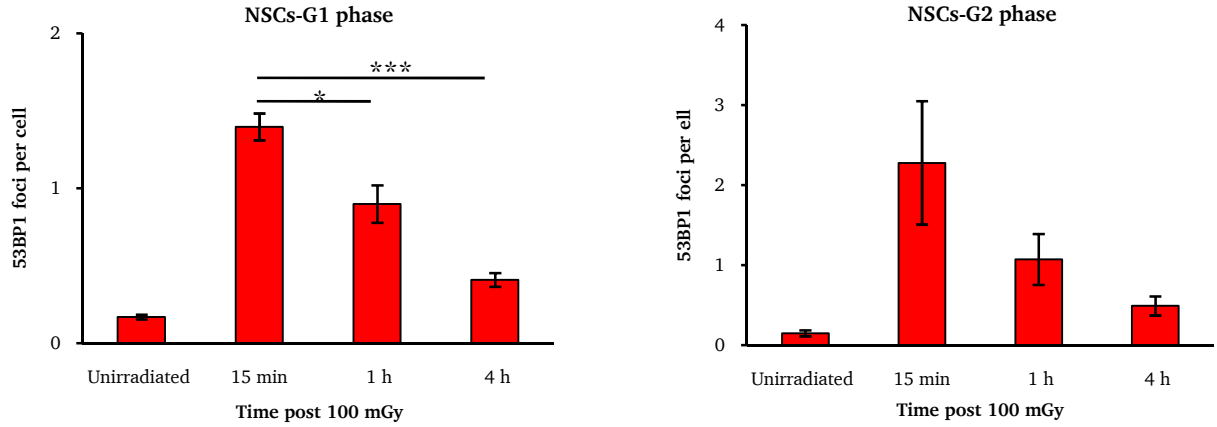

b.

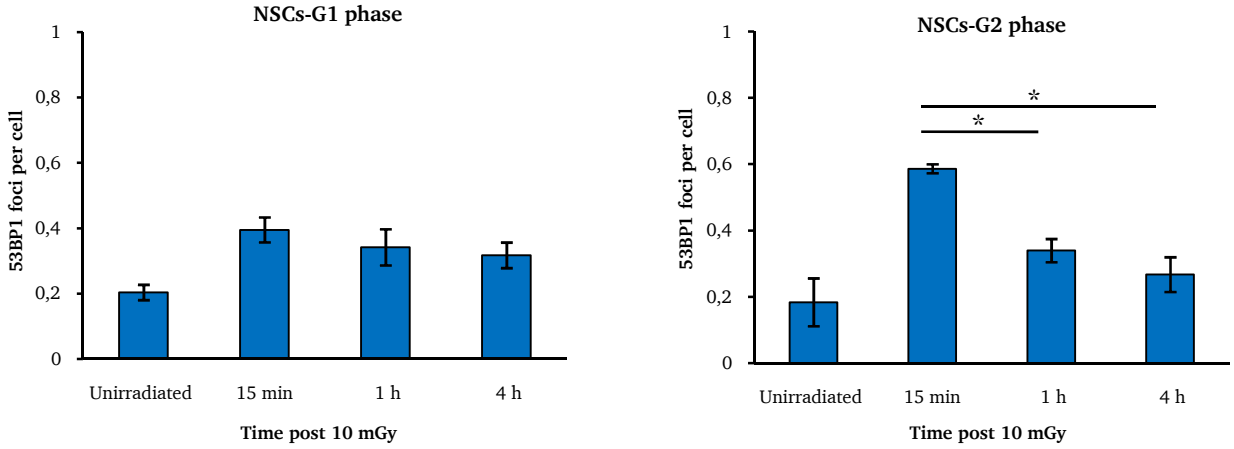

Figure 4.6. DSB repair after low dose irradiation in G1- and G2-phase NSCs. Cells were seeded on coverslips and incubated for one day under normal cell culture conditions. Then, cells were irradiated with 10 or 100 mGy X-rays and 53BP1 foci were quantified at the indicated time points. Repair incubation times took place in the presence of EdU and Nocodazole. G1- and G2-phase cells were identified by negative EdU staining and a negative or positive CyclinB1 staining, respectively. Error bars in G1 phase represent the SEM of three independent experiments and in G2 phase two independent experiments. P-value: *≤ 0.05, ***≤ 0.001 (using student t-test). a. Quantification of 53BP1 foci in G1- (left panel) and G2- (right panel) phase cells after 100 mGy. b. Quantification of 53BP1 foci in G1- (left panel) and G2- (right panel) phase cells after 10 mGy. Error bars in G1 phase represent the SEM of five independent experiments.

4.2.1.2 ATM and DNA-PKcs kinase activities

It has been shown that ATM and DNA-PKcs signalling are essential for DSB repair (Shrivastav, et al., 2009; Jiang, et al., 2015). Furthermore their kinase activities are required for the phosphorylation of H2AX and subsequent 53BP1 foci formation (Burma, et al., 2001; Stiff, et al., 2004). The lack of DSB repair in G1-phase NSCs after 10 mGy X-rays irradiation (Figure 4.6b) might be caused by an insufficient kinase activity of ATM and DNA-PKcs. To inspect the kinase activity of ATM and DNA-PKcs after irradiation in NSCs, ATM and DNA-PKcs were inactivated using small molecule inhibitors (see Table 3.1). At 1 h after irradiation with high (1 Gy) and low (10 mGy) doses of X-rays, the formation of 53BP1 foci was assessed as a readout for ATM and DNA-PKcs kinase activities in G1-phase cells.

After 1 Gy, the size of 53BP1 foci formed in ATM-inhibited cells was smaller than in wild type cells (Figure 4.7a). However, neither ATM nor DNA-PKcs inhibition significantly reduced 53BP1 foci level. Reduction in foci formation was observed only after combining both inhibitors (Figure 4.7b). In contrast, after 10 mGy, the formation of 53BP1 foci was dramatically reduced by ATM inhibition, whereas DNA-PKcs inhibition had no impact on the foci level. Combination of both inhibitors dropped the 53BP1 foci level to the ATM inhibition alone (Figure 4.7b).

a.

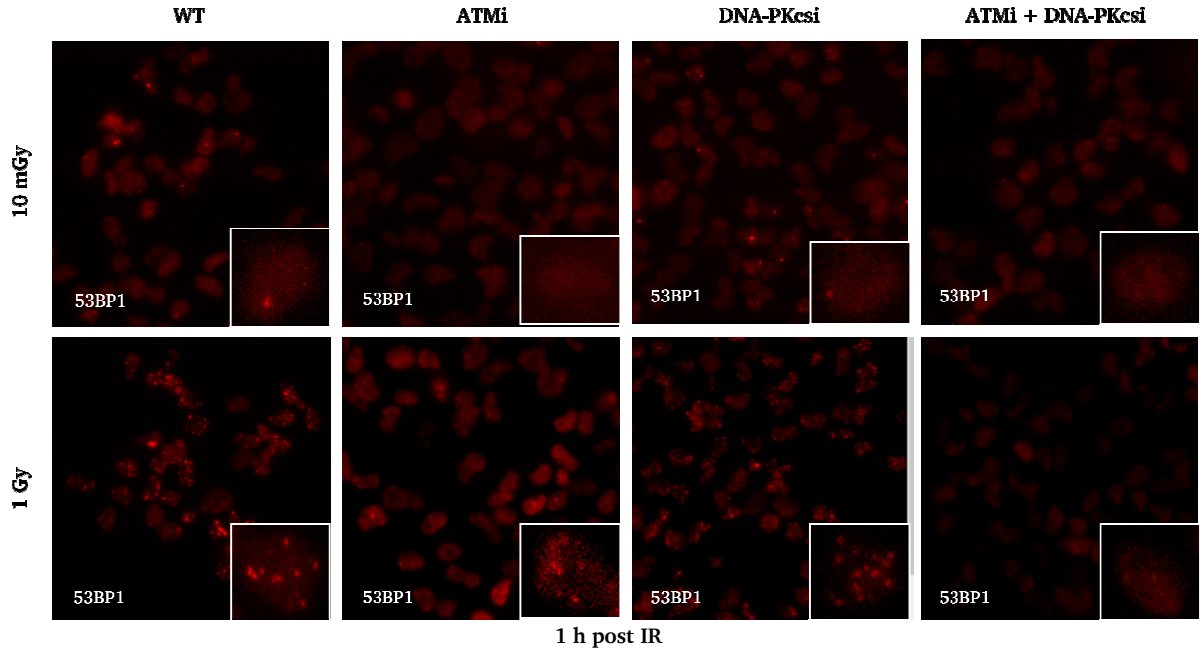

b.

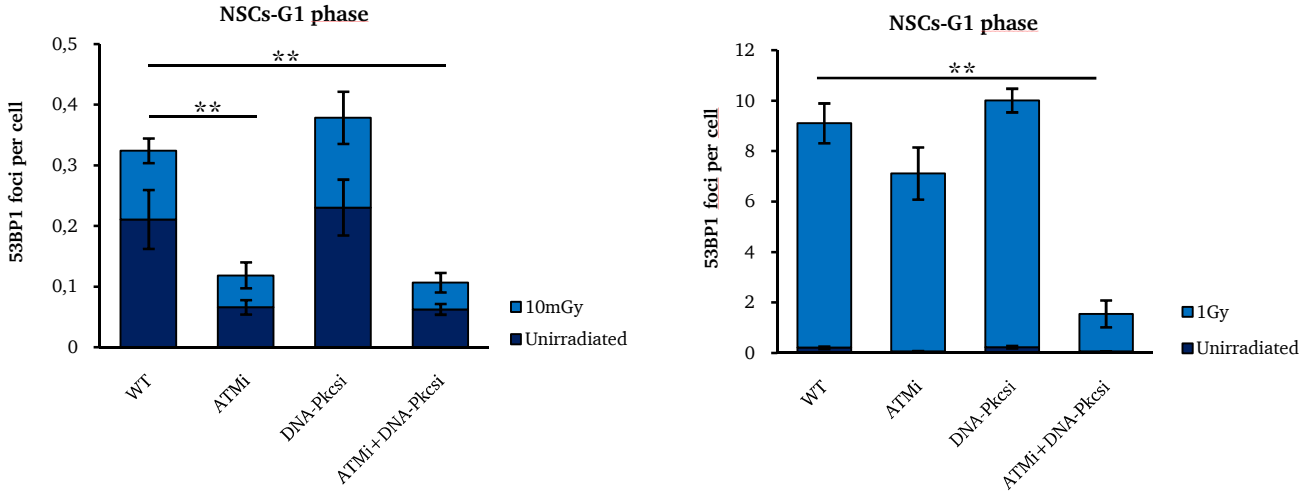

Figure 4.7. Role of ATM and DNA-PKcs in 53BP1 foci formation in G1-phase NSCs. Cells were treated with ATM (ATMi) and DNA-PKcs (DNA-PKcsi) inhibitors 30 min before irradiation. At 1 h after irradiation with 10 mGy or 1 Gy X-rays, cells were fixed and stained for 53BP1 and CyclinB1. Repair incubation took place in the presence of EdU and Nocodazole. 53BP1 foci level was evaluated in G1 phase cells (EdU-, CyclinB1-negative). a. Representative microscopy images of irradiated NSCs treated with ATM and DNA-PKcs inhibitors. b. Quantification of 53BP1 foci formation at 1 h post irradiation with 1 Gy (right panel) or 10 mGy (left panel). Error bars represent the SEM of three independent experiments. P-value: **≤ 0.01 (using student t-test).

4.2.1.3 Impact of H_2O_2 on DSB repair

It was shown that artificially induced oxidative stress by H_2O_2 treatment enhances DSB repair capacity after low dose irradiation in human fibroblasts (Grudzenski, et al., 2010). This indicated that the oxidative stress level after exposure to the low doses of IR is not sufficient to activate kinase signalling. To assess whether oxidative stress influences kinase activities and enhances DSB repair capacity in stem cells, NSCs were treated with H_2O_2 before irradiation (section 3.2.3). To determine an optimal level of oxidative stress, in a preliminary experiment, NSCs were treated with different concentrations of H_2O_2. Quantification of 53BP1 foci in G1-phase cells at 15 min after H_2O_2 treatment revealed that 10 μM H_2O_2 did not induce additional foci (Figure 4.8). Thus, the 10 μM H_2O_2 was used as an optimal concentration to induce oxidative stress in the following experiments.

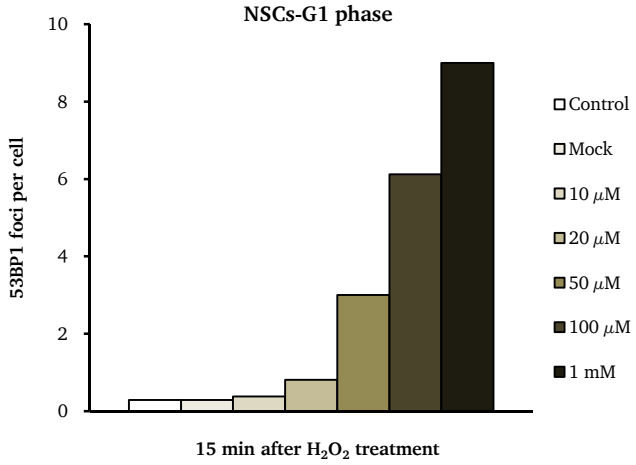

Figure 4.8. DSB induction by H_2O_2 treatment in G1-phase NSCs. Cells were treated with H_2O_2 for 30 min at 4°C. Mock was treated with PBS. 53BP1 foci were quantified after replacing the H_2O_2 with normal media contained EdU and Nocodazole. G1 phase were identified by negative EdU and CyclineB1 staining. The experiment performed only one time.

To investigate the impact of H_2O_2 on DSB repair, NSCs were pre-treated with 10 μM H_2O_2 and irradiated with 10 mGy. Scoring 53BP1 foci in G1-phase cells, demonstrated nearly similar foci level in control (H_2O_2 untreated) and H_2O_2 treated cells at 1 h post IR (Figure 4.9). Interestingly, our results showed that only cells pre-treated with H_2O_2 were able to significantly repair the IR-induced DSBs to the background level within 4 h post 10 mGy (Figure 4.9).

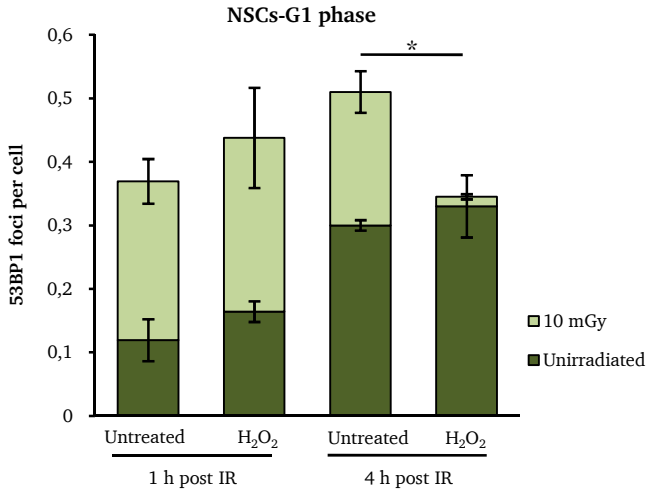

Figure 4.9. DSB repair in G1-phase NSCs after H_2O_2 treatment. 3 h prior to 10 mGy X-rays irradiation, cells were treated with 10 µM H_2O_2 for 30 min at 4°C. 53BP1 foci were quantified at 1 and 4 h after IR in G1-phase cells. Repair incubation took place in the presence of EdU and Nocodazole. G1-phase cells were identified by negative EdU and CyclinB1 staining. Error bars represent the SEM of three and two independent experiments for 1 and 4 h time points, respectively. P-value: *≤ 0.05 (using student t-test).

Since oxidative stress enhances the repair capacity after low dose of irradiation (Grudzenski, et al., 2010) (Figure 4.9), we hypothesized that the triggered DSB repair after oxidative stress might be facilitated by enhancement of ATM and DNA-PKcs kinase activities. Thus, to evaluate this hypothesis, the activity of ATM and DNA-PKcs was inhibited and the ability NSCs to form 53BP1 foci after H_2O_2 treatment was assessed. To this end, NSCs were treated with H_2O_2 as well as ATM and DNA-PKcs inhibitors. At 1 h post 10 mGy X-rays irradiation, cells were fixed and analyzed for 53BP1 foci. Oxidative stress had no impact on ATM and DNA-PKcs activities and H_2O_2 treated cells demonstrated similar level of 53BP1 foci as in untreated cell (Figure 4.10).

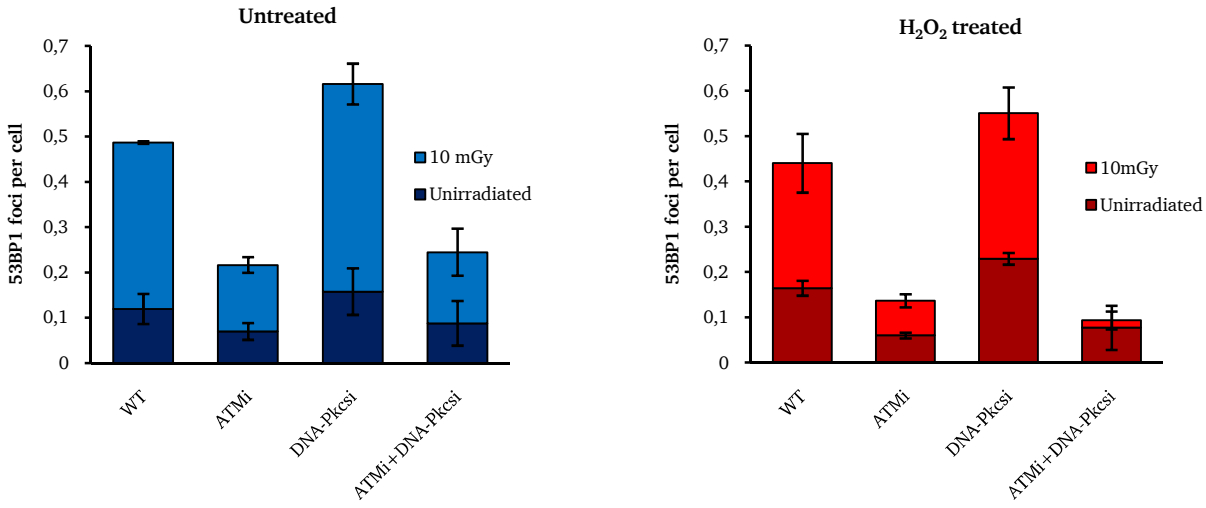

Figure 4.10. Impact of oxidative stress on ATM and DNA-PKcs kinase activities in G1-phase NSCs. 3 h before 10 mGy irradiation, cells were treated with 10 µM H_2O_2 for 30 min at 4°C. ATM and DNA-PKcs inhibitors (ATMi and DNA-PKcsi) were added 30 min prior to irradiation. 53BP1 foci were quantified at 1 h post IR in G1-phase cells (EdU-negative, CyclinB1-negative). Repair incubation took place in the presence of EdU and Nocodazole. Error bars represent the SEM of three independent experiments.

4.2.2 DSB repair after high X-rays doses

Using 2 Gy X-rays (as high dose of IR), the DSB repair mechanisms in a cell cycle-specific manner were investigated in ESCs and NSCs. To analyze DSB repair in G1 and G2 phase, cell cycle discrimination was conducted in a semi-automated way using Metafer software (section 3.2.2.3). G1-phase cells were identified by negative EdU and CyclinB1 staining, while G2-phase cells were EdU- negative and CyclinB1-positive (Figure 3.3).

4.2.2.1 DSB repair capacity

It has been shown that DSBs repair in somatic cells is a biphasic process involving a fast and a slow repair component (Dianov, et al., 2007; Riballo, et al., 2004). To test whether the same phenomenon could be observed in stem cells, wild type (WT) ESCs and NSCs were exposed to 2 Gy X-rays. Quantification of 53BP1 foci after IR demonstrated nearly similar repair capacity in both cell types in G1 and G2 phase (Figure 4.11). Furthermore, similar to somatic cells, a biphasic DSB repair has been observed in ESCs and NSCs. As seen in Figure 4.11, at induction time point (15 min after IR), both cell types displayed ~20 DSBs in G1 phase and ~40 DSBs in G2 phase. Almost 50 % of IR-induced DSBs were quickly repaired within 2 h post IR and the residual foci were slowly repaired nearly to the background level within 6 h after 2 Gy X-rays (Figure 4.11).

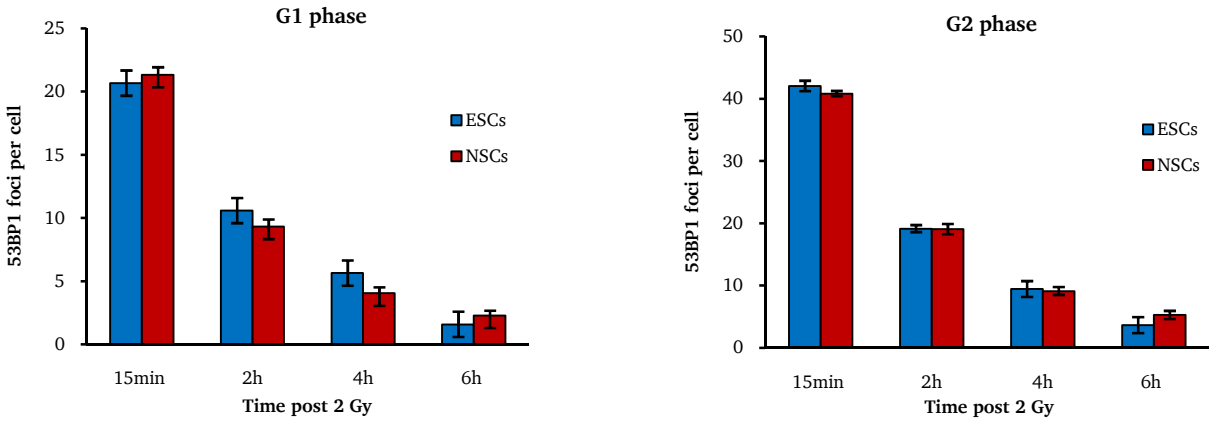

Figure 4.11. DSB repair capacity in WT ESCs and NSCs. Cells were treated with EdU and Nocodazole 30 min before 2 Gy irradiation and incubated for repair. At the indicated time points cells were fixed and 53BP1 foci were quantified in G1- and G2-phase cells. G1- and G2-phase cells were identified by negative EdU staining and negative or positive CyclinB1 staining, respectively. Foci numbers of unirradiated cells were subtracted. Error bars represent the SEM of three independent experiments.

4.2.2.2 Contribution of fast and slow component of DSB repair

It has been reported that in differentiated cells immediately after irradiation the majority of IR-induced DSBs are repaired via canonical-on-homologous end-joining (c-NHEJ) with DNA-PKcs being one of the core enzymes. While, a sub-fraction of DSBs is repaired slowly via an ATM-dependent repair pathway,

which represents resection-dependent non-homologous end-joining pathway (Res.-dep.-NHEJ) in G1 and homologous recombination (HR) in G2 phase (Beucher, et al., 2009; Biehs, et al., 2017).

The role of ATM and DNA-PKcs in the DSB repair in G1- and G2-phase ECSs and NSCs were assessed using specific inhibitors (see Table 3.1). The results revealed that in both cell types, inhibition of ATM induced a significant repair defect, which became apparent from 2 h post IR and caused almost 40-50 % unrepaired breaks to persist until 6 h post IR (Figure 4.12). On the other hand, inhibition of DNA-PKcs illustrated a clear difference between the repair behaviour of ESCs and NSCs. In ESCs, DNA-PKcs inhibition impaired DSB repair within the first 2 h post IR followed by an efficient repair identical to wild type cells (WT). In contrast, similar to somatic cells (Biehs, et al., 2017), inhibition of DNA-PKcs induced a severe repair defect in NSCs (Figure 4.12).

a.

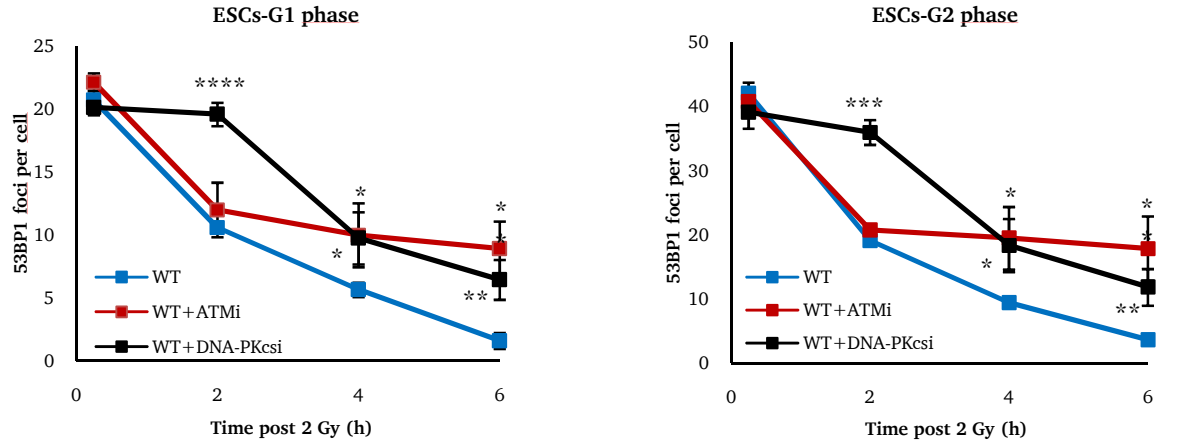

b.

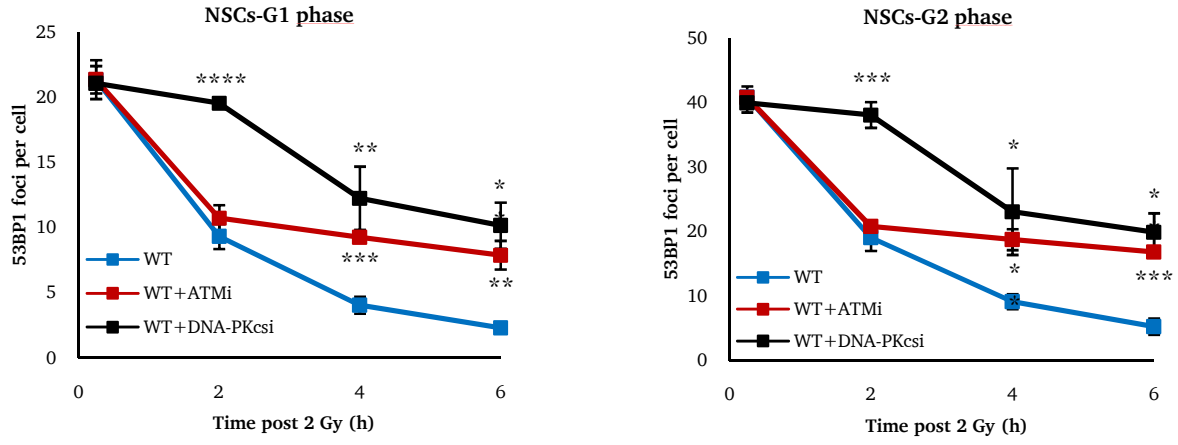

Figure 4.12. ATM- and DNA-PKcs-dependency of DSB repair in G1 and G2 phase. ESCs and NSCs were treated with ATM (ATMi) and DNA-PKcs (DNA-PKcsi) inhibitors 30 min before 2 Gy X-rays irradiation. 53BP1 foci were quantified at the indicated time points. Repair incubation took place in the presence of EdU and Nocodazole. G1- and G2-phase cells were identified by negative EdU staining and negative or positive CyclinB1 staining, respectively. Foci numbers of unirradiated cells were subtracted. Error bars represent the SEM of three independent experiments. P-value: *≤ 0.05, **≤ 0.01, ***≤ 0.001, ****≤ 0.0001 (using student t-test). a. Quantification of 53BP1 foci level after 2 Gy irradiation in G1- and G2-phase ESCs. b. Quantification of 53BP1 foci level after 2 Gy irradiation in G1- and G2-phase NSCs.

Next, the contribution of HR in G2-phase stem cells has been investigated. In somatic cells, it was previously shown that ATM-dependent repair pathway represents HR in G2 and a resection-dependent pathway in G1 phase (Beucher, et al., 2009; Biehs, et al., 2017). To verify whether the ATM-dependent repair pathway in G2-phase stem cells is the same pathway as in somatic cells, DSB repair was monitored after inhibition of Rad51 (a HR core protein) in ESCs and NSCs (Figure 4.13). Quantification of 53BP1 foci at 2 h post IR showed that the foci level in WT and Rad51-inhibited ESCs and NSCs was similar (Figure 4.13). Furthermore, since Rad51 is only involved in HR (Lambert, et al., 2000), inhibition of Rad51 did not show any significant impact on DSB repair in G1-phase cells, as expected (Figure 4.13). Interestingly, at 6 h post IR a significant repair defect became apparent in Rad51 inhibited-NSCs, whereas ESCs did not exhibit any repair defect (Figure 4.13).

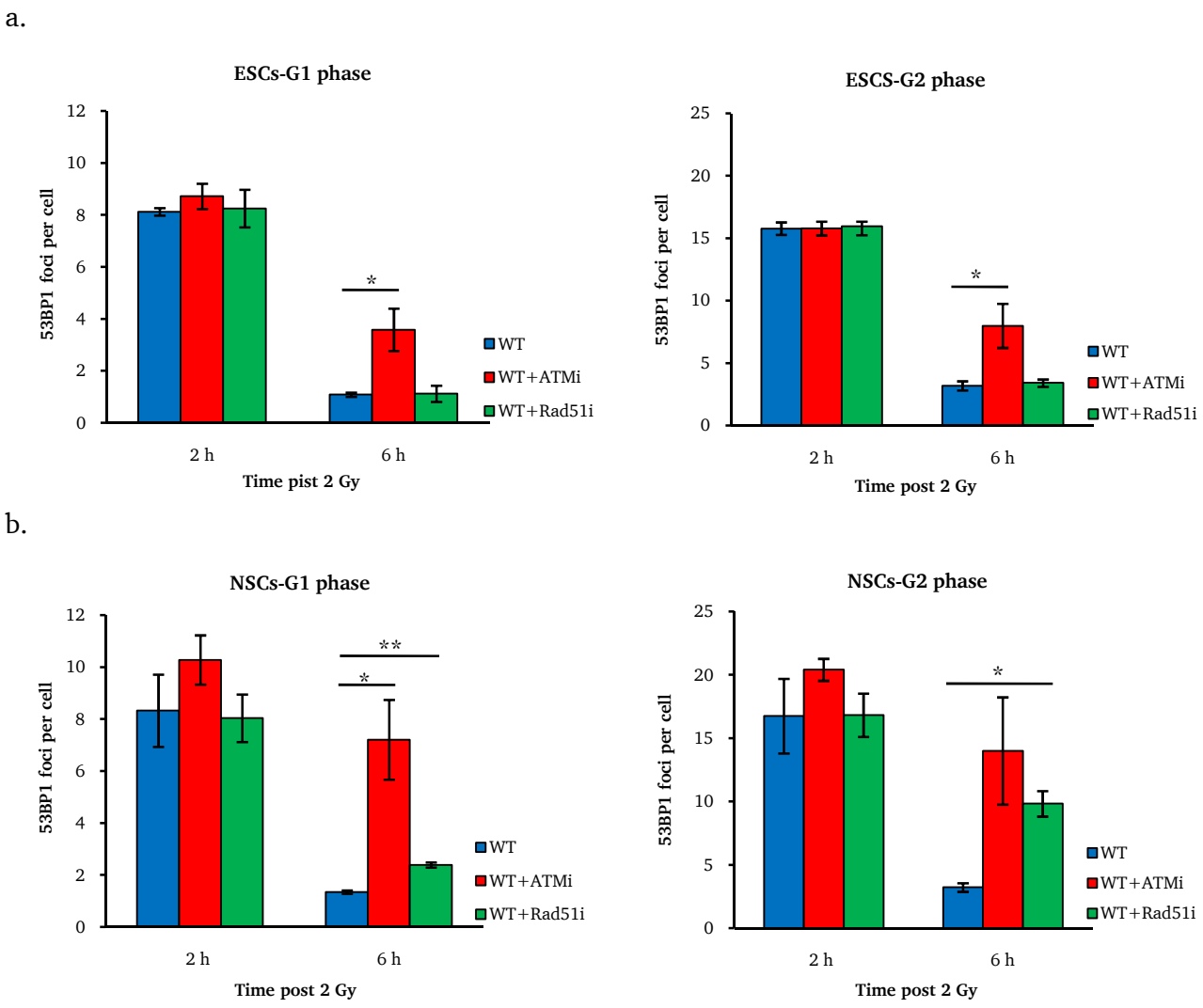

Figure 4.13. Rad51-dependency of DSB repair in G1- and G2- phase stem cells. ESCs and NSCs were treated with Rad51 inhibitor (Rad51i) 30 min before 2 Gy X-rays irradiation. At the indicated time points, cells were fixed and stained for 53BP1 and CyclinB1. The experiment was performed in the presence of EdU and Nocodazole. 53BP1 cells were quantified in G1- (EdU-negative, CyclinB1-negative) and G2- (EdU-negative, CyclinB1-positive) phase cells. The background foci level was subtracted. Error bars represent the SEM of three independent experiments for ESCs and two independent experiments for NSCs. P-value: *≤ 0.05, **≤ 0.01 (using student t-test). a. Quantification of 53BP1 foci level after 2 Gy X-rays in G1- and G2-phase ESCs. b. Quantification of 53BP1 foci level after 2 Gy X-rays in G1- and G2-phase NSCs.

In somatic cells, it was shown that Rad51 is involved in HR (Lambert, et al., 2000). To evaluate the implication of Rad51 in DSB repair in G2-phase stem cells, Rad51 foci level in ESCs and NSCs was assessed and compared to MEFs. The outcomes revealed that Rad51 foci were formed after 2 Gy X-rays in G2 phase ESCs and NSCs (Figure 4.14a). Since the formation of Rad51 foci is dependent on the slow process of resection (Bakr, et al., 2015), the generation of Rad51 foci was slowly enhanced after IR (Figure 4.14b). Interestingly, Rad51 foci formed faster and also in a higher level in ESCs than in NSCs and MEFs (Figure 4.14b). In ESCs, the level of Rad51 foci peaked at 1 h post IR, whereas in NSCs and MEFs the highest level of Rad51 foci formed at 2 h (Figure 4.14b). To verify the role of ATM in HR and consequently Rad51 foci formation, Rad51 foci number was analyzed after ATM inhibition in G2-phase ESCs, NSCs and MEFs. The results showed that the formation of Rad51 foci after ATM inhibition was completely abolished in all three cell types (Figure 4.14b).

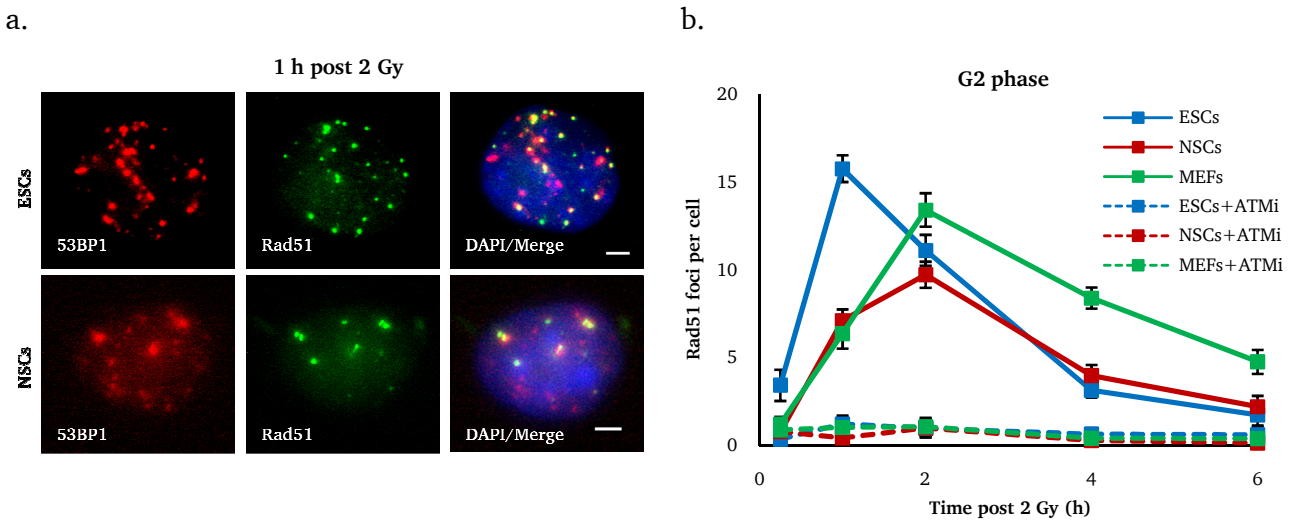

Figure 4.14. Formation of Rad51 foci in G2-phase cells. Cells were irradiated with 2 Gy and incubated under normal cell culture condition in presence of EdU and Nocodazole. Cells were fixed and stained at the indicated time points. Rad51 foci were quantified in EdU-negative and CyclinB1-positive cells. Foci numbers of unirradiated cells were subtracted. Error bars represent the SEM of three independent experiments. Scale bars represent 5 µm. a. Representative microscopy image of Rad51 foci in G2-phase ESCs and NSCs. b. Quantification of Rad51 foci in G2 phase ESCs, NSCs and MEFs.

4.2.2.3 PARP1-dependent alt-NHEJ

It has been shown that alt-NHEJ is a PARP1-dependent repair pathway (Iliakis, 2009). The role of alt-NHEJ pathway was investigated using PARP1-inhibitor in both ESCs and NSCs. Analyzing 53BP1 foci exhibited no impairment in DSB repair after PARP1-inhibition in WT or ATM-inhibited cells (Figure 4.15). In contrast, PARP1-inhibition influenced DSB repair in DNA-PKcs-inhibited cells (Figure 4.15). Interestingly, PARP1-inhibition induced a strong repair defect in DNA-PKcs-deficient ESCs (Figure 4.15). Whereas, inhibition of PARP1 had a moderate impact on NSCs DSB repair (Figure 4.15). A preliminary analysis of 53BP1 foci in MEFs revealed that the inhibition of PARP1 had no impact on DSB repair in these cells, even after DNA-PKcs inhibition (Figure 4.15).

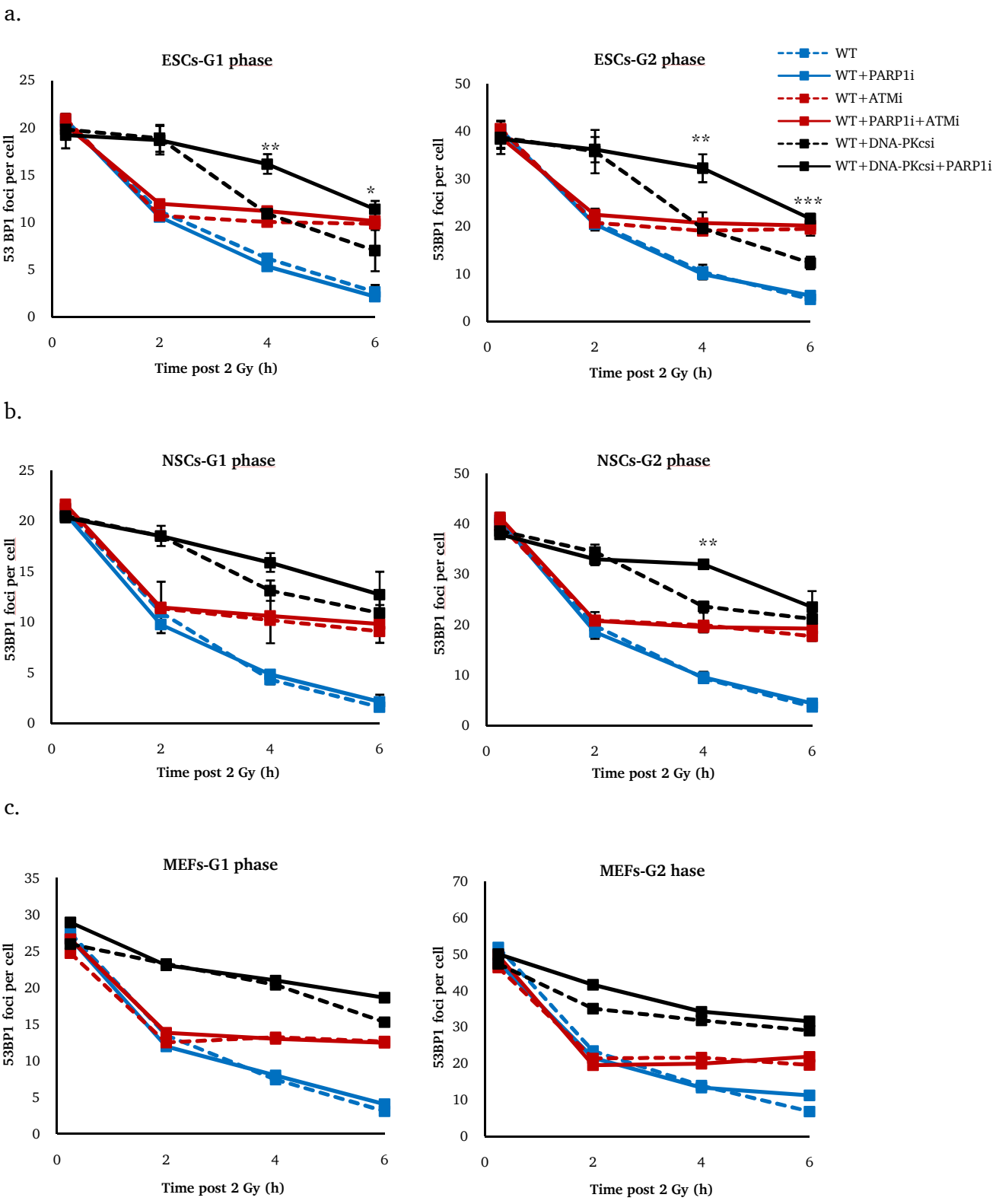

Figure 4.15. PARP1-dependent alt-NHEJ in G1 and G2 phase cells. Cells were treated with inhibitors (ATM-, DNA-PKcs- and PARP1-inhibitor) 30 min before irradiation. After 2 Gy X-rays, repair incubation took place in presence of EdU and Nocodazole. At the indicated time points, 53BP1 foci were quantified in G1 (EdU-negative, CyclinB1-negative) and G2 (EdU-negative, CyclinB1-positive) cells. Foci numbers of unirradiated cells were subtracted. Error bars represent the SEM of three and two independent experiments in ESCs and NSCs respectively. The experiment with MEFs was only performed once. P-value: *≤ 0.05, **≤ 0.01, ***≤ 0.001 (using student t-test). a. Quantification of 53BP1 foci level after 2 Gy X-rays in G1- and G2-phase ESCs. b. Quantification of 53BP1 foci level after 2 Gy X-rays in G1- and G2-phase NSCs. c. Quantification of 53BP1 foci level after 2 Gy X-rays in G1- and G2-phase MEFs.

Next, the PARP1-dependency of the observed efficient DSB repair in Rad51 inhibited G2 phase ESCs was inspected. The result revealed that PARP1 inhibition caused a significant repair defect in Rad51-inhibited ESCs. In contrast, NSCs did not exhibit an additional impairment in DSB repair after PARP1-inhibition (Figure 4.16).

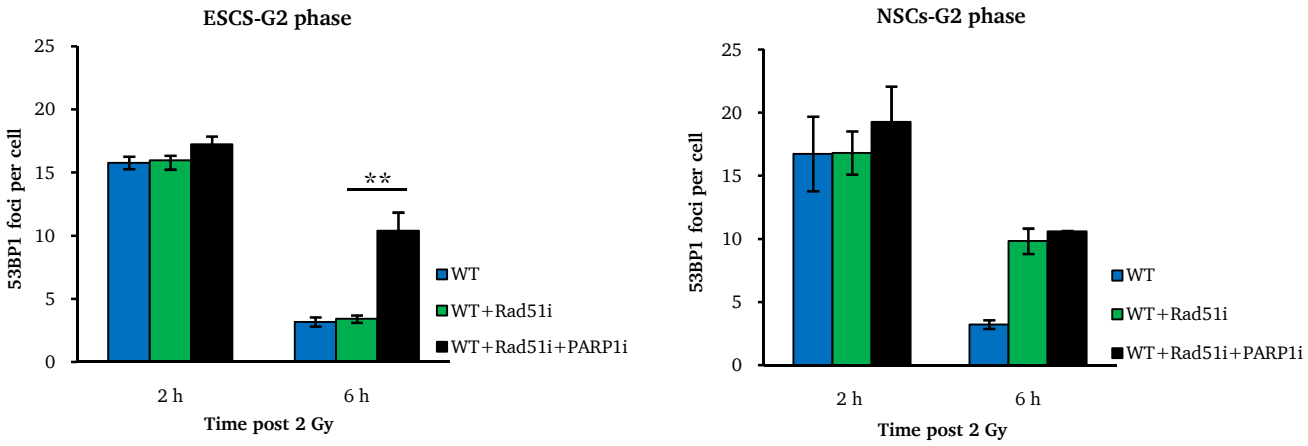

Figure 4.16. PARP1-dependent alt-NHEJ in G2 phase ESCs and NSCs. Inhibitors (Rad51- and PARP1-inhibitor) were added to the cells 30 min before IR. After irradiation with 2 Gy, 53BP1 foci were quantified at the indicated time points in EdU-negative and CyclinB1-positive cells. The WT and WT + Rad51i are the same values as in Figure 4.13. Foci numbers of unirradiated cells were subtracted. Error bars represent the SEM of three independent experiments for ESCs and two independent experiments for NSCs. P-value: **≤ 0.01 (using student t-test).

4.3 Slow component of DSB repair in G1-phase stem cells

Since the mechanism of the slow component of DSB repair in G1-phase stem cells was unclear, in the following experiments, the nature of the ATM-dependent repair pathway was investigated in G1-phase ESCs and NSCs.

4.3.1 Resection in G1 phase

It has been reported that resection is an essential process to repair complex DSBs (Niu, et al., 2009; Quennet, et al., 2010). The resection mediating proteins, like CtIP, regulate limited DNA-end resection in G1, S, and G2 phase (Niu, et al., 2009; Yajima, et al., 2013). Since resection in G1 phase is not extensive as it is in S or G2 phase, the formation of resection dependent foci, e.g. pRPA, could only be detected after induction of very complex DSBs which normally arise after heavy ions or alpha-particles irradiation (Averbeck, et al., 2014; Barton, et al., 2014). To consolidate these results, using laser micro-irradiation, the accumulation of pRPA foci at the DSB sites was observed in G1-phase HeLa cells (Figure 4.17). The pRPA laser track overlaid with γH2AX in irradiated cells, however, pRPA signal in G1 phase was weak, compared to G2 and S phase cells.

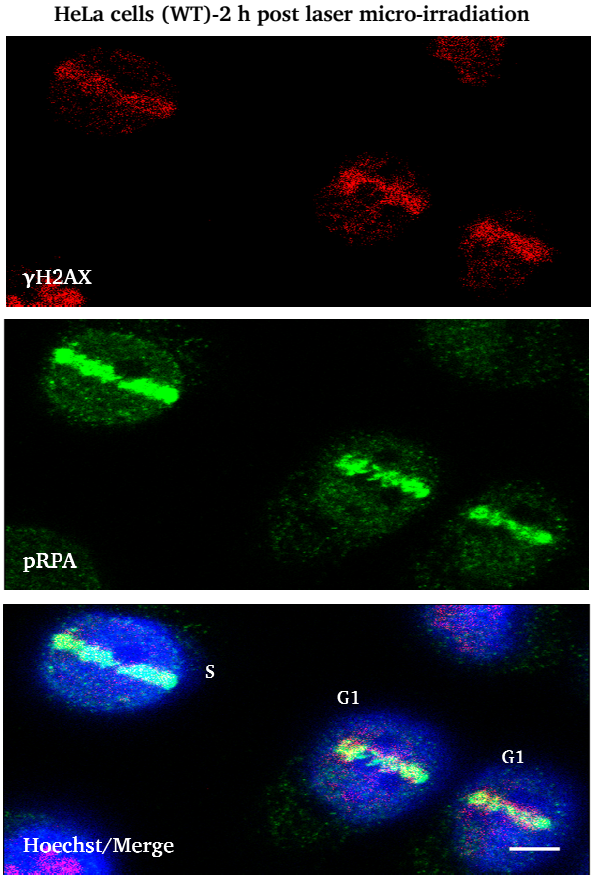

Figure 4.17. pRPA laser track formation in G1-phase HeLa cells. Cells were seeded in µ-Slide one day prior to irradiation and stained with Hoechst for 10 min immediately before irradiation. At 2 h post micro-irradiation, cells were fixed and stained with γH2AX and pRPA antibodies. Images were taken by confocal microscope. Scale bar represents 5 µm.

To investigate the role of resection in pRPA laser track formation in HeLa cells, particularly in G1 phase, resection was inactivated using CtIP siRNA. The formation of pRPA laser track was completely abolished in all cell cycle phases in CtIP-deficient cells (Figure 4.18). This indicates that the accumulation of pRPA foci at the break sites is a resection dependent process, even in G1 phase.

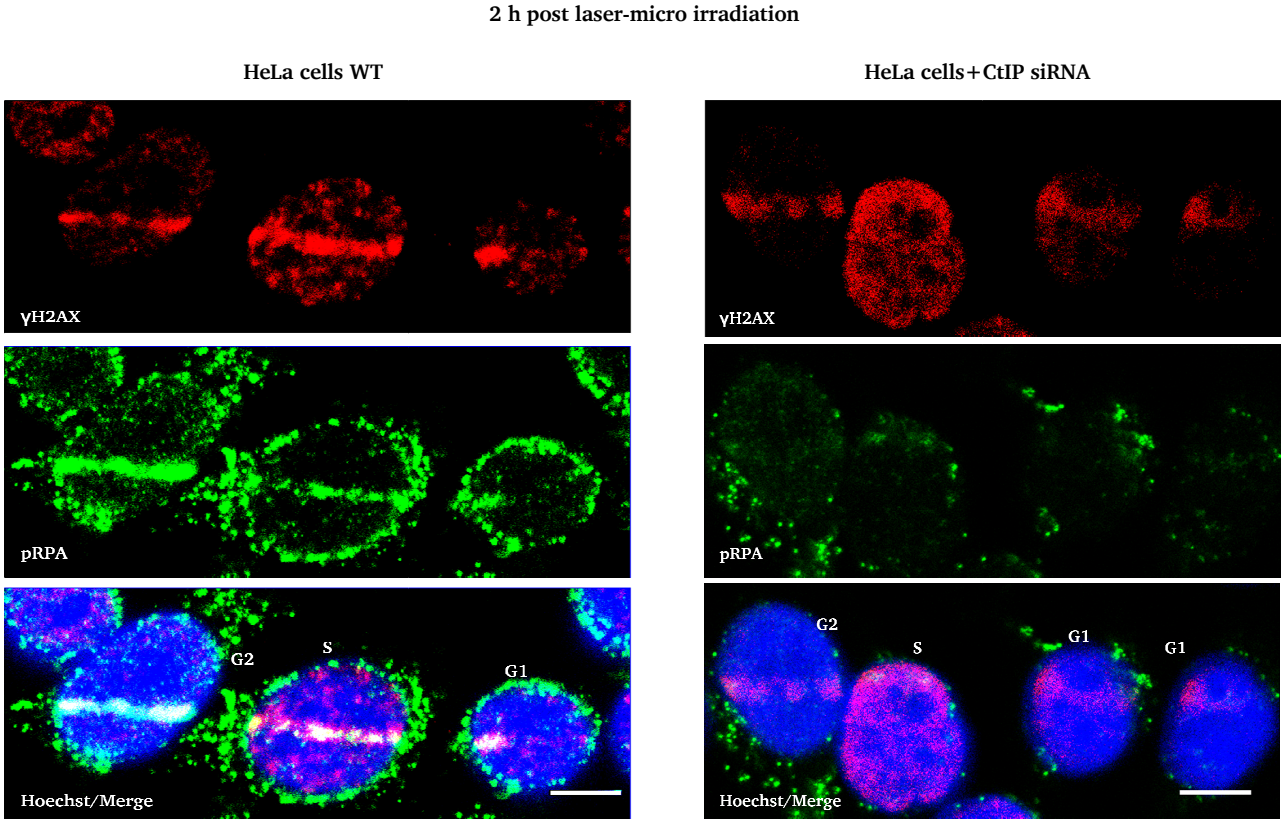

Figure 4.18. Impact of CtIP siRNA on pRPA laser track formation. Cells were treated with CtIP siRNA and incubated for 48 h at normal cell culture condition. One day prior to irradiation, cells were seeded in µ-Slide and stained with Hoechst for 10 min immediately before irradiation. At 2 h post micro-irradiation, cells were fixed and stained with γH2AX and pRPA antibodies. Images were taken by confocal microscope. Scale bar represents 5 µm.

Analyzing resection in stem cells after 2 Gy X-rays uncovered that ESCs formed pRPA foci in G1 phase, whereas NSCs did not (Figure 4.19a). The maximum number of pRPA foci in G1-phase ESCs was observed at 1 h post IR, similar to Rad51 foci in G2 phase (Figure 4.14b). The formation of pRPA foci indicated that the range of resection in G1-phase ESCs is longer than in differentiated cells. Furthermore, almost all pRPA foci formed in G1-phase ESCs were co-localized with γH2AX (Figure 4.19b). Since the formation of pRPA foci is resection dependent, similar to Rad51 foci (Figure 4.14b), pRPA foci formation was also increased after IR. Moreover, the reduction of pRPA foci level after 1 h post IR indicated the ongoing DSB repair via a resection dependent pathway in G1-phase ESCs (Figure 4.19a).

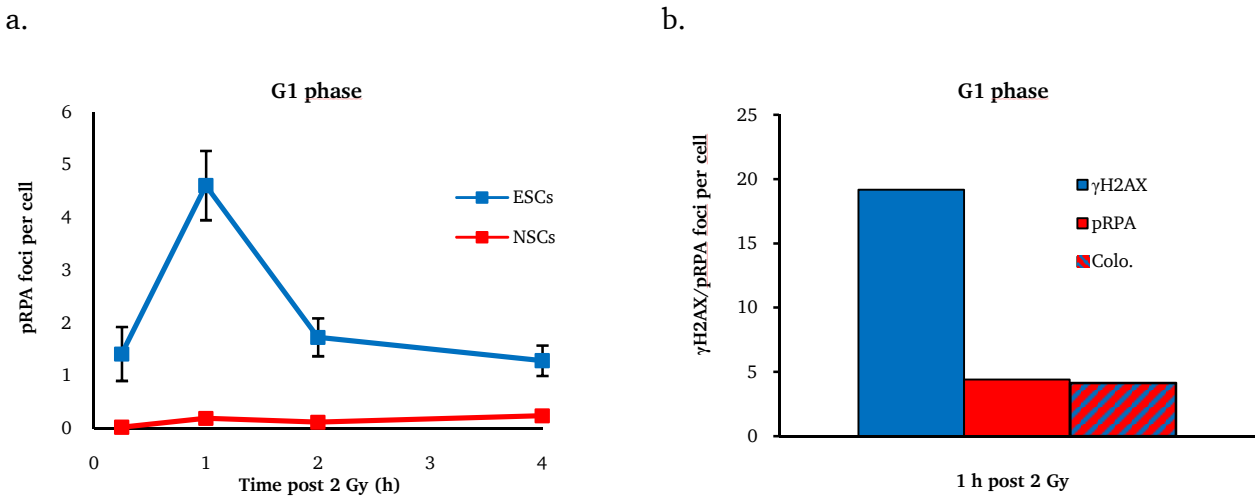

Figure 4.19. Resection in G1-phase ESCs and NSCs. After irradiating with 2 Gy X-rays, cells were incubated with EdU and Nocodazole. At the indicated time points pRPA or γH2AX foci were quantified in G1-phase (EdU-negative, CyclinB1-negative) cells. a. Quantification of pRPA foci in G1-phase ESCs and NSCs. Foci numbers of unirradiated cells were subtracted. Error bars represent the SEM of five independent experiments. b. Co-localization (Colo.) of γH2AX and pRPA foci at 1 h post IR in G1-phase ESCs.

To confirm the formation of pRPA foci after X-ray irradiation in G1-phase ESCs, pRPA foci were evaluated in another murine ESC line, ESC iB10. In a preliminary experiment, ESC J1 and iB10 were irradiated with 2 Gy X-rays and pRPA foci were scored at 1 h post IR in G1-phase cells (Figure 4.20). The result showed that, similar to ESCs J1, ESCs iB10 formed visible pRPA foci in G1 phase (Figure 4.20).

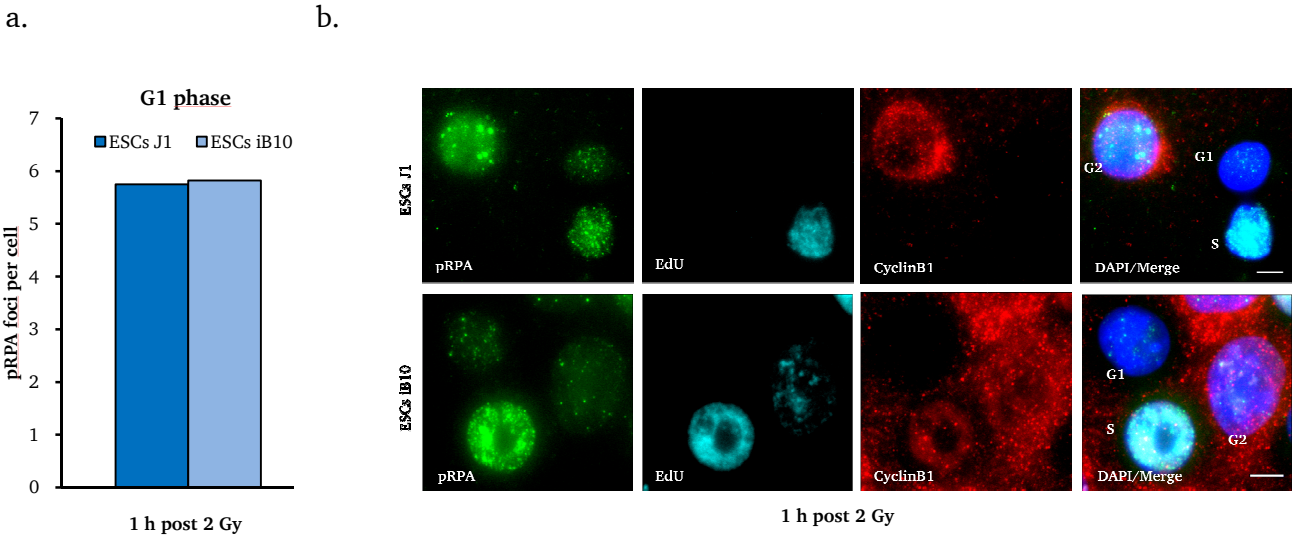

Figure 4.20. pRPA foci formation in murine ESCs. ESCs J1 and ESCs iB10 were irradiated with 2 Gy and incubated in the presence of EdU and Nocodazole. At 1 h post IR, pRPA foci were quantified in G1-phase cells (EdU-negative, CyclinB1-negative). Scale bars represent 5 µm. a. Quantification of pRPA foci at 1 h after IR in G1-phase ESCs J1 and ESCs iB10. Foci numbers of unirradiated cells were subtracted. This experiment was performed once .b. Representative microscopy images of irradiated ESCs J1 and ESCs iB10 stained for EdU, CylinB1, pRPA and DAPI.

4.3.2 Resection-dependent DSB repair

It was recently described that the slow component of DSB repair in G1-phase somatic cells is resection-dependent c-NHEJ (Res.-dep.-NHEJ) (Biehs, et al., 2017). PLK3 is one the factors mediating resection in G1 phase via phosphorylation of downstream factors, e.g. CtIP endonuclease (Barton, et al., 2014). To assess the role of PLK3 in resection and DSB repair in G1-phase ESCs, cells were treated with PLK3-inhibitor. After 2 Gy X-ray irradiation, γH2AX and pRPA foci were analyzed in each single G1-phase cells. Monitoring pRPA foci revealed that the resection in G1-phase ESCs was PLK3-dependent and the formation of pRPA foci was completely abolished after inhibition of PLK3 (Figure 4.21a). Analyzing γH2AX foci level demonstrated that the inhibition of PLK3 induced a clear impairment in DSB repair at times >2 h post IR (Figure 4.21b).

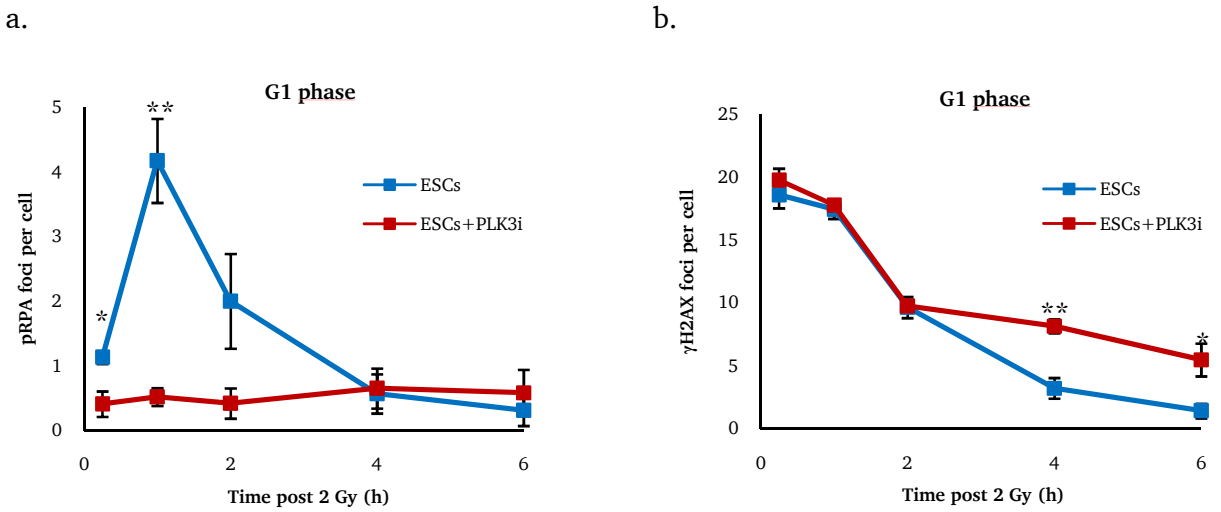

Figure 4.21. Role of PLK3 in resection and DSB repair in G1 phase ESCs. Cells were treated with PLK3 inhibitor (PLK3i) 30 min before irradiation. After 2 Gy X-rays irradiation, cells were fixed at the indicated time points and stained with γH2AX and pRPA antibodies. Repair incubation took place in the presence of EdU and Nocodazole. Foci were quantified in EdU-negative and CyclinB1-negative G1-phase cells. Foci numbers of unirradiated cells were subtracted. Error bar represent the SEM of three independent experiments. P-value: *≤ 0.05, **≤ 0.01 (using student t-test). a. Quantification of pRPA foci in WT and PLK3-inhibited (PLK3i) G1-phase ESCs. b. Quantification of γH2AX foci in WT and PLK3-inhibited (PLK3i) G1-phase ESCs.

4.3.3 Role of Artemis in slow component of DSB repair

Resection in G1 phase renders a big fragment of single-strand DNA (ssDNA). This ssDNA may fold back on the DNA to form a transient hairpin structure (Williams, et al., 2008; Jette, et al., 2015). The formation of stable hairpins protects DNA-ends against nucleases. To facilitate further repair, the hairpin end is opened by Artemis nuclease and ssDNA is immediately decorated by pRPA (Biehs, et al., 2017). Recently it was shown that the depletion of Artemis abolished pRPA foci formation after α-particle irradiation and also impaired DSB repair in somatic cells (Biehs, et al., 2017). Thus, the involvement of Artemis in resection and DSB repair in G1 phase ESCs and HeLa cells has been evaluated using siRNA (section 3.2.1.5). As expected, the quantification of γH2AX foci at 8 h post IR

demonstrated a significant repair impairment in Artemis-depleted HeLa cells (Figure 4.22a). In contrast, ESCs did not exhibit any repair defect after Artemis down regulation (Figure 4.22b). Moreover, to assess the role of Artemis in pRPA foci formation, pRPA foci level was monitored after Artemis depletion in G1-phase ESCs. Artemis siRNA strongly diminished pRPA foci level after 2 Gy X-rays in G1-phase ESCs (Figure 4.22c). The efficiency of siRNAs used for Artemis depletion in ESCs and HeLa cells was tested using western blot analysis. Artemis protein band was not detected in ESCs and HeLa cells after siRNA transfection (Figure 4.22d).

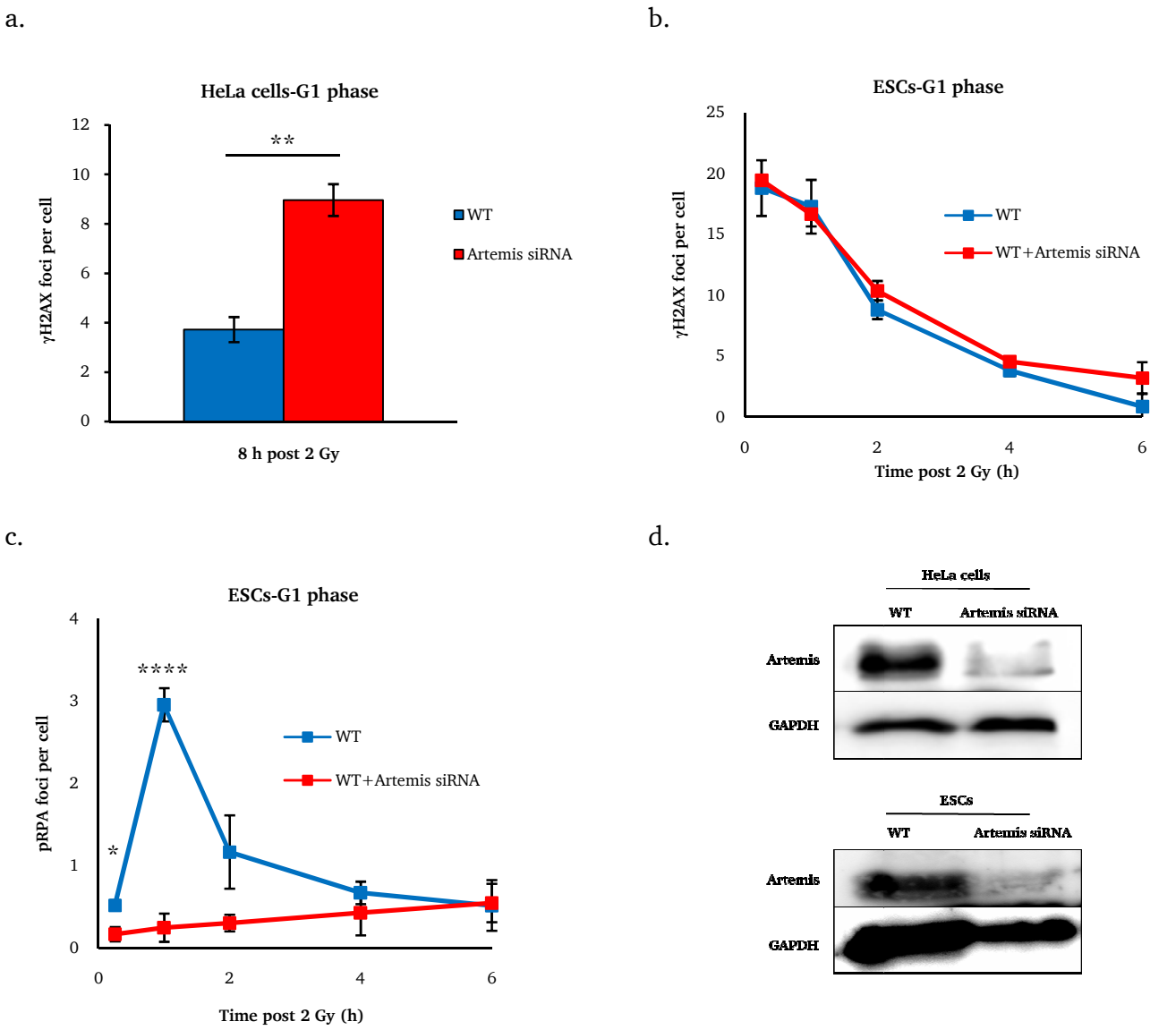

Figure 4.22. Role of Artemis in DSB repair and resection in G1 phase. ESCs and HeLa cells were transfected with Artemis siRNA 2 days prior 2 Gy X-rays irradiation. Repair incubation occurred in the presence of EdU and Nocodazole. At the indicated time points, cells were fixed and stained for γH2AX or pRPA. Foci were analyzed in EdU-negative G1-phase cells. The foci numbers of unirradiated cells were subtracted. Error bars represent the SEM of three individual experiments. P-value: *≤ 0.05, ****≤ 0.0001 (student t-test). a. Quantification of γH2AX foci level in WT and Artemis-depleted G1 phase HeLa cells. b. Quantification of γH2AX foci level in WT and Artemis-depleted G1 phase ESCs. c. Quantification of pRPA foci formation in WT and Artemis-depleted G1 phase ESCs. d. The western blot of Artemis protein level in WT and Artemis-depleted ESCs and HeLa cells.

4.3.4 Detection of RNA-DNA hybrids at DSB sites

Recently, different studies suggested that RNA is involved in DSB repair (Chakraborty, et al., 2016; Ohle, et al., 2016; Elf, 2016; Keskin, et al., 2016). In a yeast cell system, Ohle et al. demonstrated that RNA regulates resection in HR (Ohle, et al., 2016). Thus, to inspect the role of RNA in long range resection in G1-phase ESCs as detected by pRPA foci appearance (Figure 4.19), the formation of RNA-DNA hybrids at DSB sites was assessed after 2 Gy X-rays in G1 phase ESCs and HeLa cells using the S9.6 antibody. Since the S9.6 foci are too tiny and not detectable by wide field fluorescence microscopy, the formation of S9.6 foci at DSB sites (γH2AX) were evaluated utilizing confocal microscopy. To investigate the formation of RNA-DNA hybrids at DSB sites, the overlap between S9.6 and γH2AX signal intensities in each single focus layer was evaluated. The co-localization of S9.6 and γH2AX signals was observed in ESCs and HeLa cells (Figure 4.23a). As seen in Figure 4.23b, quantification of γH2AX and S9.6 foci at 15 min post IR in ESCs (n=18) and HeLa cells (n=10) demonstrated that 14 % of total γH2AX foci overlapped with S9.6 foci. At 2 h after IR, the co-localization of γH2AX and S9.6 foci in ESCs (n=11) and HeLa cells (n=10) increased to 35 % and 25 %, respectively (Figure 4.23b).

a.

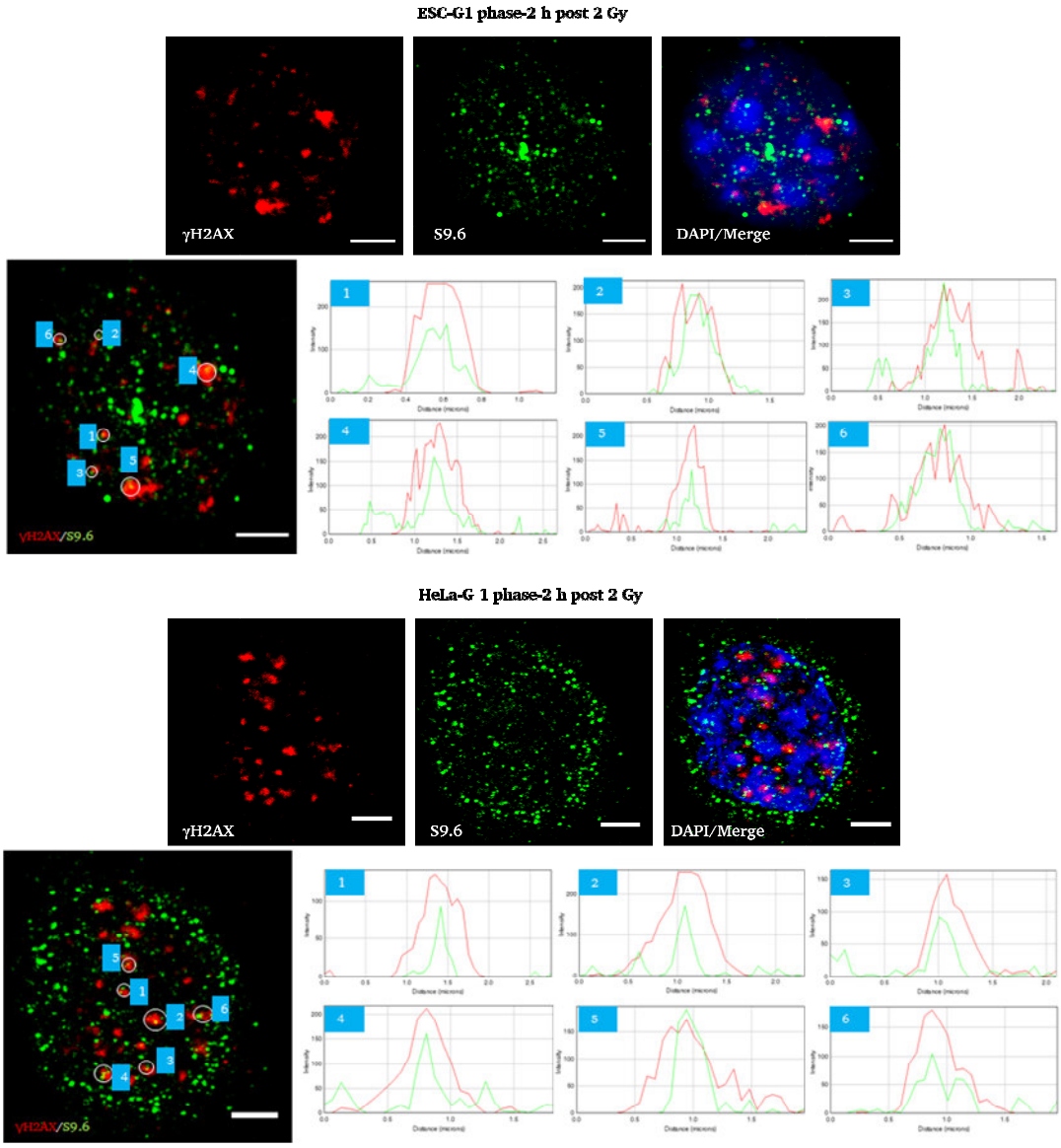

b.

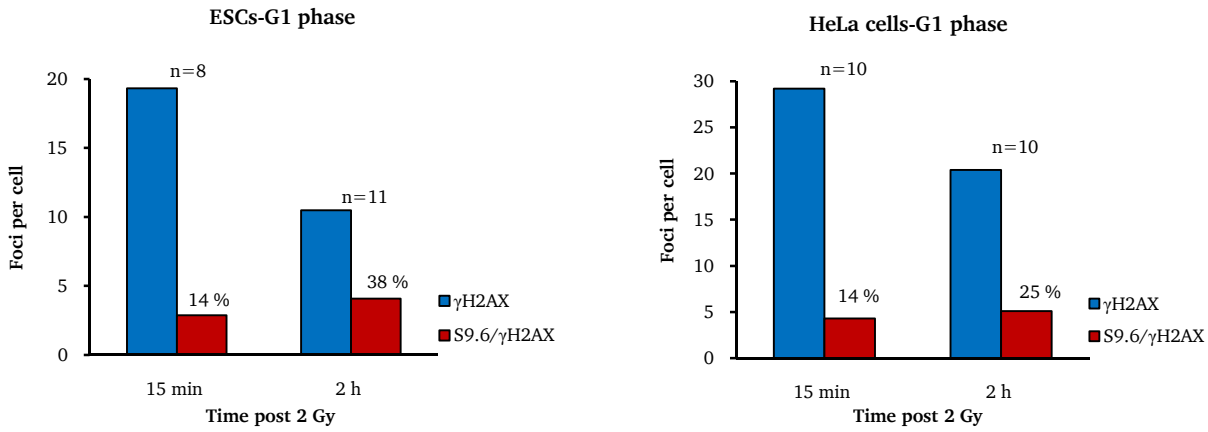

Figure 4.23. RNA-DNA hybrids formation at X-rays-induced DSB sites in G1-phase ESCs and HeLa cells. Cells were irradiated with 2 Gy X-rays and stained for S9.6 and γH2AX foci at indicated time points. Incubation time took place in the presence of Nocodazole. To evaluate the data, confocal microscopy was employed. The G1 phase cells were detected manually based on cell size and nucleus brightness (DAPI). a. Representation of the confocal image analysis of G1-phase ESCs and HeLa cells stained with S9.6 and γH2AX antibodies at 2 h post IR. Scale bars represent 5 µm. b. Quantification of S9.6 and γH2AX overlapping foci at 15 min and 2 h IR in G1-phase ESCs and HeLa cells.

To confirm the specificity of S9.6 antibody, as well as to validate the presence of S9.6 foci at DSB sites, laser-micro irradiation has been utilized. Growing ESCs in colony prevented applying laser-micro irradiation in these cells. Thus, only HeLa cells have been used for this study (chapter 3.2.1.8). The result showed that laser miro-irradiation generated a visible γH2AX track in HeLa cells (Figure 4.24). At 2 h post IR, the S9.6 foci were present at DSB sites and formed a track that overlaid with the γH2AX track (Figure 4.24). Similar to X-rays irradiation, after micro-irradiation, many S9.6 foci formed in the nucleus independently of DNA-damage.

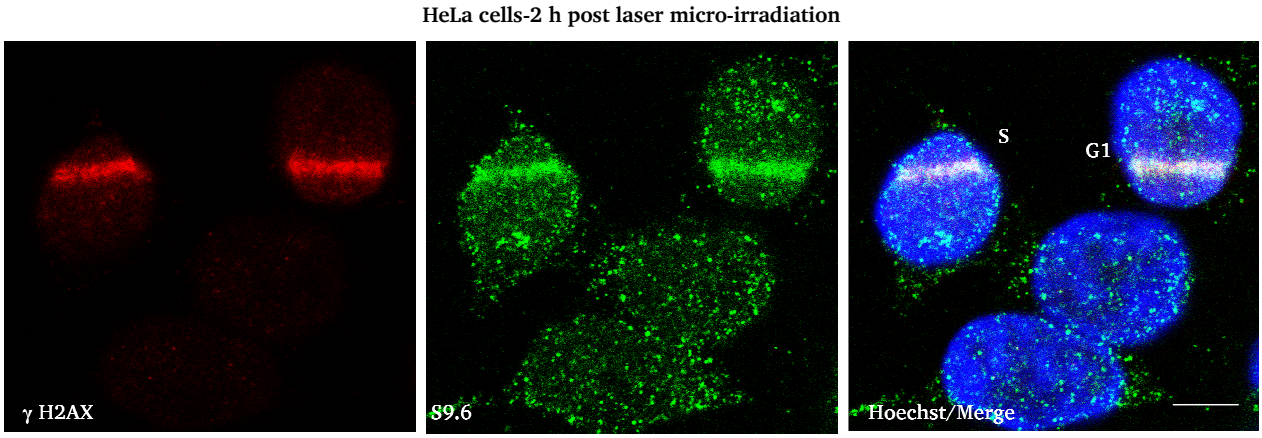

Figure 4.24. S9.6 foci accumulation at laser-induced DNA damage sites in HeLa cells. Cells were seeded in µ-Slide one day before irradiation and stained with Hoechst for 10 min immediately before irradiation. At 2 h post micro-irradiation, cells were fixed and stained with γH2AX and S9.6 antibodies. Images were taken by confocal microscope. Scale bar represents 5 µm.

4.3.5 Role of RNA-DNA hybrids in resection dependent DSB repair

PLK3 inhibition

To better understand the involvement of RNA in DSB repair, the resection dependency of the formation of RNA-DNA hybrids at DSB sites in G1 phase was addressed. Using a PLK3 inhibitor 30 min prior to micro-irradiation, resection was blocked in HeLa cells. 2 h post DNA-damage induction, clear γH2AX laser tracks were observed in both WT and PLK3-inhibited cells. The formation of a S9.6 track was abolished in PLK3-inhibited cells, whereas in WT cells, a visible S9.6 track formed overlaying with γH2AX (Figure 4.25a). Furthermore, co-localization of γH2AX and S9.6 was quantified after X-rays irradiation in PLK3-inhibited cells. To this end, ESCs and HeLa cells were exposed to 2 Gy X-rays irradiation and the co-localization of γH2AX with S9.6 foci at 15 min and 2 h post IR was analyzed in G1-phase cells. Inhibition of PLK3 decreased the co-localization level. At 15 min post IR, 30 % and 51 % decrease in S9.6 and γH2AX overlapping level was observed in ESCs (n=6) and HeLa cells (n=11), respectively. At 2 h after IR, the impact of PLK3-inhibition was more pronounced and the co-localization level was reduced to 50 % in ESCs (n=5) and 70 % in HeLa cells (n=11) (Figure 4.25b).

a.

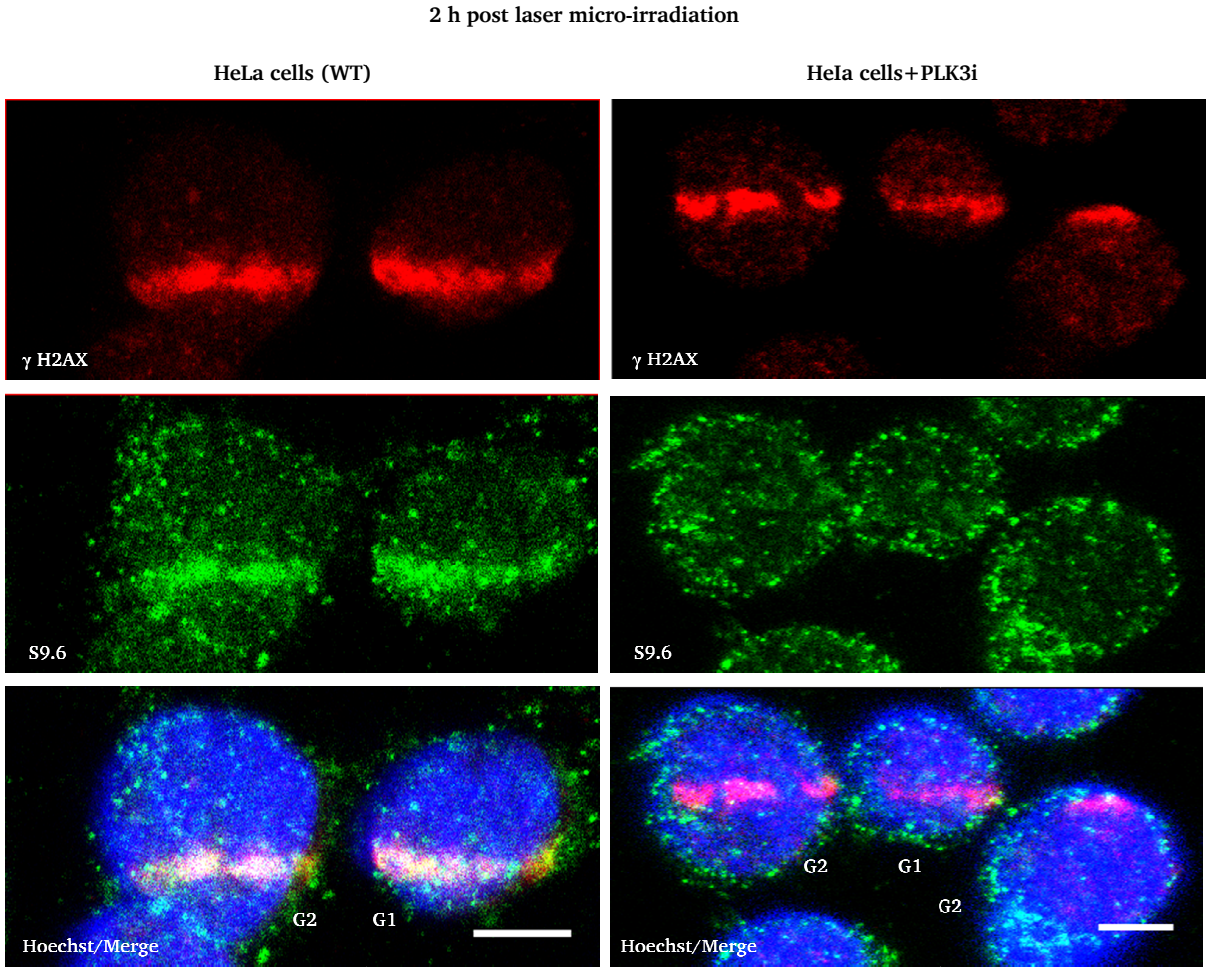

b.

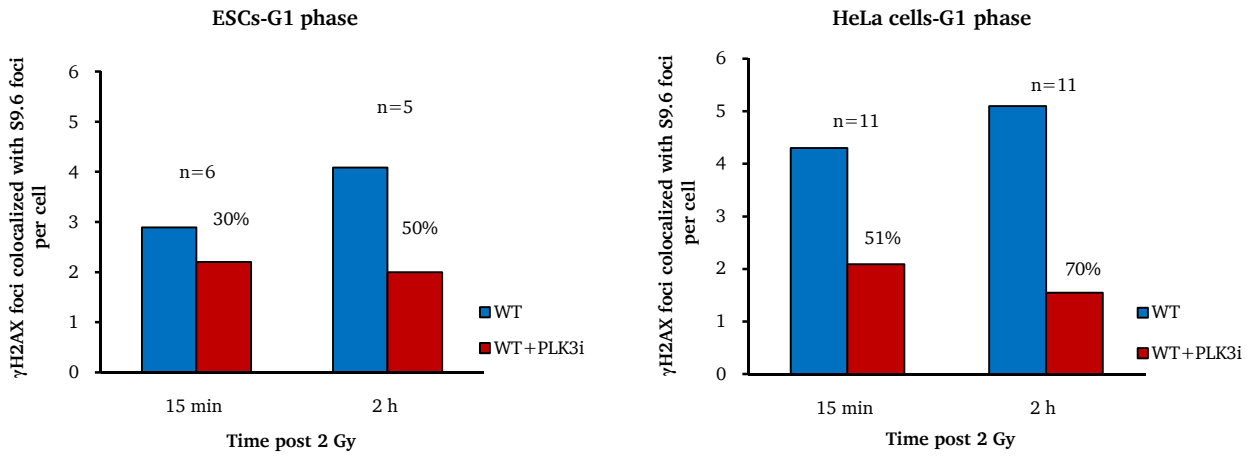

Figure 4.25. Role of PLK3 in S9.6 foci formation at DSB sites. Cells were treated with PLK3 inhibitor (PLK3i) 30 min prior to X-rays or micro-irradiation. At the indicated time points, cells were fixed and stained with γH2AX and S9.6 antibodies. Then the level of co-localization (γH2AX and S9.6) was analyzed in WT and PLK3-inhibited cells. Scale bars represent 5 μm. a. Representation of confocal image analysis in G1-phase HeLa cells. Utilizing ImageJ software, the co-localization of γH2AX track and S9.6 track was analyzed in a single focus layer at 2 h post micro-irradiation. b. Quantification of γH2AX overlaid with S9.6 foci in WT and PLK3-inhibited G1 phase ESCs and HeLa cells. The level of co-localization was analyzed at 15 min and 2 h after IR in WT and PLK3-inhibited cells. At 15 min time point, ESCs (n=6) and HeLa cells (n=11) in G1 phase were analyzed. At 2 h time point, 5 ESCs (n=5) and HeLa cells (n=11) were analyzed.

RNaseH1 overespression

It was previously shown that RNaseH1 enzyme can degrade RNA-DNA hybrid structures by cleaving the RNA moiety (Ohle, et al., 2016). Furthermore, the overexpression of RNhaseH1 suppressed the formation of RNA-DNA hybrids (Paulsen, et al., 2009; Stirling, et al., 2012). To characterize the role of RNaseH1 in S9.6 foci formation, HeLa cells were transfected with GFP-tagged RNaseH1 plasmid and seeded in μ-slides 1 day prior to irradiation (section 3.2.1.6). Then, laser micro-irradiation was performed (section 3.2.1.8). As seen in Figure 4.26, the laser tracks were generated in G1-phase HeLa cells as marked by γH2AX. Confocal image analysis showed that the overexpression of RNaseH1 not only abolished the formation of S9.6 track but also eliminated the DNA-damage independent S9.6 foci in transfected cells (Figure 4.26). The G1-phase transfected cells were identified by their size, Hoechst signal intensity and green bright nucleus.

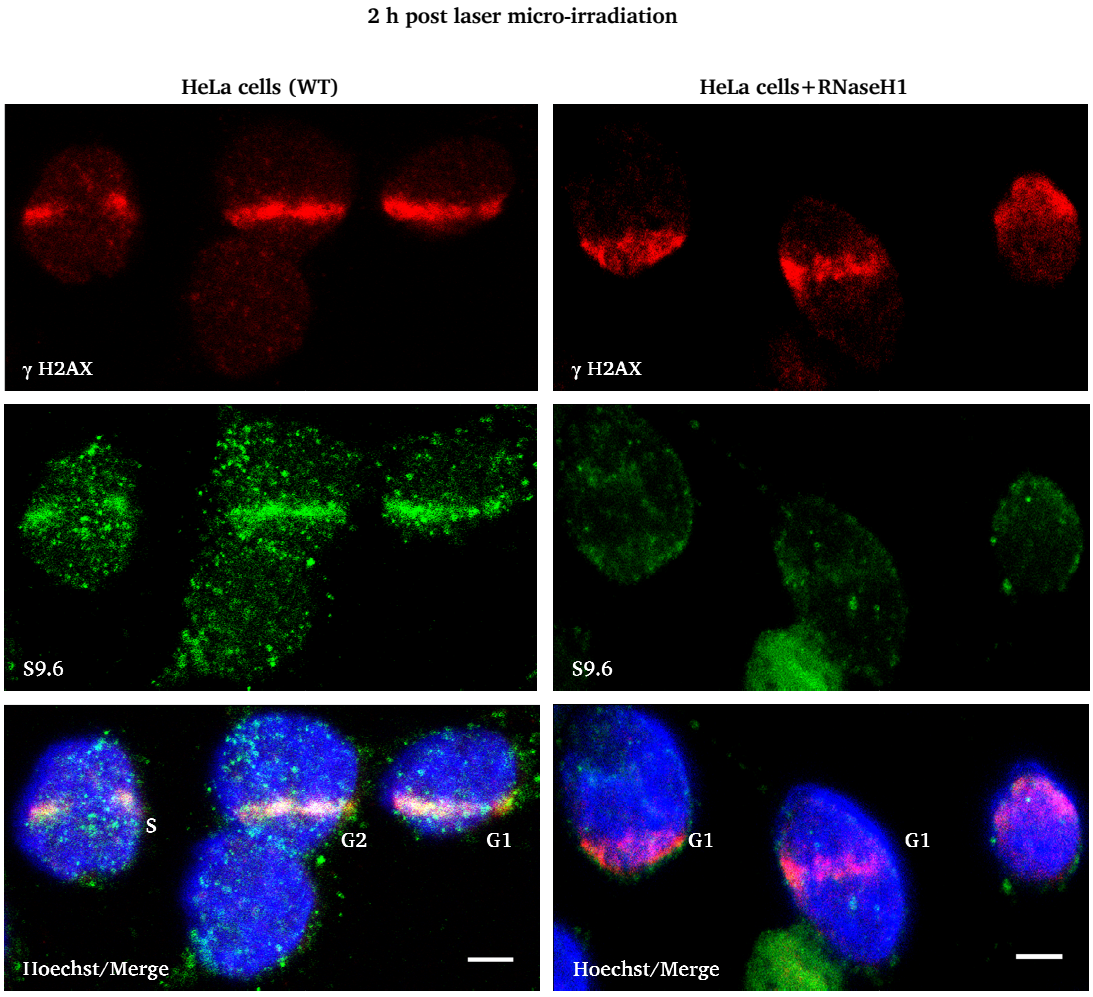

Figure 4.26. Impact of RNaseH1 overexpression on RNA-DNA hybrid formation. HeLa cells were transfected with GFP-tagged RNaseH1 plasmid three days before damage induction. One day prior to irradiation, cells were seeded in µ-slides. Hoechst staining was performed 10 min before irradiation. For laser track generation, the transfected cells were identified by their green bright nucleus and exposed to micro-irradiation. At 2 h post irradiation, cells were fixed and stained with S9.6 and γH2AX antibodies. Using confocal microscope and ImageJ software, the formation of S9.6 and γH2AX laser tracks was analyzed.

To investigate the involvement of RNA in DSB repair in G1 phase, ESCs and HeLa cells were transfected with GFP-tagged RNaseH1 plasmid. Two days after transfection, almost 80 % of cells were transfected and identified by their green nucleus (pan nuclear staining) (Figure 4.27a). Then, cells were irradiated with 2 Gy X-rays and DSB repair was assessed at different time points post IR. Monitoring γH2AX foci in G1 phase ESCs revealed that the overexpression of RNaseH1 impaired DSB repair from 1-2 h post IR (Figure 4.27b). In contrast to ESCs, G1 phase HeLa cells did not show any repair defect after RNaseH1 overexpression (Figure 4.27b). These results are identical to what has been observed after inhibition of PLK3 in G1-phase cells (Figure 4.21b)(Biehs, et al., 2017). Since the formation of RNA-DNA hybrids is an essential factor for resection (Figure 4.26), the lack of hybrids, similar to PLK3, might be compensated by a resection-independent c-NHEJ in G1 phase HeLa cells (Biehs, et al., 2017).

a.

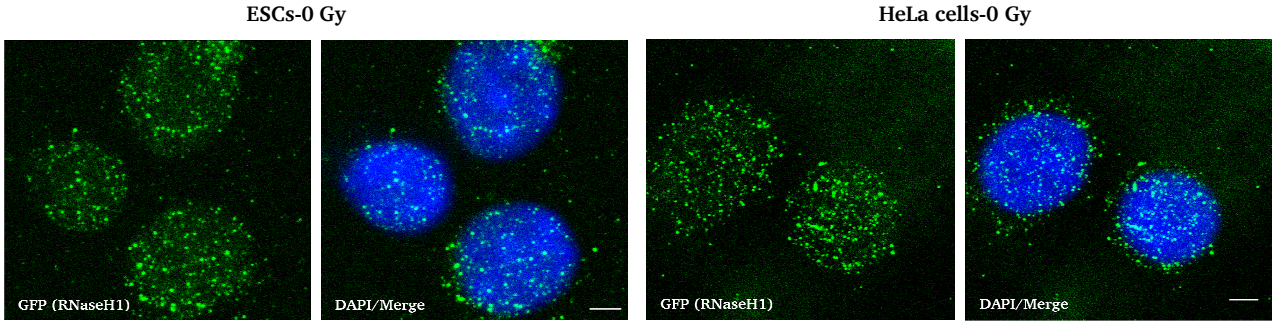

b.

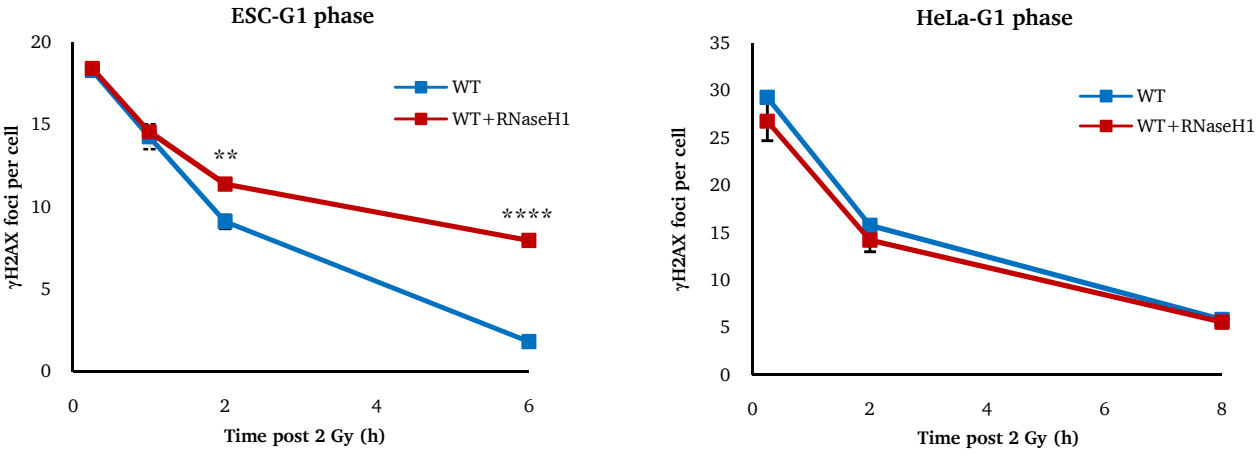

Figure 4.27. DSB repair after RNaseH1 overexpression in G1-phase cells. ESCs and HeLa cells were transfected with GFP-tagged RNaseH1 plasmid and incubated for two days. After irradiation with 2 Gy X-rays, cells were fixed at the indicated time points and stained with GFP and γH2AX antibodies. The repair incubation time took place in the presence of EdU and Nocodazole. The γH2AX foci were quantified in G1-phase cells (EdU-negative). Foci numbers of unirradiated cells were subtracted. Error bars represent the SEM of four and three individual experiments in ESCs and HeLa cells, respectively. P-value: **≤ 0.01, ****≤ 0.0001 (using student t-test). a. Representative confocal microscopy images of GFP-tagged RNaseH1 plasmid transfection in ESCs and HeLa cells. b. Quantification analysis of γH2AX foci levels in G1-phase WT and RNaseH1 overexpressed ESCs and HeLa cells after 2 Gy X-rays irradiation.

Since the inhibition of PLK3 and overexpression of RNaseH1 hindered DSB repair in G1-phase ESCs (Figure 4.26a; Figure 4.27a), next the interaction between resection and RNA-DNA hybrids formation in DSB repair was investigated. ESCs were transfected with GFP-tagged RNaseH1 plasmid and incubated for two days. Then, PLK3 inhibitor was added to the cells 30 min prior to 2 Gy X-rays irradiation. Analyzing γH2AX foci at 6 h post IR revealed that the inhibition of PLK3 and overexpression of RNaseH1 induced a repair defect in G1-phase ESCs (Figure 4.28). The level of residual DSBs at 6 h post IR was higher in RNaseH1 transfected cells, compared to PLK3 inhibited cells (Figure 4.28). The impact of RNaseH1 overexpression was rescued after combination with PLK3 inhibitor and DSB level dropped to the PLK3 inhibitor alone (Figure 4.28). This indicates that PLK3 is an upstream factor for RNA-DNA hybrids activity.

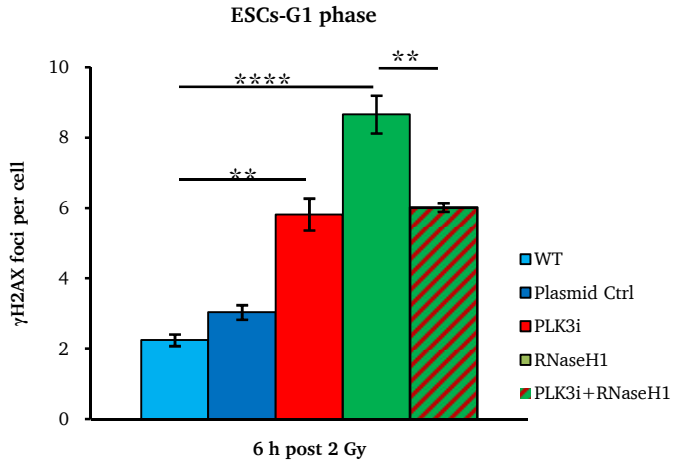

Figure 4.28. PLK3 and RNaseH1 interplay in G1-phase ESCs. Two days before irradiation, ESCs were transfected with GFP-tagged RNaseH1 plasmid. 30 min prior to 2 Gy X-rays irradiation, cells were treated with PLK3 inhibitor. After irradiation cells were incubated under normal cell culture condition in presence of EdU and Nocodazole. 6 h post IR cells were spun down on glass slides, fixed and stained with γH2AX and GFP antibodies. To quantify the γH2AX foci only G1-phase cells (EdU-negative) were evaluated. Foci numbers of un-irradiated cells were subtracted. Error bars represents SEM of three individual experiments. P-value: **≤ 0.01, ****≤ 0.0001 (using student t-test).

Artemis is an essential factor regulating resection in G1 phase (Biehs, et al., 2017). As it has been observed in Figure 4.22a, and also reported by previous studies (Biehs, et al., 2017), depletion of Artemis impaired DSB repair in G1-phase HeLa cells. Hence, the interplay between Artemis and RnaseH1 was checked. Using GFP-tagged RNaseH1 plasmid, the RNaseH1 enzyme was overexpressed in HeLa cells. Artemis was depleted by siRNA one day prior to irradiation. Cells were irradiated with 2 Gy X-rays and the level of γH2AX foci at 8 h post IR was analyzed in G1-phase HeLa cells. The increased number of residual foci demonstrated that the depletion of Artemis induced a repair defect in HeLa cells, whereas, overexpression of RNaseH1 had no impact on DSB repair (Figure 4.29). Interestingly, depletion of Artemis in RNaseH1 overexpressed cells did not induce a repair defect

(Figure 4.29). This is evident that Artemis is not involved in the initial steps of resection in G1 phase and its failure cannot be compensated by other resection-independent c-NHEJ.

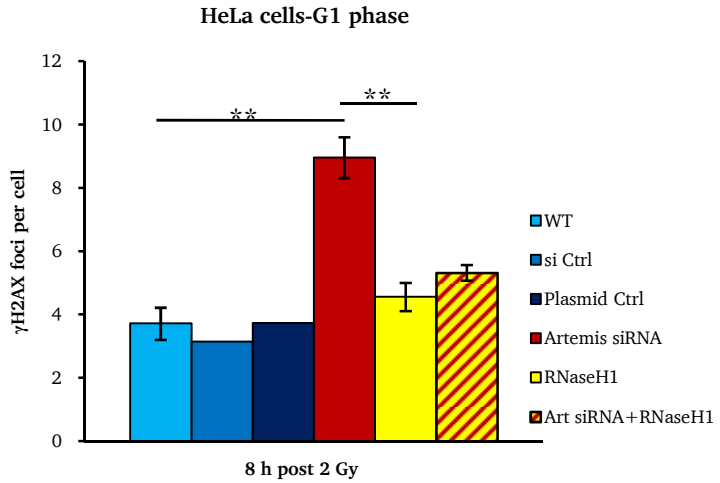

Figure 4.29. Artemis and RNaseH1 interplay in G1-phase HeLa cells. Cells were transfected with GFP-tagged RNaseH1 plasmid two days before irradiation. One day prior to 2 Gy X-rays irradiation, Artemis siRNA was added to the cells. After irradiation, cells were incubated under normal cell culture condition in the presence of EdU and Nocodazole. At 8 h post IR cells were fixed and stained with γH2AX and GFP antibodies. Using a semi-automatic microscopy analysis, γH2AX foci were scored in G1-phase cells (EdU-negative). Foci numbers of unirradiated cells were subtracted. Error bars represent SEM of three individual experiments. P-value: **≤ 0.01 (using student t-test).

To better understand the mechanism of pRPA foci formation in G1-phase ESCs, the role of RNA in modulating long range resection was investigated. To this end, ESCs were transfected with GFP-tagged RNaseH1 plasmid and irradiated with 2 Gy X-rays. Following IR, the formation of pRPA was monitored in WT and RNaseH1 transfected G1-phase cells. As seen in Figure 4.18, the WT cells formed visible pRPA foci in a time dependent manner. The maximum level of pRPA foci formed at 1 h post IR, then the foci level was slowly decreased (Figure 4.30a). In contrast to the WT cells, the RNaseH1 overexpressed cells did not form pRPA foci at 1 h post IR. However, at time points >1 h after IR, the level of pRPA foci formation was slowly enhanced in RNaseH1 transfected cells (Figure 4.30a). These pRPA foci were of the same size as in S- and G2-phase ESCs (Figure 4.30b).

a.

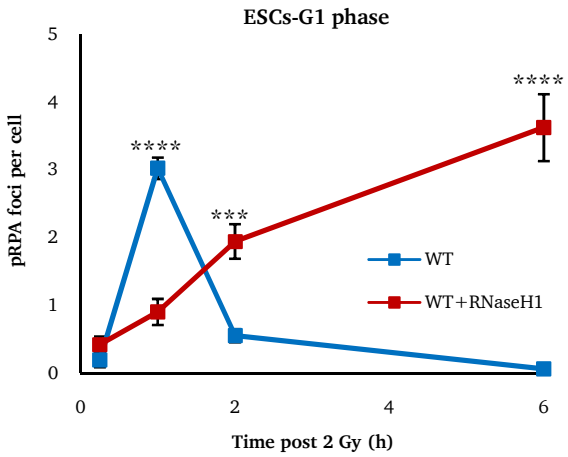

b.

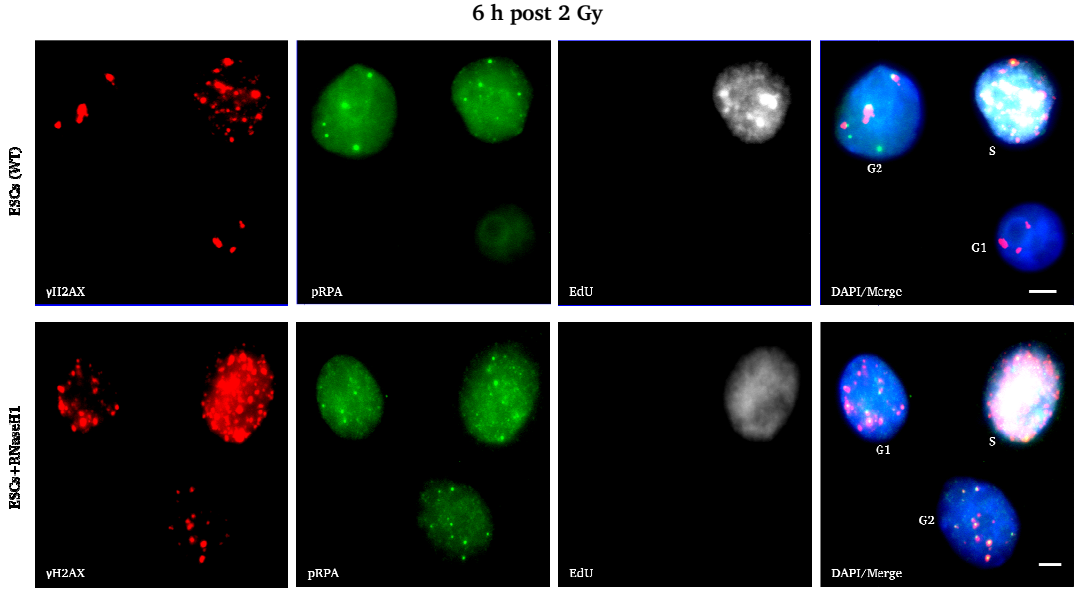

Figure 4.30. Impact of RNaseH1 overexpression on pRPA foci formation in G1-phase ESCs. Cells were transfected with GFP-tagged RNaseH1 plasmid. At two days post transfection, cells were irradiated with 2 Gy X-rays and fixed at the indicated time points. Then, cells were stained with pRPA and γH2AX antibodies. Incubation time took place in the presence of EdU and Nocodazole. pRPA foci were quantified in G1-phase cells (EdU-negative). Foci numbers of unirradiated cells were subtracted. Error bars represent SEM of four independent experiments. P-value: ***≤ 0.001, ****≤ 0.0001 (using student t-test). a. Quantification of pRPA foci in WT and RNaseH1 overexpressed G1-phase ESCs. b. Representative microscopy images of pRPA foci at 6 h post IR in WT and RNaseH1 transfected G1-phase ESCs.

To investigate whether the formation of pRPA foci at DSB sites in G1 phase is dependent on the activity of transcription machinery, using DRB (RNA Pol II inhibitor) transcription was deactivated in ESCs. Cells were incubated with 10 μM DRB in the normal cell culture condition. Following irradiation with 2 Gy X-rays, cells were fixed and stained with pRPA antibody. Monitoring pRPA foci in G1-phase ESCs revealed that the inhibition of Pol II diminished the formation of pRPA in G1-phase ESCs (Figure 4.31). This indicates that the transcription machinery promotes the long-range resection in G1-phase ESCs.

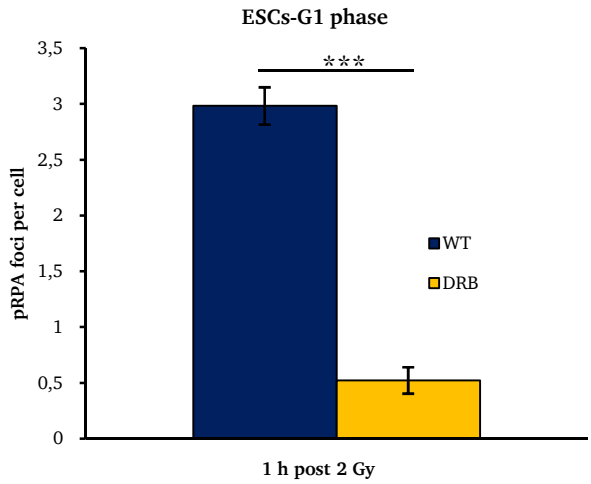

Figure 4.31. Impact of RNA Pol II inhibition on pRPA foci formation in G1-phase ESCs. Cells where treated with 10 µM DRB 3 h prior to 2 Gy X-rays irradiation. At 1 h post IR, cells were fixed and stained with pRPA and γH2AX antibodies. Repair incubation time took place in the presence of EdU and Nocodazole. pRPA foci were quantified in G1-phase cells (EdU-negative). Foci numbers of unirradiated cells were subtracted. Error bars represent SEM of three independent experiments. P-value: ***≤ 0.001 (using student t-test).

DDX1 foci

Similar to RNaseH1, DDX1 protein also unwinds RNA-DNA hybrid structures (Li, et al., 2008). It has been shown that, upon irradiation, DDX1 foci rapidly form at DSB sites (almost at 30 % of DSBs) (Li, et al., 2008). Thus, as a factor mediating RNA processing in DSB repair, the role of DDX1 was assessed in our cell system. Unfortunately, the DDX1 foci could not be detected by the commercial available antibodies in ESCs and HeLa cells. An efficient antibody to detect DDX1 foci, was specific for human cells. Therefore, the formation of DDX1 foci was analyzed only in HeLa cells. The formation of DDX1 at DSB sites was evaluated after irradiation with 2 Gy X-rays. As seen in Figure 4.32a, the majority of DDX1 foci detected in G1-phase HeLa cells formed at the DSB sites (Figure 4.32a). Quantification of DDX1 and γH2AX foci revealed that, upon irradiation, DDX1 foci formed at 50 % and 30 % of DSB sites respectively in G1 and G2 phase (Figure 4.32b). The level of DDX1 and γH2AX foci were identical at late time points (Figure 4.32b). Note, foci were quantified in the same cells.

a.

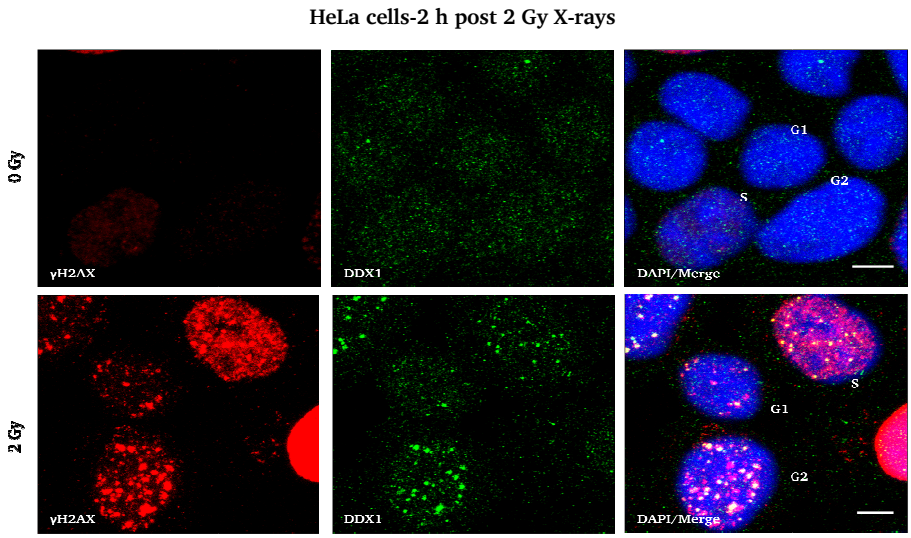

b.

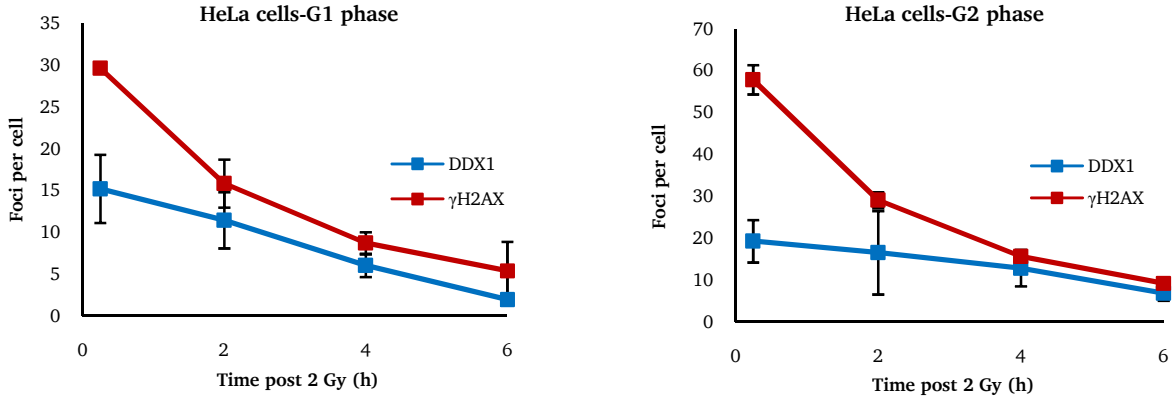

Figure 4.32. Formation of DDX1 foci in G1- and G2-phase HeLa cells. Cells were seeded on coverslips one day prior to irradiation. EdU and Nocodazole were added to the cells 30 min before 2 Gy X-rays irradiation. After irradiation cells were fixed at the indicated time points and stained with DDX1 (kindly provided by Prof. Godbout) and γH2AX antibodies. Using a semi-automatic microscopy approach, DDX1 and γH2AX foci were quantified in G1- (EdU-negative) and G2- (EdU-negative) phase cells. Foci numbers of unirradiated cells were subtracted. Error bars represent SEM of three individual experiments. a. Representative confocal microscopy images of DDX1 and γH2AX foci formation at 2 h post IR in G1-phase HeLa cells. b. Quantification of DDX1 and γH2AX foci in G1- and G2- phase HeLa cells.

To investigate whether the formation of DDX1 foci relays on the presence of ssDNA, resection was inactivated using CtIP siRNA (Table 3.2). Two days after CtIP siRNA treatment, cells were exposed to 2 Gy X-rays irradiation. Quantification of DDX1 foci at 2 h post IR in G1-phase showed 50 % reduction in DDX1 foci level in CtIP depleted cells compared to WT cells (Figure 4.33a). The depletion of CtIP had no impact on DSB repair at 8 h post IR (Figure 4.33b). Since CtIP is an essential factor to regulate resection in G1 and G2 phase (Sartori, et al., 2007; Barton, et al., 2014), Rad51 foci (a marker for resection in G2 phase) was quantified as a read out to check the efficiency of CtIP siRNA. Quantification of Rad51 foci at 2 h after IR showed a significant reduction in Rad51 foci level in G2-phase cells (Figure 4.33c). This indicated that resection was hindered by CtIP siRNA.

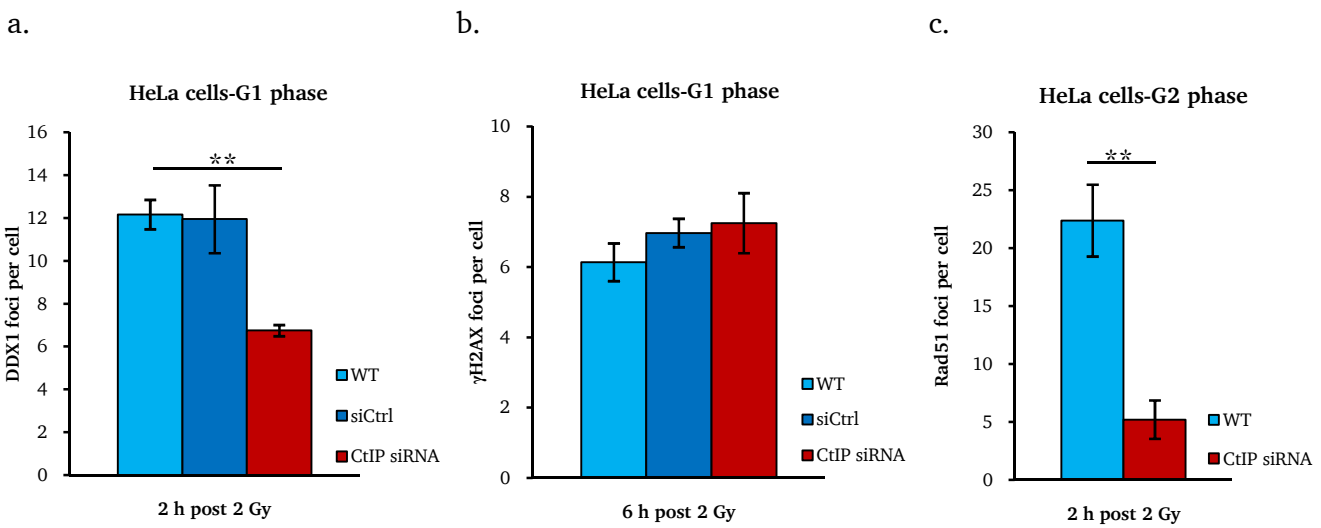

Figure 4.33. Resection dependency of DDX1 foci formation in G1-phase HeLa cells. Cells were transfected with CtIP siRNA two days before irradiation. After 2 Gy X-rays irradiation cells were incubated in normal cell culture condition. The repair incubation took place in the presence of EdU and Nocodazole. At the indicated time points cells were fixed and stained with different antibodies. DDX1 and γH2AX foci were quantified in G1-phase cells (EdU-negative, CyclinB1-negative) and Rad51 foci analyzed in G2-phase cells (EdU-negative, CyclinB1-positve). Foci numbers of unirradiated cells were subtracted. Error bars represent SEM of three individual experiments. P-value: **≤ 0.01 (using student t-test). a. Quantification of DDX1 foci at 2 h post IR in G1-phase HeLa cells. b. Quantification of γH2AX foci at 6 h post IR in G1-phase HeLa cells. c. Quantification of Rad51 foci at 2 h post IR in G2-phase HeLa cells.

DDX1 siRNA

In order to check the role of DDX1 in DSB repair, DDX1 protein was downregulated in HeLa cells using siRNA (Table 3.2). Following the standard DDX1 siRNA transfection protocol (Li, et al., 2016), cells were split 72 h after the first round of siRNA transfection and underwent a second round of siRNA transfection. One day after the second siRNA transfection, cells were irradiated with 2 Gy X-rays and incubated under normal cell culture conditions in presence of EdU and Nocodazole. Quantification of DDX1 foci in G1-phase cells revealed almost 50 % decrease in foci level 15 min post IR in DDX1 siRNA transfected cells (Figure 4.34a). Furthermore, fluorescence microscope image analysis showed the reduction in DDX1 foci formation after DDX1 siRNA transfection (Figure 4.34b). Monitoring the γH2AX foci level after irradiation indicated a significant repair defect at late time points in DDX1 depleted cells (Figure 4.34c). This indicated the involvement of DDX1 protein in the slow component of DSB repair in G1 phase cells.

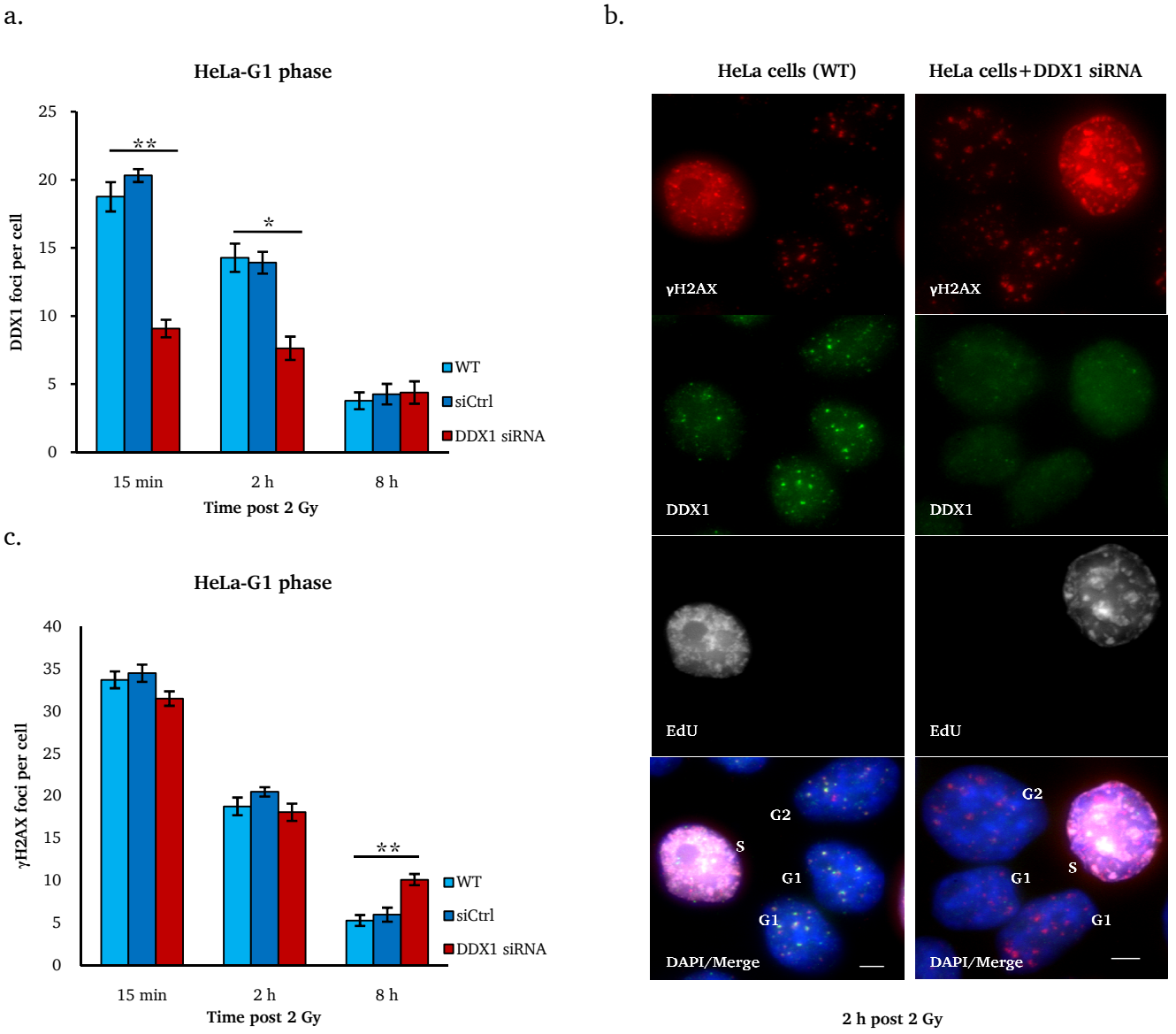

Figure 4.34. Role of DDX1 in DSB repair in G1-phase HeLa cells. Cells were transfected with DDX1 siRNA one day before 2 Gy X-rays irradiation. EdU and Nocodazole were added to the cells 30 min prior to irradiation. After damage induction, cells were fixed at the indicated time points and stained with γH2AX and DDX1 antibodies. Using a semi-automated microscopy, the foci were quantified in G1-phase cells (EdU-negative). Foci numbers of unirradiated cells were subtracted. Error bars represent SEM of three individual experiments. P-value: *≤ 0.05, **≤ 0.01 (using student t-test). a. Quantification of DDX1 foci after 2 Gy irradiation in G1-phase HeLa cells. b. Representative microscopy image of DDX1 and γH2AX foci formation at 2 h post IR in WT and DDX1 depleted G1-phase HeLa cells (using ImageJ). c. Quantification of γH2AX foci after 2 Gy irradiation in G1-phase HeLa cells.

PLK3 inhibitor, EdU and Nocodazole were added to the cells 30 min before 2 Gy X-rays irradiation. Following irradiation, cells were incubated under normal cell culture conditions. At 8 h post IR, the level of residual γH2AX foci were quantified in each condition. Inhibition of PLK3 had no impact on DSB repair and the residual γH2AX foci level was identical to the WT and siCtrl (Figure 4.35). The impact of DDX1 siRNA on DSB repair was rescued after combination with PLK3 inhibitor (Figure 4.35).

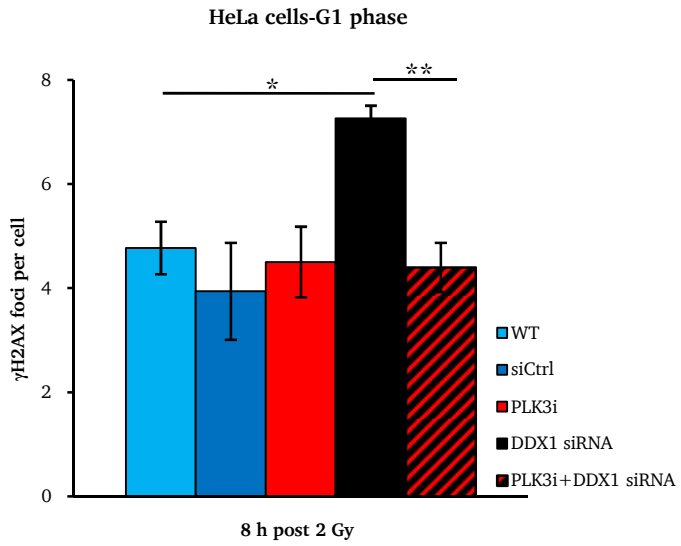

Figure 4.35. Interaction of DDX1 and PLK3 in DSB repair in G1 phase HeLa cells. Cells were transfected with DDX1 siRNA. PLK3 inhibitor was added to the cells 30 min prior to 2 Gy X-rays irradiation. The repair incubation took place in presence of EdU and Nocodazole. 8 h post IR, cells were fixed and stained with γH2AX and CylinB1 antibodies. γH2AX foci were quantified in G1 phase cells (EdU-negative, CyclinB1-negative). Foci numbers of unirradiated cells were subtracted. Error bars represent SEM of three individual experiments. P-value: *≤ 0.05, **≤ 0.01 (using student t-test).

Both RNaseH1 and DDX1 proteins unwind RNA-DNA hybrid structure by cleaving the RNA moiety (Li, et al., 2008; Ohle, et al., 2016). In HeLa cells, overexpression of RNaseH1 had no impact on DSB repair (Figure 4.26b), whereas DDX1 siRNA induced repair defect at late time points after irradiation (Figure 4.34). To better understand the role of these two proteins in DSB repair, the RNaseH1 was overexpressed in DDX1 depleted cells. EdU and Nocodazole were added to the cells 30 min before irradiation. At 8 h post 2 Gy X-rays irradiation, the γH2AX foci level was evaluated in G1-phase cells. As previously seen, quantification of the γH2AX foci revealed that the DSB repair was impaired only in DDX1 depleted cells, and no indication of the impaired DSB repair was observed in RnaseH1 transfected cells (Figure 4.36). The combination of DDX1 siRNA and RNaseH1 overexpression rescued the impact of DDX1 (Figure 4.36).

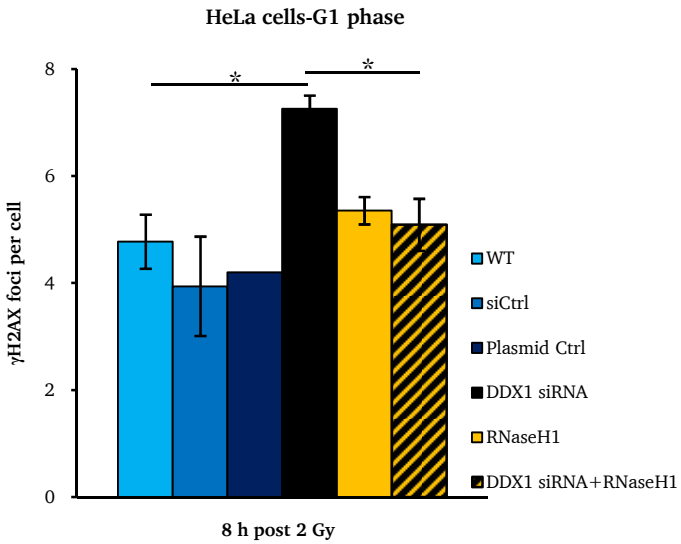

Figure 4.36. DDX1 and RNaseH1 interplay in DSB repair in G1 phase HeLa cells. Cells were transfected with DDX1 siRNA two days before irradiation RNaseH1 plasmid transfection was performed one day before irradiation. EdU and Nocodazole were added to the cells 30 min prior 2 Gy X-rays irradiation. After IR, cells were incubated in normal cell culture conditions. At 8 h post IR, cells were fixed and stained with γH2AX and CylinB1 antibodies. γH2AX foci were quantified in G1-phase cells (EdU-negative, CyclinB1-negative). Foci numbers of unirradiated cells were subtracted. Error bars represent SEM of three individual experiments. P-value: *≤ 0.05 (using student t-test).

5 Discussion

DNA double-strand breaks (DSBs) can be arised by low and high doses of ionizing radiations (IR) (UNSCEAR, 2000). Any failure to repair these genetic lesions may change the cells fate (Harper, et al., 2007; Jackson, et al., 2009). In somatic cells, the majority of IR-induced DSBs are repaired quickly via canonical-non-homologous end-joining (c-NHEJ) with DNA-PKcs being one of the core enzymes. In contrast, a sub-fraction of breaks is repaired with slow kinetics in an ATM-dependent manner, which represents homologous recombination (HR) in G2 phase and a resection-dependent end-joining pathway in G1 phase (Beucher, et al., 2009; Biehs, et al., 2017). The nuclease CtIP mediates resection in G1 and G2 phase. In somatic cells, the resection in G1 is not as extensive as it is in S or G2 phase. Thus, the formation of resection-dependent foci in G1 phase, like pRPA foci, could only be detected after the induction of very complex breaks or clustered damages, which arise after irradiation with alpha-particles or heavy ions (Averbeck, et al., 2014; Barton, et al., 2014). In addition, in the absence of c-NHEJ core factors, the residual DSBs are repaired by an alternative end-joining pathway (alt-NHEJ) (Iliakis, 2009; Mansour, et al., 2013). This pathway requires PARP1, Ligase I and Ligase III as well as nucleases that conduct limited resection of the break ends (Wang, et al., 2006; Liang, et al., 2008; Iliakis, 2009; Mansour, et al., 2013).

Similar to somatic cells, DNA of stem cells can be damaged by exogenous or endogenous sources of DNA damaging factors. DSB repair impairment in stem cells can affect intracellular heterogeneity and also organ development (Blampain, et al., 2013; Behrens, et al., 2014). The essential concern about ESCs and their derivatives, e. g. NSCs, is their ability to restore physiological functionality in response to DSBs. As it has been observed in Figure 4.2 and also shown by previous studies, ESCs are more resistant to the IR-induced DSBs than somatic cells (Saretzki, et al., 2004; Maynard, et al., 2008). Furthermore, it was reported that the mutation frequency in ESCs is about 100-fold lower than in somatic cells (Munroe, et al., 2000; Cervantes, et al., 2002). Global gene expression analysis revealed that the level of gene transcription and proteins involved in DNA repair is higher in ESCs than in differentiated cells (Momcilovic, et al., 2010; Fan, et al., 2011). It was shown that ESCs rely more on HR for DSB repair compared to other DSB repair pathways (Adams, et al., 2010; Tichy, et al., 2010; Serrano, et al., 2011; Lan, et al., 2012). However, in these studies the cell cycle phase as well as the contribution of DSB repair pathways was not considered.

Extensive studies have indicated that, in contrast to somatic cells, ESCs have a specific cell cycle timing with a short G1/G2 and a long S phase (Kapinas, et al., 2013). In agreement with previous studies (Hong, et al., 2004; van der Laan, et al., 2013), we observed that the G1/S checkpoint was not activated in ESCs and NSCs after exposure to 2 Gy X-rays (Figure 4.3). In the absence of G1/S checkpoint in ESCs and NSCs, cells may enter into S phase with unrepaired DSBs. To protect genome

integrity in stem cells, DSBs must be repaired through a robust repair mechanism which may differ from somatic cells.

In the current work, the mechanisms by which ESCs and ESC-derived NSCs minimize the IR-induced DSBs, particularly in G1-phase, have been studied. This may shed light on how mammals preserve their genome during embryonic development.

5.1 DSB repair after low X-rays doses

DSB repair capacity

In clinical practice, the diagnostic and therapeutic procedures are usually accompanied by low doses of X-rays irradiation (up to 100 mGy). The cell response to the low doses of IR is different from high doses (Collis, et al., 2004). It was reported that DSB repair efficiency is reduced after irradiation with low doses of X-rays (Rothkamm, et al., 2003). In agreement with previous studies, we observed that the DSB level induced by 100 mGy X-rays was significantly reduced within 4 h post IR in G1- and G2-phase NSCs (Figure 4.6a). The cell response to 100 mGy X-rays in NSCs was similar to what was observed after irradiation with 2 Gy (Figure 4.11). Preliminary experiments with ESCs also showed the same repair capacity after exposure to 100 mGy (Figure 4.5). This indicated that, similar to higher doses of X-rays, 100 mGy induces an efficient DSB repair response in stem cells. In contrast, cells exposed to 10 mGy X-rays did not show a proficient DSB repair (Figure 4.6b). In G2 phase, almost 50 % of IR-induced DSBs were repaired within 1 h post 10 mGy and the residual DSBs remained unrepaired until 4 h after irradiation (Figure 4.6b). While, no DSB repair was observed in G1 phase and IR-induced DSB level was remained constant up to 4 h post IR (Figure 4.6b). This observation is consistent with previous studies indicated that DSB repair efficiency decreases after irradiation with doses below 20 mGy (Rothkamm, et al., 2003; Grudzenski, et al., 2010). Depending on the dose of irradiation and also the number of accumulated DSBs, the DNA repair machinery becomes active with different potency (Rodriguez-Rocha, et al., 2011; Talaeei, et al., 2013). The level of DSBs produced by 10 mGy is probably insufficient to activate the DSB repair machinery in the cells, especially in G1 phase.

ATM and DNA-PKcs signaling are essential for DSB repair (Shirvastav, et al., 2008; Beucher, et al., 2009), and their kinase activities are required for γH2AX and subsequent 53BP1 foci formation (Stiff, et al., 2004). Thus, analyzing 53BP1 foci as a readout, the activation of ATM and DNA-PKcs after 10 mGy X-rays was assessed in G1-phase NSCs (Figure 4.7). The formation of 53BP1 foci after 10 mGy was found to rely on ATM kinase activity, not DNA-PKs (Figure 4.7). This finding is consistent with the previous studies indicating that ATM is the main kinase to phosphorylate H2AX (Burma, et al., 2001). DNA-PKcs-inhibited NSCs demonstrated similar level of 53BP1 foci as in WT cells (Figure 4.7). This suggests that in the absence of DNA-PKcs, ATM phosphorylates H2AX inducing the formation of 53BP1

foci. In contrast, after 1 Gy X-rays, the similar levels of 53BP1 foci formed in WT, ATM- and DNA-PKcs-inhibited cells (Figure 4.7). This indicated that both kinases become activate after irradiation with high doses of X-rays. However, in ATM-inhibited cells, the 53BP1 foci formed in smaller size than in WT and DNA-PKcs-inhibited conditions. In the absence of ATM, DNA-PKcs phosphorylates H2AX with slightly lower efficiency (Stiff, et al., 2004). This may explain the formation of small 53BP1 foci in ATM-inhibited cells compare to other conditions. The significant reduction in 53BP1 foci level was observed only after inhibition of ATM combined with DNA-PKcs inhibitors. This is in agreement with previous studies reported that ATM-deficiency can be compensated by DNA-PKcs activity (Stiff, et al., 2004).

H_2O_2 pre-treatment

When the IR-induced DSB level is insufficient to activate DSB repair machinery, low levels of oxygen radicals may induce a response that is required for repair (Grudzenski, et al., 2010). Previously, it was shown that H_2O_2 pre-treatment induces an efficient DSB repair in somatic cells by generating oxygen radicals (Grudzenski, et al., 2010). In line with these studies, pre-treatment of NSCs with H_2O_2 enhanced the repair capacity in G1-phase NSCs after irradiation with 10 mGy X-rays (Figure 4.9), whereas, H_2O_2 had no impact on ATM and DNA-PKcs kinase activities (Figure 4.10). ATM is initially an inactive, noncovalently-associated dimer in mammalian cells (Bakkenist, et al., 2003). In response to IR-induced DNA damage, the inactive dimer form of ATM is converted into an active monomer. Unlike irradiation, H_2O_2 generates intra-molecular disulfide bounds between ATM monomers (Gou, et al., 2010). The H_2O_2-activated ATM does not phosphorylate H2AX, which in consequence does not form foci (Gou, et al., 2010). Thus, ATM activation induced by H_2O_2 can take place in the apparent absence of γH2AX or 53BP1 foci formation (Gou, et al., 2010). Altogether, the increase in DSB repair capacity observed in H_2O_2 treated NSCs after 10 mGy X-rays might be explained by the over activation of ATM under oxidative stress. The over activated ATM may compensate for the lack of DNA-PKcs activity and enhance repair in G1 phase. Moreover, H_2O_2 pre-treatment as well as high doses of IR up-regulate a set of genes involved in DSB repair, whereas 10 mGy does not (Grudzenski, et al., 2010). This also might be the reason for elevated DSB repair capacity in H_2O_2 treated cells.

5.2 DSB repair after high X-rays doses

DSB repair in G1 and G2 phase

Similar to somatic cells (DiBiase, et al., 2000; Riballo, et al., 2004), wild type ESCs and NSCs displayed biphasic DSB repair kinetics after 2 Gy X-rays in G1 and G2 phase (Figure 4.11). Moreover, the DSB repair capacity was almost similar in both cell types (Figure 4.11). It was previously reported that the majority of IR-induced DSBs are repaired via c-NHEJ in G1 and G2 phase. However, a subfraction of

breaks localized to heterochromatin is repaired with slow kinetics in an ATM-dependent manner (Jackson, et al., 2009; Lukas, et al., 2013). In heterochromatic regions, DSB repair requires ATM to facilitate the entry of DNA-repair machinery by phosphorylating the transcriptional co-repressor Kruppel-associated box (KRAB)-associated protein-1 (KAP1). This repair pathway represents HR in G2 and a Resection-dependent-NHEJ pathway (Res-dep-NHEJ) in G1 phase (Beucher, et al., 2009; Biehs, et al., 2017). As in somatic cells, inhibition of ATM in ESCs and NSCs revealed that the slow component of DSB repair in G1 and G2 phase stem cells is ATM-dependent (Figure 4.12). The inhibition of ATM induced 40-50 % unrepaired DSBs in ESCs and NSCs (Figure 4.12), whereas in somatic cells, it was reported to induce only 15-20 % (Riballo, et al., 2004; Goodarzi, et al., 2008). This indicated that in stem cells almost half of the IR-induced DSBs are repaired via the slow component of DSB repair in G1 and G2 phase.

In agreement with previous studies demonstrated that DNA-PKcs inhibition stalled DSB repair in somatic cells (Beucher, et al., 2009; Biehs, et al., 2017), inhibition of DNA-PKcs induced a sever repair defect in G1- and G2-phase NSCs after exposure to 2 Gy X-rays (Figure 4.12). Interestingly, in ESCs, DNA-PKcs inhibition induced a transient repair defect (up to 2 h post IR), which was followed by an efficient repair (Figure 4.12). This observation indicated that ESCs are able to minimize the number of IR-induced DSBs in the absence of DNA-PKcs. This result is in line with previous studies reporting that DNA-PKcs inhibition has a small impact on c-NHEJ in ESCs compared to NSCs and differentiated cells (Adams, et al., 2010).

Several studies have indicated that ESCs preferentially employ HR over c-NHEJ (Adams, et al., 2010; Tichy, et al., 2010; Serrano, et al., 2011; Lan, et al., 2012). A central player in HR is Rad51 protein which is involved in the strand-pairing stages and also DNA homology search (Valerie, et al., 2003). Inhibition of Rad51 induced a significant repair defect in G2-phase NSCs after irradiation with 2 Gy X-rays, as it was expected (Figure 4.13). This effect was identical to the impact of ATM inhibition on DSB repair in G2 phase (Figure 4.13). This indicated that both ATM and Rad51 are involved in HR. Surprisingly, despite to the fact that HR is the predominant repair pathway in G2-phase ESCs, inhibition of Rad51 did not show any impact on DSB repair in G2-phase ESCs (Figure 4.13). Since HR is not available in G1 phase (Orthwein, et al., 2015), inhibition of Rad51 did not have any effect on DSB repair in G1-phase ESCs and NSCs. However, the repair defect induced by ATM inhibitor confirmed the role of ATM in the slow component of DSB repair in G1-phase ESCs and NSCs (Figure 4.13).

Upon DSB induction, Rad51 protein re-localizes to distinct foci around the DSB sites (Sung, et al., 2003; Sinha, et al., 2008). Analysis of Rad51 foci formation after 2 Gy X-rays in G2 phase revealed that, in an ATM dependent manner, Rad51 foci were formed faster and in a higher level in ESCs than in NSCs and MEFs (Figure 4.14). This observation is in line with previous studies demonstrated that Rad51 protein level in ESCs is higher than in more differentiated cells, e.g. MEFs (Tichy, et al., 2010;

Serrano, et al., 2011). In contrast to G2 phase, Rad51 foci were not detected in G1-phase cells (data not shown). This determined the lack of HR in G1-phase stem cells. The higher level of Rad51 foci in ESCs compared to NSCs and MEFs indicated that the usage of HR is reduced through cell differentiation, as shown in previous studies (Adams, et al., 2010; Tichy, et al., 2010).
Then we asked whether the efficient DSB repair observed in DNA-PKcs- and Rad51-deficient ESCs was provided by an alternative repair pathway.

alt-NHEJ DSB repair pathway

Previously, it has been described that an alt-NHEJ repair pathway operates in the absence of Ku protein (a c-NHEJ core factors) in somatic cells (Mansour, et al., 2013). Several proteins are involved in this DSB repair pathway including PARP1, Ligase I, Ligase III and Pol θ (Audebert, et al., 2004; Liang, et al., 2008; Mansour, et al., 2010; Mateos-Gomez, et al., 2015). Inhibition of PARP1 in DNA-PKcs-deficient ESCs revealed that a substantial fraction of the DSB repair in DNA-PKcs-inhibited cells (Figure 4.12), was performed by a PARP1-dependent repair pathway in G1 and G2 phase (Figure 4.15). Inhibition of PARP1 in DNA-PKcs-deficient NSCs displayed a slight additional repair defect which indicated that the residual repair in these cells might be partially conducted by a PARP1-dependent pathway. Whereas, in DNA-PKcs-deficient MEFs, no additional repair defect was observed after inhibition of PARP1 (Figure 4.15). Moreover, inhibition of PARP1 did not have any effect on the repair capacity in WT and ATM-inhibited cells (Figure 4.15). This observation was consistent with previous studies in which it was defined that PARP1-inhibition has no effect on WT cells (Yang, et al., 2004; Mansour, et al., 2010). PARP1 is also known as a chromatin remodeler (Luijsterburg, et al., 2016), required for employing and the efficient functioning of c-NHEJ and HR repair pathways (Spagnolo, et al., 2012; Zhang, et al., 2015). These functions of PARP1 may facilitate an efficient DSB repair via alt-NHEJ to compensate for the lack of c-NHEJ in ESCs. The decrease in DSB repair capacity in the absence of DNA-PKcs from ESCs to NSCs and MEFs might be caused by an inability to use a PARP1-dependent alt-NHEJ.
The simultaneously inhibition of PARP1 and Rad51 resulted in a substantial repair defect in G2-phase ESCs (Figure 4.16). Whereas, in Rad51-deficient NSCs, no additional repair defect was observed after inhibition of PARP1 (Figure 4.16). This result indicated that ESCs are more flexible in their repair pathway choice and they can compensate for a HR-deficiency using a PARP1-dependent repair pathway. In contrast, NSCs cannot switch to an alt-NHEJ pathway when breaks have been committed to repair via HR.
PARP1-dependent alt-NHEJ is a resection dependent pathway (Ceccaldi, et al., 2015). The formation of Rad51 foci after irradiation in stem cells and differentiated cells displayed an active resection process in G2 phase cells (Figure 4.14). The higher level of Rad51 foci in ESCs than in NSCs and MEFs indicated that more DSBs undergo resection in ESCs than in others cell types. In G1 phase, the

formation of pRPA foci (a resection marker) was observed only after inducing complex DSBs using α-particles or very high doses of X-rays (Barton, et al., 2014; Biehs, et al., 2017). In line with these studies, using laser micro-irradiation, the accumulation of pRPA foci at the DNA break sites has been observed in G1-phase HeLa cells (Figure 4.17). In stem cells, analyzing pRPA foci after 2 Gy X-rays uncovered that ESCs, but not NSCs, form pRPA foci in G1 phase (Figure 4.19a). Similar to what was observed for Rad51 foci in G2-phase ESCs (Figure 4.14), the highest level of pRPA foci in G1 phase was observed at 1 h post IR (Figure 4.19a). This observation suggests that the maximum level of resection in G1- and G2-phase ESCs takes place within 1 h after 2 Gy X-rays irradiation. Then, these DSBs are committed to repair via resection dependent pathways. It is worth to note that pRPA foci analysis in another murine ESC line (ESCs iB10) confirmed the formation of pRPA foci in G1-phase ESCs (Figure 4.20).

Inhibition of resection, using PLK3-inhibitor, abolished the formation of pRPA foci in G1-phase ESCs (Figure 4.21a). In addition, the formation of pRPA tracks generated by laser micro-irradiation in HeLa cells was diminished after CtIP down regulation (Figure 4.18). These results are consistent with previous studies reporting that the formation of pRPA foci was abolished after inhibition of resection in G1 phase (Barton, et al., 2014; Biehs, et al., 2017). Furthermore, inhibition of resection hindered DSB repair in G1-phase ESCs (Figure 4.21b), where as in HeLa cells, no repair defect was observed (Figure 4.33b). As it was suggested by Biehs et al., HeLa cells by utilizing a resection-independent c-NHEJ compensate for the lack of resection in G1 phase (Biehs, et al., 2017), whereas in ESCs, resection is apparently crucial for DSB repair and its failure cannot be compensated by other repair pathways.

These findings were interpreted in a way that the PLK3-dependent repair pathway plays a more prominent role in the DSB repair of G1-phase ESCs than it does in differentiated cells. Furthermore, the similar repair impairment induced by PLK3- and ATM-inhibitors (Figure 4.21b; Figure 4.12), validated that the slow component of DSB repair in G1-phase ESCs is a resection-dependent pathway.

Ceccaldi et al. showed that when resection has been occurred, HR and alt-NHEJ may compete with each other to repair DSBs in G2 phase. Once HR is impeded, PARP1 may serve as a platform for employing alt-NHEJ factors (Ceccaldi, et al., 2016). In G1- and G2-phase ESCs, since the majority of DSBs undergo resection, in the absence of classical DSB repair pathways, PARP1-dependent alt-NHEJ takes the advantage of resected DNA-ends and promotes an efficient repair (Figure 5.1).

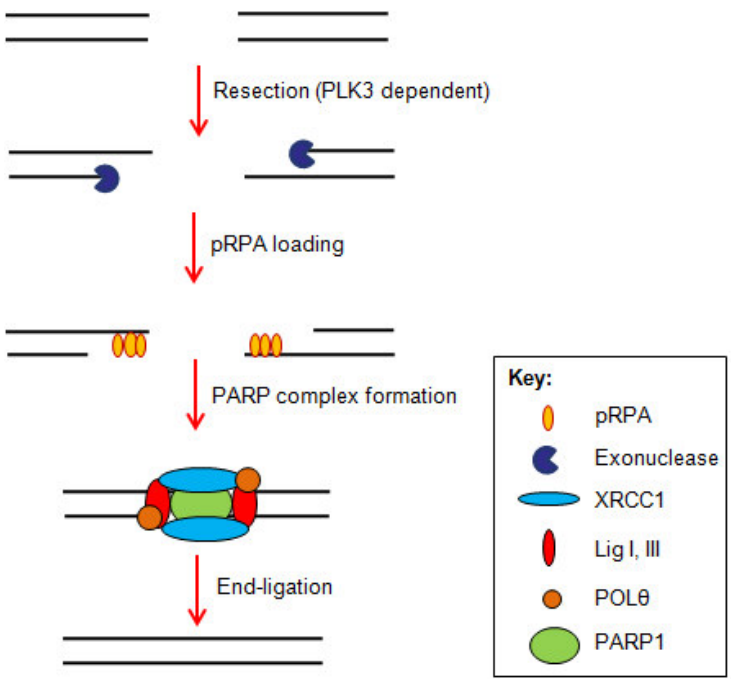

Figure 5.1. Model for the mechanism of PARP1-dependent alt-NHEJ in G1- and G2-phase ESCs. In the absence of classical DSB repair pathways, following resection, the pRPA-coated ssDNA is used as a platform for recruiting PARP1-dependent alt-NHEJ factors. The DNA-ends are re-joined via PARP1-dependent alt-NHEJ.

Role of Artemis in resection dependent DSB repair in G1 phase

Rieballo et al. demonstrated that Artemis is a downstream component of the ATM signaling pathway which is involved in the slow component of DSB repair (Riballo, et al., 2004). In addition, Artemis and CtIP function in the same repair pathway in G1 phase of somatic cells (Biehs, et al., 2017). Consistent with the model proposed by Löbrich and Jeggo (Figure 5.2), following resection in G1 phase, the single strand overhangs fold back into the DNA-PKcs to form an intermediate hairpin structure. To complete the repair process, Artemis is required to open up the loop (Biehs, et al., 2017). Depletion of Artemis in ESCs did not have any impact on repair kinetics in G1 phase (Figure 4.22b), whereas, consistent with previous studies (Biehs, et al., 2017), Artemis siRNA let to a higher residual γH2AX foci level at 8 h post 2 Gy X-rays in G1-phase HeLa cells (Figure 4.22a). The repair impairment induced by Artemis depletion in G1-phase HeLa cells was rescued by CtIP down-regulation (Biehs, et al., 2017). This indicated that in somatic cells, the main distinction between resection initiation factors, e.g. CtIP, and Artemis is that DSBs are repaired without resection initiation factors but remain unrepaired without Artemis. The lack of CtIP may prevent the initiation of resection but allows resection-independent c-NHEJ to repair DSBs. In contrast, loss of Artemis prevents downstream c-NHEJ usage.

In addition, the nuclease activity of Artemis is required for pRPA foci formation in G1-phase somatic cells (Biehs, et al., 2017). Consistent with this study, Artemis siRNA diminished the formation of pRPA foci in G1-phase ESCs (Figure 4.22c). This indicated that Artemis is involved in the resection process in G1-phase ESCs.

Taken together, Artemis regulates pRPA foci formation in G1-phase ESCs and HeLa cells. Nevertheless, the mechanistic role of this protein in DSB repair in G1-phase ESCs is unclear.

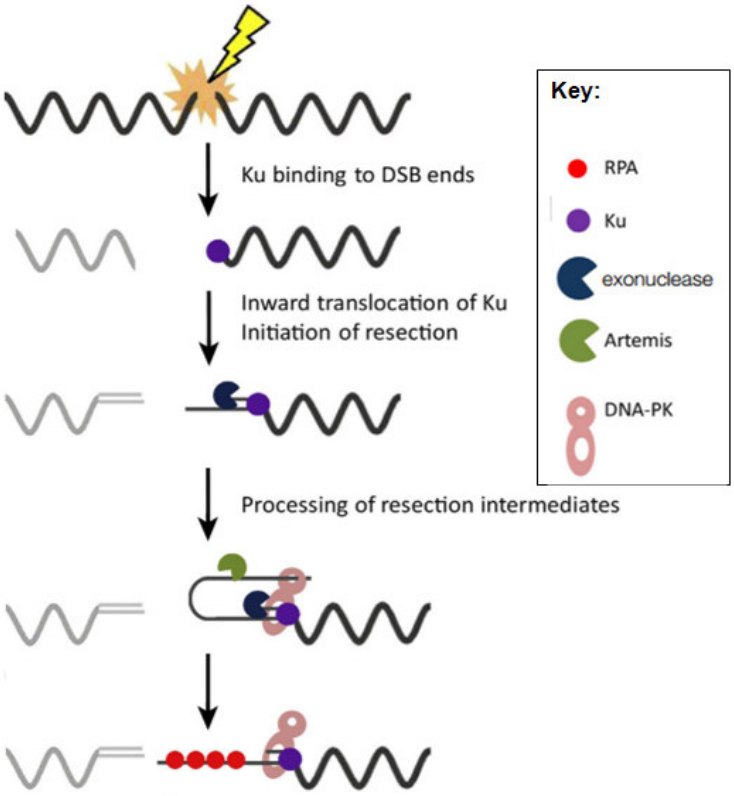

Figure 5.2. Model for the role of Artemis in resection-dependent c-NHEJ in G1-phase somatic cells. The inward translocation of Ku from DNA-ends facilitates resection at damage sites. Then, the single strand overhang might be captured by a channel in DNA-PKcs, to generate a hairpin structure, which requires resolution by Artemis to complete the process. The loading of pRPA on ss-DNA and downstream repair require Artemis and might be prevented by the hairpin intermediate (Modified from Löbrich and Jeggo 2017).

5.3 Involvement of RNA in resection dependent DSB repair

The presence of RNA at sites of DSB has been detected by several studies (Francia, et al., 2012; Wei, et al., 2012; Lee, et al., 2012). Using S9.6, a specific antibody to detect RNA-DNA hybrids (Boguslawski, et al., 1986; Ginno, et al., 2012), the formation of RNA-DNA hybrids at the break sites was confirmed in ESCs and HeLa cells (Figure 4.23a). This observation was evaluated by measuring the signal intensity of the γH2AX and S9.6 foci (Figure 4.23a). Quantification of the γH2AX foci overlaid with S9.6 at 15 min post 2 Gy X-rays, revealed that only 14 % of all IR-induced DSBs in G1-phase ESCs and HeLa cells contained RNA (Figure 4.23b). This indicates that the RNA-DNA hybrids do not form at all break sites and a big fraction of DSBs is repaired in an RNA-independent manner, especially in the first 2 h post IR. The increase in co-localization level of γH2AX and S9.6 foci from 15 min to 2 h post IR in both cell types suggests that the formation of RNA-DNA hybrids at the DSB sites is a slow process and probably needs some pre-processing. In addition, the higher level of γH2AX and

S9.6 foci overlapping at 2 h post IR in ESCs than in HeLa cells points towards a crucial role of RNA in DSB repair of ESCs with respect to differentiated cells (Figure 4.23b).

The formation of RNA-DNA hybrids may also take place in a DNA-damage independent manner during natural processes in the cells, e.g. transcription and R-Loop formation (Bhatia, et al., 2014; Nguyen, et al., 2017). This may explain the formation of abundant S9.6 foci out of the γH2AX focus in the cells (Figure 4.23a). In addition, the formation of S9.6 tracks overlapping with γH2AX tracks generated by laser micro-irradiation verified the accumulation of S9.6 at DSB sites, as well as the specificity of the antibody (Figure 4.24).

The involvement of RNA-DNA hybrids in DSB repair process has been defined differently in various organisms. Several studies proposed that the small non-coding RNAs play role in DSB repair by directing chromatin modification and also recruiting repair proteins to the DSB sites (Lee, et al., 2009; Wei, et al., 2012; Francia, et al., 2012; Chowdhury, et al., 2013; Ohsawa, et al., 2013). In addition, the role of transcript RNAs as template to restore damaged sequences in yeast was shown in previous studies (Shen, et al., 2011; Keskin, et al., 2014). In mammalian cells, the RNA-templated DSB repair was described recently (Chakraborty, et al., 2016). These studies suggested that nascent transcripts provide the missing genetic information for restoring the original sequence at the DSB sites. The presence of RNA at DSB site, which we observed by co-localization of S9.6 with γH2AX (Figure 4.23a; Figure 4.24), indicates an active transcription at the break sites. The transcripts might be transcribed before DNA damage induction and hybridized with ssDNA to form RNA-DNA hybrids in the course of DSB repair. Alternatively, transcription might be stimulated by DSB induction using ssDNA as templates to form fresh RNA at the damage sites. Ohle et al. demonstrated that the transcription was initiated after DSB induction and nascent transcripts were produced by RNA Pol II (Pol II) using 3' ssDNA overhangs as templates (Ohle, et al., 2016). This process requires the initial step of DNA-end resection, which generates short ssDNA segments (Ohle, et al., 2016). Consistent with this study, inhibition of resection, using PLK3 inhibitor, abolished the accumulation of S9.6 foci at γH2AX laser tracks in G1-phase HeLa cells (Figure 4.25a). Furthermore, inhibition of PLK3 reduced the number of S9.6 foci overlapping with γH2AX foci after 2 Gy X-rays in G1-phase ESCs and HeLa cells (Figure 4.25b). This effect was more apparent at 2 h post IR than 15 min. The rapid formation of S9.6 foci at the DSB sites can be partially explained by the fact that the phosphorylation of CtIP initiates upon IR and continuously enhances until 2 h post IR (Barton, et al., 2014). The small proportion of phosphorylated CtIP and consequently the short range of resection at 15 min post IR might be sufficient for the formation of RNA-DNA hybrids. These observations indicated that the formation of RNA-DNA hybrids at DSB sites is a resection dependent process.

RNaseH1 is a ribonuclease which degrades RNA-DNA hybrids by cleaving the RNA moiety (Cerritelli, et al., 2009; Aguilera, et al., 2012). Previously it has been reported that the overexpression of RNaseH1 enzyme degrades RNA-DNA hybrids and reduces S9.6 signal (Paulsen, et al., 2009; Stirling,

et al., 2012; Chakraborty, et al., 2016; Ohle, et al., 2016). In agreement with these studies, after laser micro-irradiation, HeLa cells transfected with a plasmid containing RNaseH1 did not form S9.6 tracks at the damage sites (Figure 4.26). In addition, the DNA-damage-independent S9.6 foci were also eliminated in these cells. This data confirmed that the formation of S9.6 foci is a dynamic biological process in the cells and the antibody specifically recognizes the DNA-bound RNAs.

There are lines of evidence to support the role of RNaseH1 as an essential factor for efficient DSB repair. In yeast, deletion of the *RNaseH1* gene caused hypersensitivity to DNA damage (Lazzaro, et al., 2012). In addition, Ohle et al. observed a strong delay in DSB repair in yeast when overexpressing RNaseH1 (Ohle, et al., 2016). In line with these studies, overexpression of RNaseH1 impaired DSB repair from 2 h post IR in G1-phase ESCs, whereas, in HeLa cells repair kinetics were not affected (Figure 4.27b). An explanation of this observation could be that the formation of RNA-DNA hybrids was not required for DSB repair in G1-phase HeLa cells. Alternatively, it is possible that the lack of RNA-DNA hybrids was compensated by a resection-independent c-NHEJ; similar to what was observed after inhibition of resection in G1-phase HeLa cells (Biehs, et al., 2017). Furthermore, the repair defect induced by Artemis siRNA in WT HeLa cells was not observed in RNaseH1 overexpressed cells (Figure 4.29). These results suggest that RNA-DNA hybrids are involved in the pre-resection process in G1-phase cells.

In ESCs, inhibition of PLK3 after overexpression of RNaseH1 rescued the repair defect induced by destabilization of RNA-DNA hybrids in G1 phase (Figure 4.28). This result is consistent with the previous model which proposed that RNA-DNA hybrids are required for the initiation of long-range resection (Ohle, et al., 2016). In this model, Pol II takes the advantage of the initial step of resection and binds to the short ssDNA segment generated by a CtIP/PLK3-dependent process. In a second step, Pol II initiates transcription around the DSB sites. During transcription elongation, Pol II machinery employs the chromatin remodelers to open up the chromatin ahead of the transcription bubble (Figure 2.5). The length of resection depends on the length of the Pol II translocation (Ohle, et al., 2016). The inhibition of Pol II significantly diminished the formation of pRPA foci in G1-phase ESCs (Figure 4.31). This finding proves the involvement of Pol II in the extent of resection and formation of pRPA in G1-phase ESCs. During resection, due to the lack of a non-homologous DNA strand, the nascent RNA would be more prone to re-hybridize with the single strand-template DNA, directly competing with the recruitment of the RPA (Ohle, et al., 2016). The formation of RNA-DNA hybrids leads to stalling of Pol II and termination of transcription (Skourti-Stathaki, et al., 2014; Zhao, et al., 2016). Furthermore, the DNA-bound RPA molecules stimulate the activity of the RNaseH1 enzyme resulting in the degradation of RNA (Petzold, et al., 2015). The overexpression of RNaseH1 changed the pattern of pRPA foci formation in G1-phase ESCs. At 1 h post 2 Gy X-rays, the formation of pRPA foci was diminished in RNaseH1 transfected cells (Figure 4.30a). Consistent with the previous studies showing that RPA foci

is increased after RNaseH1 overexpression (Ohle, et al., 2016), the level of pRPA foci has been increased up to 4 h post IR in G1-phase ESCs (Figure 4.30a). Upon RNaseH1 overexpression, Pol II transcription machinery probably moves slowly through ssDNA. In this scenario the nascent transcripts cannot bound to the template strand and form RNA-DNA hybrids. During this slow but continuously translocation of Pol II, the ssDNA-end will be covered by pRPA.

Despite the fact that the RNA-DNA hybrids regulate long-range resection in the cells (Ohle, et al., 2016), the formation of pRPA foci after 2 Gy X-rays was only observed in G1-phase ESCs (Figure 4.19). Presumably, the translocation of Ku protein after damage induction controls the length of DNA-end resection. On the molecular level, upon DNA break, the Ku70/80 heterodimer binds to the DNA-ends. Then, the DNA-bound Ku recruits the protein kinase DNA-PKcs to the DSB sites to form the DNA-PK holoenzyme (Yoo, et al., 1999; Ma, et al., 2001). DNA-PK (Ku together with DNA-PKcs) is a barrier at the DNA-ends that prevents repair (Mahaney, et al., 2013). Phosphorylation of DNA-PKcs at T2609 cluster leads to a conformational shift that induces DNA-PK dissociation from DNA-ends. This increases the access of other repair proteins to the DSB sites (Merkle, et al., 2002; Ding, et al., 2003). Biehs et al. showed that Ku remains bound to DSBs during resection in G1 phase. In addition, the inward translocation of Ku along DNA is essential for resection and pRPA foci formation in G1 phase (Biehs, et al., 2017).

We proposed a model that attempts to reconcile our observations in the light of published data about the role of RNA in resection (Figure 5.3). Based on our model, the initial steps of resection in G1 phase are similar in ESCs and HeLa cells. Upon translocation of Ku and initiation of resection, Pol II binds to the small ssDNA-ends and start transcription at the DSB sites. In ESCs, the transcription machinery uses the advantage of Ku long relocation and promotes an excessive resection. Next, the nascent transcripts hybridize to the single strand template-DNA in competing with RPA and forming RNA-DNA hybrids. After degradation of RNA by RNaseH1, the extra-long ssDNA fragments will be fully covered by pRPA. These pRPA prevent the formation of hairpin at the DNA-ends (Chen, et al., 2013). In HeLa cells, the elongation of transcription and eventually the extension of resection is limited by Ku. After removal of RNA by RNaseH1 enzyme, since the resected DNA-ends are not long enough to be covered by pRPA and form a focus, the short single strand overhang folds into the DNA-PK and forms a hairpin structure. Next, to complete repair, Artemis chops off the loop. Cutting off the hairpin structure by Artemis may cause the unwanted removal of some nucleotides. In ESCs, since the long ssDNA-ends are covered by nascent RNA and pRPA, the formation of a hairpin is not possible, or inessential, for these cells. Consistent with this model, depletion of Artemis did not impair repair kinetics in G1-phase ESCs, whereas in HeLa cells did (Figure 4.22a; Figure 4.22b). This data indicates that Artemis activity is unnecessary for DSB repair in G1-phase ESCs.

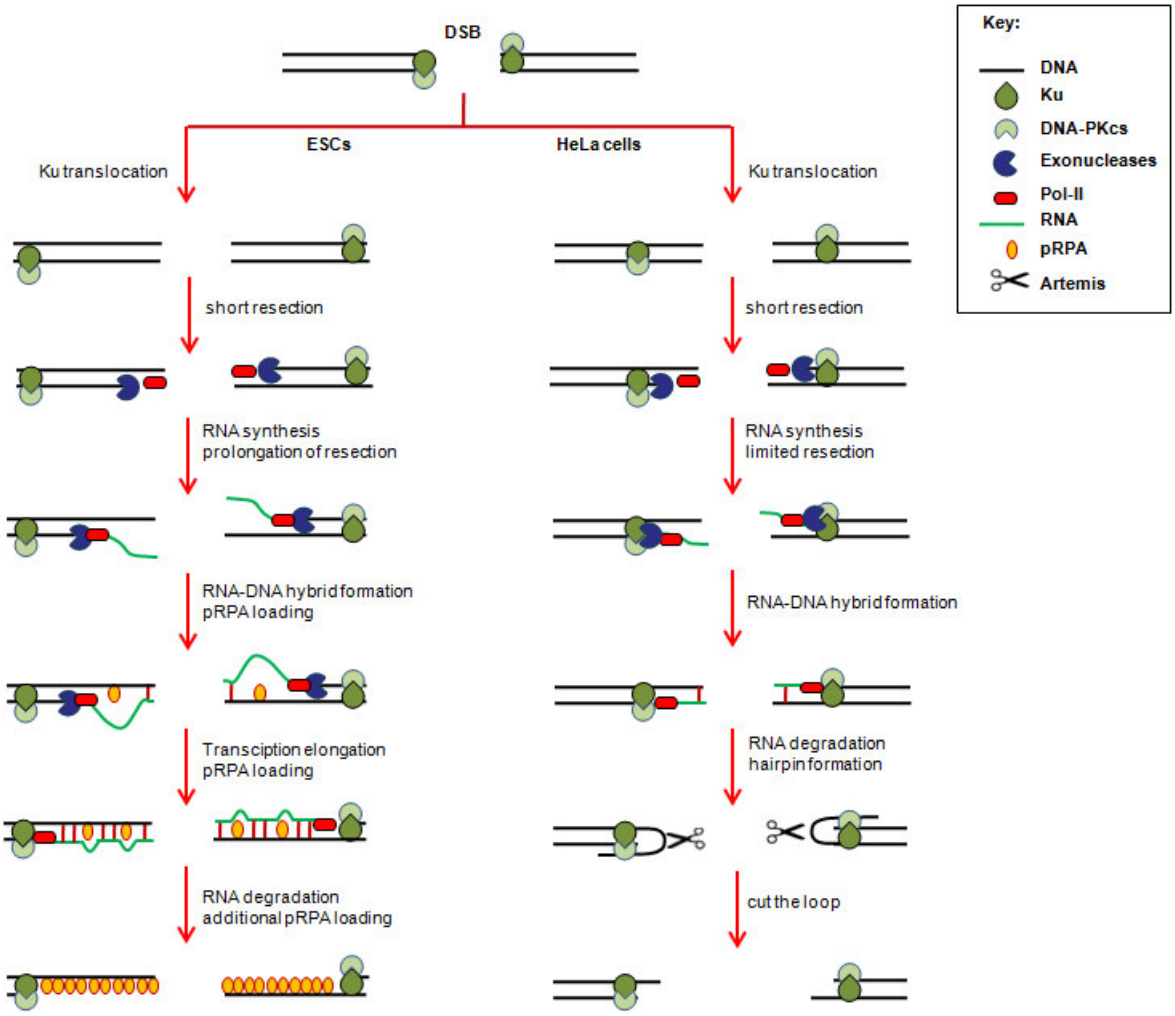

Figure 5.3. Model for the mechanism of resection in G1-phase ESCs vs. HeLa cells. In the slow component of DSB repair in G1 phase, both cell types generate small segments of ssDNA via a CtIP/PLK3-dependent resection process. Upon short resection, RNA Pol II binds to the single strand overhang and initiates transcription. The decondensation of the chromatin during transcription elongation promotes an extended DNA resection process. Presumably, in HeLa cells, the short translocation of the Ku protein prohibits the extension of transcription and consequently prevents long resection. After degradation of the RNA molecule, ssDNA folds into DNA-PK and forms a loop. Next, the loop will be opened by the Artemis endonuclease activity. The short length of ssDNA-ends in HeLa cells are not sufficient to be covered by pRPA. In contrast, in ESCs, the long movement of Ku along DNA facilitates transcription elongation and resection prolongation. During resection, the single strand overhang binds to the transcribed RNA and RPA. DNA-bound RPA activates RNaseH1 which cleaves RNA from RNA-DNA hybrids. After degradation of RNA, to protect the nucleotides and perhaps to promote further repair, the long ssDNA will be covered by pRPA.

The short length of G1 phase and the lack of G1/S checkpoint in ESCs, increases the risk of mutation in these cells. Using a fast and robust DNA repair machinery, ESCs minimize the level of mutations and maintain genomic integrity (Maynard, et al., 2008; Tichy, et al., 2010). Prolongation of resection by employing the transcription machinery in G1 phase, instead of forming a hairpin, is presumably part of a highly efficient and reliable DSB repair machinery in ESCs. In G1-phase HeLa cells, the processing of ssDNA-ends facilitates the ligation of these ends. This repair pathway is potentially error-prone and may induce chromosomal translocations (Biehs, et al., 2017).

Since the mechanism of how ESCs repair long ssDNA-ends in G1 phase is unclear, we proposed three possible ways through by repair can be proceeded (Figure 5.4). In G2 phase, the microhomology-mediated repair pathway (MMR), is known as a backup repair pathway for HR (Chiruvella, et al., 2013). MMR shares the initial steps of DNA-end resection with HR (Truong, et al., 2013). The long stretched of ss-DNA-ends covered by pRPA in G1-phase ESCs, raised the possibility that MMR mediates DSB repair in these cells (Figure 5.4a). In this repair pathway, the exposed complementary sequences on both sides of the DSBs closely move and perform annealing to form an intermediate with 3´-flaps and gaps. Then, the gaps are filled in by a DNA polymerase which stabilizes the annealed intermediate (Wang, et al., 2017). Since MMR is an error prone repair pathway and contributes to genomic instabilities (Rai, et al., 2010; Simsek, et al., 2010), the usage of this repair pathway by ESCs is highly unlikely. As a second possible way for repair, we proposed that the missing sequence at resected DNA-ends might be restored by DNA-polymerase activity (Figure 5.4b). In this model, following resection, a DNA polymerase binds to the 5'-DNA-ends and initiates 5'—>3' DNA synthesis at the DSB sites (similar to the Okazaki fragments). As there is no template sequence available to recover the nucleotides missing between the break ends, after restoration of the resected sequences, the DNA-end ligation will take place resulting in some nucleotides deletion. Therefore, as this pathway might potentially lead to the loss of genomic information, it might not be the ideal repair pathway for accurate repair in ESCs. For a faithful DSB repair in G1-phase ESCs, we proposed a novel model in which RNA may play a prominent role (Figure 5.4c). In this model, the RNA transcribed immediately before DSB induction (at the same or second allele), provides a template to restore the missing information at the resected DNA and also between the DNA-ends via a reverse transcription process. In this pathway, the reverse transcriptase (RT) enzyme promotes the synthesis of a new DNA-strand from the template-RNA. Since the transcript contains the backup information identical to the damaged DNA, the restoration of the original sequence will take place at a high fidelity level. The RNA-templated DSB repair in yeast and mammalian cells was recently shown by other group (Mazina et al., 2017). In addition, previous studies reported that RT is physiologically activated in the early stages of embryogenesis, whereas, in differentiated cells RT activity is repressed (Pittoggi, et al., 2003; Garcia-Perz, et al., 2007; Sciamanna, et al., 2016).

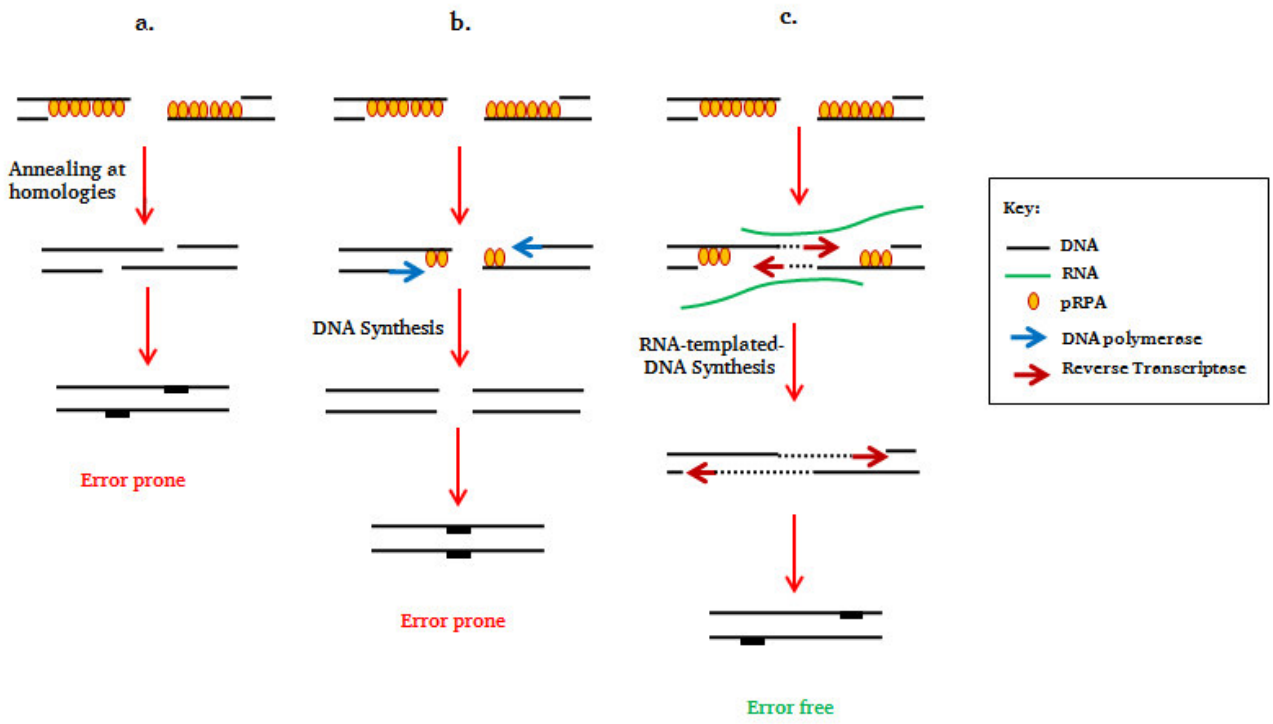

Figure 5.4. Model for DSB repair following resection in G1-phase ESCs. Following an extensive resection in G1-phase ESCs, DSBs might be repaired via three plausible repair mechanisms: a. The DSB repair is boosted by microhomologous sequences. In this model, after annealing of complementary nucleotides located at each DNA-end, the remaining gap will be filled in by a DNA-polymerase. The annealing of homologous sequences might cause genetic rearrangement. b. The single strand overhangs may be used as a template by DNA polymerases to restore the resected sequences. As there is no template available to restore the damaged nucleotides between the DNA-ends, the ligation will take place with some base deletion. c. The RNA, which is transcribed before damage induction, will be used as a template to restore the missing sequence by reverse transcriptase. Since the transcript contains the entire genetic information at the DSB site, it can bridge the gap between the DNA-ends and restore the missing sequence. In this model, since the whole nucleotide sequence will be recovered by reverse transcription, the repair is error free.

To gain further insight into the role of RNA in regulating resection in G1 phase, we focused on DDX1, a protein that identified as a factor required for unwinding the RNA-DNA hybrids (Li, et al., 2008). DDX1 is recruited to the DSBs containing RNA-DNA hybrids (Li, et al., 2008). Analyzing DDX1 foci after 2 Gy X-rays in G1- and G2-phase HeLa cells revealed that rapidly after irradiation, DDX1 foci formed at a subset of DSBs (Figure 4.32b). This observation is in line with previous studies indicating that DDX1 accumulates at 30 % of DSB sites and forms IR-induced foci (Li, et al., 2008). The correlation between DDX1 and γH2AX kinetics at late time points after IR revealed that DDX1 is involved in the slow component of DSB repair (Figure 4.32b). This is in accordance with the previous report suggesting that DDX1 is involved in HR (Li, et al., 2016). It has been observed that the depletion of DDX1 impaired DSB repair at 8 h post IR in G1 phase (Figure 4.34c). These data implied that DDX1 has a role in the slow component of DSB repair not only in G2 phase but also in G1. Since the DDX1 protein is involved in different biological processes in the cell, e.g. RNA metabolism (Chou, et al., 2013), the DSB repair impairment observed in DDX1 depleted cells might not be induced directly by irradiation.

Then, we asked whether the formation of DDX1 foci at DSB sites resides downstream of DNA-end resection. To answer this question, resection was deactivated in HeLa cells using CtIP siRNA. Reduction in the level of DDX1 foci after depletion of CtIP (Figure 4.33a), revealed that the formation of DDX1 foci in G1 phase relies on resection. Furthermore, after combination of PLK3 inhibitor and DDX1 siRNA, it was observed that the repair defect induced by DDX1 siRNA in G1-phase HeLa cells was rescued by inhibition of PLK3 (Figure 4.35). In addition, the repair impairment induced by DDX1 siRNA was abolished in RNaseH1 overexpressed G1-phase cells (Figure 4.36). These results revealed that DDX1 is not involved in the initial steps of resection and in the absence of resection initiation factors or RNA-DNA hybrids, the DDX1 function is not required for DSB repair in G1-phase.

The work performed during this thesis has been devoted to the characterization of DSB repair in ESCs and NSCs. Our results revealed a higher DSB repair capacity in ESCs than in NSCs and differentiated cells. By employing the transcription machinery, ESCs are able to perform long-range DNA-end resection and, thereby, they are prone to use resection-dependent repair pathways. These novel findings not only extend our understanding of DNA repair mechanism in stem cells but also have broader implications of the genetic conservation during embryonic development in mammals.

6 References

Adachi, K., Suemori, H., Yasuda, S., Nakatsuji, N., & Kawase, E. (2010). *Role of SOX2 in maintaining pluripotency of human embryonic stem cells.* Genes Cells, (5), S. 455-469.

Adams, B., Golding, S., Rao, R., & Valerie, K. (2010). *Dynamic dependence on ATR and ATM for double-strand break repair in human embryonic stem cells and neural descendants.* PLoS One, (4), S. E10001.

Aguilera, A., & García-Muse, T. (2012). *R loops: from transcription byproducts to threats to genome stability.* Mol Cell., (2), S. 115-124.

Audebert, M., Salles, B., & Calsou, P. (2004). *Involvement of poly(ADP-ribose) polymerase-1 and XRCC1/DNA ligase III in an alternative route for DNA double-strand breaks rejoining.* J Biol Chem., (53), S. 55117-55126.

Averbeck, N., Ringel, O., Herrlitz, M., Jakob, B., Durante, M., & Taucher-Scholz, G. (2014). *DNA end resection is needed for the repair of complex lesions in G1-phase human cells.* Cell Cycle, (16), S. 2509-2516.

Bakkenist, C., & Kastan, M. (2003). *DNA damage activates ATM through intermolecular autophosphorylation and dimer dissociation.* Nature, (6922), S. 499-506.

Bakr, A., Oing, C., Köcher, S., Borgmann, K., Dornreiter, I., Petersen, C., et al. (2015). *Involvement of ATM in homologous recombination after end resection and RAD51 nucleofilament formation.* Nucleic Acid Re., (6), S. 3154-3166.

Barton, O., Naumann, S., Diemer-Biehs, R., Künzel, J., Steinlage, M., Conrad, S., et al. (2014). *Polo-like kinase 3 regulates CtIP during DNA double-strand break repair in G1.* J Cell Biol., (7), S. 877-894.

Baumann, P., Benson, F., & West, S. (1996). *Human Rad51 protein promotes ATP-dependent homologous pairing and strand transfer reactions in vitro.* Cell, (4), S. 757-766.

Behrens, A., van Deursen, J., Rudolph, K., & Schumacher, B. (2014). *Impact of genomic damage and ageing on stem cell function.* Nat Cell Biol., (3), S. 201-207.

Beucher, A., Birraux, J., Tchouandong, L., Barton, O., Shibata, A., Conrad, S., et al. (2009). *ATM and Artemis promote homologous recombination of radiation-induced DNA double-strand breaks in G2.* EMBO J., (21), S. 3413-3427.

Bhatia, v., Barroso, S., García-Rubio, M., Tumini, E., Herrera-Moyano, E., & Aguilera, A. (2014). *BRCA2 prevents R-loop accumulation and associates with TREX-2 mRNA export factor PCID2.* Nature, (7509), S. 362-365.

Biehs, R., Steinlage, M., Barton, O., Juhász, S., Künzel, J., Spies, J., et al. (2017). *DNA Double-Strand Break Resection Occurs during Non-homologous End Joining in G1 but Is Distinct from Resection during Homologous Recombination.* Mol Cell., (4), S. 671-684.

Blampain, C., & Simons, B. (2013). *Unravelling stem cell dynamics by lineage tracing.* Nat Rev Mol Cell Biol., (8), S. 489-502.

Blanpain, C., Mohrin, M., Sotiropoulou, P., & Passegue, E. (2011). *DNA-damage response in tissue-specific and cancer stem cells.* Cell Stem Cell, (1), S. 16-29.

Boguslawski, S., Smith, D., Michalak, M., Mickelson, K., Yehle, C., Patterson, W., et al. (1986). *Characterization of monoclonal antibody to DNA.RNA and its application to immunodetection of hybrids.* J Immunol Methods, (1), S. 123-130.

Boiani, M., & Schöler, H. (2005). *Regulatory networks in embryo-derived pluripotent stem cells.* Nat Rev Mol Cell Biol., (11), S. 872-884.

Burma, S., Chen, B., Murphy, M., Kurimasa, A., & Chen, D. (2001). *ATM phosphorylates histone H2AX in response to DNA double-strand breaks.* J Biol Chem., (45), S. 42462-42467.

Cannavo, E., & Cejka, P. (2014). *Sae2 promotes dsDNA endonuclease activity within Mre11-Rad50-Xrs2 to resect DNA breaks.* Nature, (7520), S. 122-125.

Cauffman, G., Van de Velde, H., Liebaers, I., & Van Steirteghem, A. (2005). *Oct-4 mRNA and protein expression during human preimplantation development.* Mol Hum Reprod., (3), S. 173-181.

Ceccaldi, R., Rondinelli, B., & D'Andrea, a. (2016). *Repair Pathway Choices and Consequences at the Double-Strand Break.* Trends Cell Biol., (1), S. 52-64.
Cerritelli, S., & Crouch, R. (2009). *Ribonuclease H: the enzymes in eukaryotes.* FEBS J., (6), S. 1494-1505.
Cervantes, R., Stringer, J., Shao, C., Tischfield, J., & Stambrook, P. (2002). *Embryonic stem cells and somatic cells differ in mutation frequency and type.* Proc Natl Acad Sci USA., (6), S. 3586-3590.
Chakraborty, A., Tapryal, N., Venkova, T., Horikoshi, N., Pandita, R., Sarker, A., et al. (2016). *Classical non-homologous end-joining pathway utilizes nascent RNA for error-free double-strand break repair of transcribed genes.* Nat Commun., (7), S. 13049.
Chen, H., Lisby, M., & Symington, LS. (2013). *RPA Coordinates DNA End Resection and prevents Formation of DNA Hairpins*. Mol Cell., (50), S. 589-600.
Chiruvella, K., Liang, Z., & Wilson, T. (2013). *Repair of Double-Strand Breaks by End Joining.* Cold Spring Harb Perspect Biol., (5), S. a012757.
Chou, C., Lin, W., Lin, C., Luber, C., Godbout, R., Mann, M., et al. (2013). *DEAD box protein DDX1 regulates cytoplasmic localization of KSRP.* PLoS One., (9), S. e73752.
Chowdhury, D., Choi, Y., & Brault, M. (2013). *Charity begins at home: non-coding RNA functions in DNA repair.* Nat Rev Mol Cell Biol., (3), S. 181-189.
Collis, S., Schwaninger, J., Ntambi, A., Keller, T., Nelson, W., Dillenhay, L., et al. (2004). *Evasion of early cellular response mechanisms following low level radiation-induced DNA damage.* J Biol Chem., (48), S. 49624-49632.
Conti, L., Pollard, S., Gorba, T., Reitano, E., Toselli, M., Biella, G., et al. (2005). *Niche-independent symmetrical self-renewal of a mammalian tissue stem cell.* PLoS One., (9), S. e283.
Deckbar, D., Jeggo, P., & Löbrich, M. (2011). *Understanding the limitations of radiation-induced cell cycle checkpoints.* Crit Rev Biochem Mol Biol., (4), S. 271-283.
Deriano, L., & Roth, D. (2013). *Modernizing the nonhomologous end-joining repertoire: alternative and classical NHEJ share the stage.* Annu Rev Genet., (47), S. 433-455.
Dianov, G., & Parsons, J. (2007). *Co-ordination of DNA single strand break repair.* DNA Repai (Amst), (4), S. 454-460.
DiBiase, S., Zeng, Z., Chen, R., Hyslop, T., Curran, W., & Iliakis, G. (2000). *DNA-dependent protein kinase stimulates an independently active, nonhomologous, end-joining apparatus.* Cancer Res., (60), S. 1245-1253.
Ding, Q., Reddy, Y., Wang, W., Woods, T., Douglas, P., Ramsden, D., et al. (2003). *Autophosphorylation of the catalytic subunit of the DNA-dependent protein kinase is required for efficient end processing during DNA double-strand break repair.* Mol Cell Biol., (23), S. 5836-5848.
Doege, C., Inoue, K., Yamashita, T., Rhee, D., Travis, S., Fujita, R., et al. (2012). *Early-stage epigenetic modification during somatic cell reprogramming by Parp1 and Tet2.* Nature, (488), S. 652-655.
Dolezalova, D., Mraz, M., Barta, T., Plevova, K., Vinarsky, V., Holubcova, Z., et al. (2012). *MicroRNAs regulate p21(Waf1/Cip1) protein expression and the DNA damage response in human embryonic stem cells.* Stem Cells, (30), S. 1362-1372.
Dunne-Daly, C. (1999). *Principles of radiotherapy and radiobiology.* Semin Oncol Nurs., (4), S. 250-259.
Elf, J. (2016). *Hypothesis: Homologous Recombination Depends on Parallel Search.* Cell Syst., (), S. 325-327.
Fan, J., Robert, C., Jang, Y., Liu, H., Sharkis, S., Baylin, S., et al. (2011). *Human induced pluripotent cells resemble embryonic stem cells demonstrating enhanced levels of DNA repair and efficacy of nonhomologous end-joining.* Mutat Res., (713), S. 8-17.
Fluckiger, A., Marcy, G., Marchand, M., Negre, D., Cosset, F., Mitalipov, S., et al. (2006). *Cell cycle features of primate embryonic stem cells.* Stem Cells, (24), S. 547-556.
Fong, H., Hoheistein, K., & Donovan, P. (2008). *Regulation of self-renewal and pluripotency by Sox2 in human embryonic stem cells.* Stem Cells, (26), S. 1931-1938.

Francia, S. (2015). *Non-Coding RNA: Sequence-Specific Guide for Chromatin Modification and DNA Damage Signaling.* Front Genet., (6), S. 320.
Francia, S., Cabrini, M., Matti, V., Oldani, A., & di Fagagna, F. (2016). *DICER, DROSHA and DNA damage response RNAs are necessary for the secondary recruitment of DNA damage response factors.* J Cell Sci., (129), S. 1468-1476.
Francia, S., Michelini, F., Saxena, A., Tang, D., de Hoon, M., Anelli, V., et al. (2012). *Site-specific DICER and DROSHA RNA products control the DNA-damage response.* Nature, (488), S. 231-235.
Fung, T., & Poon, R. (2005). *A roller coaster ride with the mitotic cyclins.* Semin Cell Dev Biol., (3), S. 335-342.
Gage, H. (2000). *Mammalian neural stem cells.* Science, (287), S. 1433-1438.
Gao, F., Kwon, S., Zhao, Y., & Jin, Y. (2009). *PARP1 poly(ADP-ribosyl)ates Sox2 to control Sox2 protein levels and FGF4 expression during embryonic stem cell differentiation.* J Biol Chem., (284), S. 22263-22273.
Garcia-Perez, J., Marchetto, M., Muotr, A., Coufal, N., Gage, F., O'Shea, K., et al. (2007). LINE-1 retrotransposition in human embryonic stem cells. *Hum. Mol. Gent.*, (16), S. 1569-1577.
Ginno, P., Lott, P., Christensen, H., Krof, I., & Chedin, F. (2012). *R-loop formation is a distinctive characteristic of unmethylated human CpG island promoters.* Mol Cell, (45), S. 814-825.
Goodarzi, A., & Jeggo, P. (2013). *The repair and signaling responses to DNA double-strand breaks.* Mol Cell, (82), S. 1-45.
Goodarzi, A., Noon, A., Deckbar, D., Ziv, Y., Shiloh, Y., Löbrich, M., et al. (2008). *ATM signaling facilitates repair of DNA double-strand breaks associated with heterochromatin.* Adv Genet., (31), S. 167-177.
Gottlieb, T., & Jackson, S. (1993). *The DNA-dependent protein kinase: requirement for DNA ends and association with Ku antigen.* Cell, (72), S. 131-42.
Gou, Z., Deshpande, R., & Paull, T. (2010). *ATM activation in the presence of oxidative stress.* Cell Cycle, (9), S. 4805-4811.
Gravel, S., Chapman, J., Magill, C., & Jackson, S. (2008). *DNA helicases Sgs1 and BLM promote DNA double-strand break resection.* Genes Dev., (22), S. 2767-2772.
Grudzenski, S., Raths, A., Conrad, S., Rübe, C., & Löbrich, M. (2010). *Inducible response required for repair of low-dose radiation damage in human fibroblasts.* Proc Natl Acad Sci USA., (107), S. 14205-14210.
Harper, J., & Elledge, S. (2007). *The DNA damage response: ten years after.* Mol Cell., (28), S. 739-745.
Helmrich, A., Ballarino, M., Nudler, E., & Tora, L. (2013). *Transcription-replication encounters, consequences and genomic instability.* Nat Struc Mol Biol., (4), S. 412-418.
Hemberger, M., Nozaki, T., Winterhager, E., Yamamoto, H., Nakagama, H., Kamada, N., et al. (2003). *Parp1-deficiency induces differentiation of ES cells into trophoblast derivatives.* Dev Biol., (257), S. 371-381.
Hervey Lodish, A. B. (2006). *Molecular Biology of the Cell, 5th ed.* .
Hong, Y., & Stambrook, P. (2004). *Restoration of an absent G1 arrest and protection from apoptosis in embryonic stem cells after ionizing radiation.* Proc Natl Acad USA., (40), S. 14443-14448.
Iliakis, G. (2009). *Backup pathways of NHEJ in cells of higher eukaryotes: cell cycle dependence.* Radiother Oncol., (3), S. 310-315.
Iliakis, G., Wang, Y., Guan, J., & Wang, H. (2003). (5847, Hrsg.) *DNA damage checkpoint control in cells exposed to ionizing radiation.* Oncogene, (37), S. 5834-5847.
Imamichi, S., Sharma, M., Kamdar, R., Fukuchi, M., & Matsumoto, Y. (2014). *Ionizing radiation-induced XRCC4 phosphorylation is mediated through ATM in addition to DNA-PK.* Proc Jpn Acad Ser B Phys Biol Sci., (9), S. 365-372.
Jackson, S., & Bartek, J. (2009). *The DNA-damage response in human biology and disease.* Nature, (7267), S. 1071-1078.
Jette, N., & Lees-Miller, S. (2015). *The DNA-dependent protein kinase: A multifunctional protein kinase with roles in DNA double strand break repair and mitosis.* Prog Biophys Mol Biol., (117), S. 194-205.

Jiang, W., Crowe, J., Liu, X., Nakajima, S., Wnag, Y., Li, C., et al. (2015). *Differential phosphorylation of DNA-PKcs regulates the interplay between end-processing and end-ligation during non-homologous end-joining.* Mol Cell., (1), S. 172-185.
Kapinas, K., Grandy, R., Ghule, P., Medina, R., Becker, K., Pardee, A., et al. (2013). *The Abbreviated Pluripotent Cell Cycle.* J Cell Physiol., (1), S. 9-20.
Kegel, P., Riballo, E., Kühne, M., Jeggo, P., & Löbrich, M. (2007). *X-irradiation of cells on glass slides has a dose doubling impact.* DNA Repair, (11), S. 1692-1697.
Keskin, H., Meers, C., & Storici, F. (2016). *Transcript RNA supports precise repair of its own DNA gene.* RNA Biol., (2), S. 157-165.
Keskin, H., Shen, Y., Huang, F., Patel, M., Yang, T., Ashley, K., et al. (2014). *Transcript-RNA-templated DNA recombination and repair.* Nature, (7527), S. 436-439.
Khanna, K., & Jackson, S. (2001). *DNA double-strand breaks: signaling, repair and the cancer connection.* Nat Genet., (3), S. 247-254.
Lai, Y., Chang, C., Pawlik, K., Zhou, D., Renfrow, M., & Townes, T. (2012). *SRY (sex determining region Y)-box2 (Sox2)/poly ADP-ribose polymerase 1 (Parp1) complexes regulate pluripotency.* Proc Natl Acad USA., (10), S. 3772-3777.
Lambert, S., & Lopez, B. (2000). *Characterization of mammalian RAD51 double strand break repair using non-lethal dominant-negative forms.* EMBO J., (12), S. 3090-3099.
Lan, M., Acharya, M., Tran, K., Bahari-Kashani, J., Patel, N., Strnadel, J., et al. (2012). *Characterizing the radioresponse of pluripotent and multipotent human stem cells.* PLoS One., (12), S. e50048.
Lazzaro, F., Novarian, D., Amara, F., Watt, D., Stone, J., Costanzo, V., et al. (2012). *RNase H and postreplication repair protect cells from ribonucleotides incorporated in DNA.* Mol Cell., (1), S. 99-110.
Leber, R., Wise, T., Mizuta, R., & Meek, K. (1998). *The XRCC4 gene product is a target for and interacts with the DNA-dependent protein kinase.* J Biol Chem., (3), S. 1794-1801.
Lee, E., & Hui, J. (2006). *The potential of stem cells in orthopaedic surgery.* J Bone Joint Surg Br., (7), S. 841-851.
Lee, H., Chang, S., Choudhary, S., Aalto, A., Maiti, M., Bamford, D., et al. (2009). *qiRNA is a new type of small interfering RNA induced by DNA damage.* Nature, (7244), S. 274-277.
Lendahl, U., Zimmerman, L., & McKay, R. (1990). *CNS stem cells express a new class of intermediate filament protein.* Cell, (4), S. 585-595.
Li, L., Germain, D., Poon, H., Hildebrandt, M., Monckton, E., McDonald, D., et al. (2016). *DEAD Box 1 Facilitates Removal of RNA and Homologous Recombination at DNA Double-Strand Breaks.* Mol Cell Biol., (22), S. 2794-2810.
Li, L., Monckton, E., & Godbout, R. (2008). *A role for DEAD box 1 at DNA double-strand breaks.* Mol Cell Biol., (28), S. 6413-6425.
Liang, L., Deng, L., Nguyen, S., Zhao, X., Maulion, C., Shao, C., et al. (2008). *Human DNA ligases I and III, but not ligase IV, are required for microhomology-mediated end joining of DNA double-strand breaks.* Nucleic Acids Res., (10), S. 3297-3310.
Lieber, M., Gu, J., Lu, H., Shimazaki, N., & Tsai, A. (2010). *Nonhomologous DNA end joining (NHEJ) and chromosomal translocations in humans.* Subcell Biochem., (50), S. 279-296.
Lindhal, T., Satoh, M., Poirier, G., & Klungland, A. (1995). *Post-translational modification of poly(ADP-ribose) polymerase induced by DNA strand breaks.* Trends Biochem Sci., (20), S. 405-411.
Lindsey-Boltz, L., & Sancar, A. (2007). *RNA polymerase: the most specific damage recognition protein in cellular responses to DNA damage?* Proc Natl Acad Sci USA., (33), S. 13213-13214.
Liu, Z., & Kraus, W. (2017). *Catalytic-Independent Functions of PARP-1 Determine Sox2 Pioneer Activity at Intractable Genomic Loci.* Mol Cell., (4), S. 589-603.
Löbrich, M., Rydberg, B., & Cooper, P. (1995). *Repair of x-ray-induced DNA double-strand breaks in specific Not I restriction fragments in human fibroblasts: joining of correct and incorrect ends.* Proc Natl Acad Sci USA., (26), S. 12050-12054.

Luijsterburg, M., de Krijger, I., Wiegan, W., Shah, R., Smeenk, G., de Groot, A., et al. (2016). *PARP1 Links CHD2-Mediated Chromatin Expansion and H3.3 Deposition to DNA Repair by Non-homologous End-Joining.* Mol Cell., (4), S. 547-562.
Lukas, J., & Likas, C. (2013). *Molecular biology. Shielding broken DNA for a quick fix.* Science, (6120), S. 652-653.
Lukas, J., Lukas, C., & Bartek, J. (2004). *Mammalian cell cycle checkpoints: signalling pathways and their organization in space and time.* DNA Repair, (8), S. 997-1007.
Ma, Y., & Lieber, M. (2001). *DNA Length-Dependent Cooperative Interactions in the Binding of Ku to DNA.* Biochemistry, (32), S. 9638-9646.
Mahaney, B., Hammel, M., Meek, K., Tainer, J., & Lees-Miller, S. (2013). *XRCC4 and XLF form long helical protein filaments suitable for DNA end protection and alignment to facilitate DNA double strand break repair.* Biochem Cell Biol., (1), S. 31-41.
Mahaney, B., Meek, K., & Lees-Miller, S. (2009). *Repair of ionizing radiation-induced DNA double-strand breaks by non-homologous end-joining.* Biochem J., (3), S. 639-650.
Mansour, M., Borgmann, K., Petersen, C., Dikomey, E., & Dahm-Daphi, J. (2013). *The absence of Ku but not defects in classical non-homologous end-joining is required to trigger PARP1-dependent end-joining.* DNA Repair (Amst), (12), S. 1134-1142.
Mansour, W., Rhein, T., & Dahm-Daphi, J. (2010). *The alternative end-joining pathway for repair of DNA double-strand breaks requires PARP1 but is not dependent upon microhomologies.* Nucleic Acids Res., (18), S. 6065-6077.
Morrison, SJ., Shan, NM., & Anderson, DJ. (1997). *Regulatory mechanism in stem cell biology.* Cell, (3), S. 287-297.
Mateos-Gomez, P., Gong, F., Nair, N., Miller, K., Lazzerini-Denchi, E., & Sfeir, A. (2015). *Mammalian polymerase θ promotes alternative NHEJ and suppresses recombination.* Nature, (7538), S. 254-257.
Maynard, S., Swistowska, A., Lee, J., Liu, Y., Liu, S., Da Cruz, A., et al. (2008). *Human embryonic stem cells have enhanced repair of multiple forms of DNA damage.* Stem Cells, (9), S. 2266-2274.
Mazina, OM., Keskin, H., Hanamshet, K., Storici, F., Mazin. AV. (2017). *Rad52 Inverese Strand Exchange Drives RNA-Templated DNA Double-Strand Break Repair.* Mol Cell, (1), 19-29.
Mazón, G., Mimitou, E., & Symington, L. (2010). *SnapShot: Homologous recombination in DNA double-strand break repair.* Cell, (4), S. 646e1.
McKay, B., Stubbert, L., CC, F., Smith, J., Cardamore, R., & Spronck, J. (2004). *Regulation of ultraviolet light-induced gene expression by gene size.* Proc Natl Acad Sci USA., (17), S. 6582-6586.
Merkle, D., Douglas, P., Moorhead, G., Leonenko, Z., Yu, Y., Cramb, D., et al. (2002). *The DNA-dependent protein kinase interacts with DNA to form a protein-DNA complex that is disrupted by phosphorylation.* Biochemistry, (42), S. 12706-12714.
Mimeault, M., & Batra, S. (2009). *Recent insights into the molecular mechanisms involved in aging and the malignant transformation of adult stem/progenitor cells and their therapeutic implications.* Ageing Res Rev., (2), S. 94-112.
Mimitou, E., & Symington, L. (2009). *DNA end resection: many nucleases make light work.* DNA Repair (Amst), (9), S. 983-995.
Mladenov, E., Magin, S., Soni, A., & Iliakis, G. (2013). *DNA double-strand break repair as determinant of cellular radiosensitivity to killing and target in radiation therapy.* Front Oncol., (3), S. 113.
Momcilovic, O., Knobloch, L., Fornsaglio, J., Varum, S., Easley, C., & Schatten, G. (2010). *DNA damage responses in human induced pluripotent stem cells and embryonic stem cells.* PLoS One, (10), S. e13410.
Morrison, S., & Kimble, J. (2006). *Asymmetric and symmetric stem-cell divisions in development and cancer.* Nature, (7097), S. 1068-1074.
Munroe, R., Bergstrom, R., Zheng, Q., Libby, B., Smith, R., John, S., et al. (2000). *Mouse mutants from chemically mutagenized embryonic stem cells.* Nat Genet., (3), S. 318-321.

Nguyen, H., Yadav, T., Giri, S., Saez, B., Graubert, T., & Zou, L. (2017). *Functions of Replication Protein A as a Sensor of R Loops and a Regulator of RNaseH1.* Mol Cell., (5), S. 832-847.
Niu, H., Raynard, S., & Sung, P. (2009). *Multiplicity of DNA end resection machineries in chromosome break repair.* Genes Dev., (13), S. 1481-1486.
Ohle, C., Tesorero, R., Schermann, G., Dobrev, N., Sinning, I., & Fischer, T. (2016). *Transient RNA-DNA Hybrids Are Required for Efficient Double-Strand Break Repair.* Cell, (4), S. 1001-1013.
Ohsawa, R., Seol, J., & Tyler, J. (2013). *At the intersection of non-coding transcription, DNA repair, chromatin structure, and cellular senescence.* Front Genet., (4), S. 136.
Orthwein, A., Noordermeer, S., Wilson, M., Landry, S., Enchev, R., Sherker, A., et al. (2015). *A mechanism for the suppression of homologous recombination in G1 cells.* Nature, (7582), S. 422-426.
Park, D., Xiang, A., Mao, F., Zhang, L., Di, G., Liu, X., et al. (2010). *Nestin is required for the proper self-renewal of neural stem cells.* Stem Cells, (12), S. 2162-2171.
Paulsen, R., Soni, D., Wollman, R., Hahn, A., Yee, M., Guan, A., et al. (2009). *A genome-wide siRNA screen reveals diverse cellular processes and pathways that mediate genome stability.* Mol Cell., (2), S. 228-239.
Pesce, M., & Schöler, H. (2001). *Oct-4: gatekeeper in the beginnings of mammalian development.* Stem Cells, (4), S. 271-278.
Petzold, C., Marceau, A., Miller, K., Marqusee, S., & Keck, J. (2015). *Interaction with Single-stranded DNA-binding Protein Stimulates Escherichia coli Ribonuclease HI Enzymatic Activity.* J Biol Chem., (23), S. 14626-14636.
Pittoggli, C., Scimanna, I., Mattel, E., Beraldi, R., Lobascio, A., Mai, A., et al. (2003). Role of Endogenous Reverse Transcriptase in Murine Early Embryo Development. *Mol Reprod. Dev.*, (3), S. 225-236.
Quennet, V., Beucher, A., Barton, O., Takeda, S., & Löbrich, M. (2010). *CtIP and MRN promote non-homologous end-joining of etoposide-induced DNA double-strand breaks in G1.* Nucleic Acids Res., (6), S. 2144-2152.
Rai, R., Zheng, H., He, H., Luo, Y., Multani, A., Carpenter, P., et al. (2010). *The function of classical and alternative non-homologous end-joining pathways in the fusion of dysfunctional telomeres.* EMBO J., (15), S. 2598-2610.
Riballo, E., Kühne, M., Rief, N., Doherty, A., Smith, G., Recio, M., et al. (2004). *A pathway of double-strand break rejoining dependent upon ATM, Artemis, and proteins locating to gamma-H2AX foci.* Mol Cell., (5), S. 715-724.
Robertson, R., Moses, D., KwoN, Y., Chan, P., Chi, P., Klein, H., et al. (2009). *Structural transitions within human Rad51 nucleoprotein filaments.* Proc Natl Acad Sci USA., (31), S. 12688-12693.
Rodda, D., Chew, J., Lim, L., Loh, Y., Wang, B., Ng, H., et al. (2005). *Transcriptional regulation of nanog by OCT4 and SOX2.* J Biol Chem., (26), S. 24731-24737.
Rodriguez-Rocha, H., Garcia-Garcia, A., Panayiotidis, M., & Franco, R. (2011). *DNA damage and autophagy.* Mutat Res., (2), S. 158-166.
Roper, S., Chrysanthou, S., Senner, C., Sienerth, A., Gnan, S., Murray, A., et al. (2014). *ADP-ribosyltransferases Parp1 and Parp7 safeguard pluripotency of ES cells.* Nucleic Acids Res., (42), S. 8914-8927.
Roque, T., Haton, C., Etienne, O., Chicheportiche, A., Rousseau, L., Martin, L., et al. (2012). *Lack of a p21waf1/cip-Dependent G1/S Checkpoint in Neural Stem and Progenitor Cells After DNA Damage In Vivo.* Stem Cells, (3), S. 537-547.
Rothkamm, K., & Löbrich, M. (2003). *Evidence for a lack of DNA double-strand break repair in human cells exposed to very low x-ray doses.* Proc Natl Acad Sci USA., (9), S. 5057-5062.
San Filippo, J., Sung, P., & Klein, H. (2008). *Mechanism of eukaryotic homologous recombination.* Annu Rev Biochem., (77), S. 229-257.
Saretzki, G., Armstrong, L., Leake, A., Lako, M., & von Zglinicki, T. (2004). *Stress defense in murine embryonic stem cells is superior to that of various differentiated murine cells.* Stem Cells, (6), S. 962-971.
Sartori, A., Lukas, C., Coates, J., Mistrik, M., Fu, S., Bartek, J., et al. (2007). *Human CtIP promotes DNA end resection.* Nature, (7169), S. 509-514.

Savatier, P., Huang, S., Szekely, L., Wiman, K., & Samarut, J. (1994). *Contrasting patterns of retinoblastoma protein expression in mouse embryonic stem cells and embryonic fibroblasts.* Oncogene, (3), S. 809-819.
Schneider, L., Fumagalli, M., & d'Adda di Fagagna, F. (2012). *Terminally differentiated astrocytes lack DNA damage response signaling and are radioresistant but retain DNA repair proficiency.* Cell Death Differ., (4), S. 582-591.
Sciamanna, I., De Luca, C., & Spadafora, C. (2016). *The Reverse Transcriptase Encoded by LINE-1 Retrotransposons in the Genesis, Progression, and Therapy of Cancer.* Front Chem., (4), S. 6.
Serrano, L., Liang, L., Chang, Y., Deng, L., Maulion, C., Nguyen, S., et al. (2011). *Homologous Recombination Conserves DNA Sequence Integrity Throughout the Cell Cycle in Embryonic Stem Cells.* Stem Cells Dev., (2), S. 363-374.
Shirvastav, M., De Haro, L., & Nickoloff, J. (2008). *Regulation of DNA double-strand break repair pathway choice.* Cell Res., (1), S. 134-147.
Shrivastav, M., Miller, C., De Haro, L., Durant, S., Chen, B., Chen, D., et al. (2009). *DNA-PKcs and ATM Co-Regulate DNA Double-Strand Break Repair.* DNA Repair (Amst), (8), S. 920-929.
Simsek, D., & Jasin, M. (2010). *Alternative end-joining is suppressed by the canonical NHEJ component Xrcc4/ligase IV during chromosomal translocation formation.* Nat Struct Mol Biol., (4), S. 410-416.
Sinha, M., & Peterson, C. (2008). *A Rad51 Presynaptic Filament Is Sufficient to Capture Nucleosomal Homology during Recombinational Repair of a DNA Double-Strand Brea.* Mol Cell., (6), S. 803-810.
Skourti-Stathaki, K., Kamieniarz-Gdula, K., & Proudfoot, N. (2014). *R-loops induce repressive chromatin marks over mammalian gene terminators.* Nature, (7531), S. 436-439.
Spagnolo, L., Barbeau, J., Curtin, N., Morris, E., & Pearl, L. (2012). *Visualization of a DNA-PK/PARP1 complex.* Nucleic Acids Res., (9), S. 4168-4177.
Stiff, T., O'Driscoll, M., Rief, N., Iwabuchi, K., Löbrich, M., & Jeggo, P. (2004). *ATM and DNA-PK function redundantly to phosphorylate H2AX after exposure to ionizing radiation.* Cancer Res., (7), S. 2390-2396.
Stirling, P., Chan, Y., Minaker, S., Aristizabal, M., Barrett, I., Sipahimalani, P., et al. (2012). *R-loop-mediated genome instability in mRNA cleavage and polyadenylation mutants.* Genes Dev., (2), S. 163-175.
Storici, F., Bebenek, K., Kunkel, T., Gordenin, D., & Resnick, M. (2007). *RNA-templated DNA repair.* Nature, (7142), S. 338-341.
Sung, P., & Robberson, D. (1995). *DNA strand exchange mediated by a RAD51-ssDNA nucleoprotein filament with polarity opposite to that of RecA.* Cell, (3), S. 453-461.
Sung, P., Krejci, L., Van Komen, S., & Sehorn, M. (2003). *Rad51 recombinase and recombination mediators.* J Biol Chem., (278), S. 42729-42732.
Suvorova, I., Grigorash, B., Chuykin, I., Pospelova, T., & Pospelov, V. (2016). *G1 checkpoint is compromised in mouse ESCs due to functional uncoupling of p53-p21Waf1 signaling.* Cell Cycle, (1), S. 52-63.
Tadokoro, T., & Kanaya, S. (2009). *Ribonuclease H: molecular diversities, substrate binding domains, and catalytic mechanism of the prokaryotic enzymes.* FEBS J., (6), S. 1482-1493.
Talaeei, H., & Nikjoo, H. (2013). *Biochemical DSB-repair model for mammalian cells in G1 and early S phases of the cell cycle.* Mutat Res., (2), S. 206-212.
Terzoudi, G., Manola, K., Pantelias, G., & Iliakis, G. (2005). *Checkpoint abrogation in G2 compromises repair of chromosomal breaks in ataxia telangiectasia cells.* Cancer Res., (24), S. 11292-11296.
Thomson, J., Itskovitz-Eldor, J., Shapiro, S., Waknitz, M., Swiergiel, J., Marshall, V., et al. (1998). *Embryonic stem cell lines derived from human blastocysts.* Science, (5391), S. 1145-1147.
Tichy, E., Pillai, R., Deng, L., Liang, L., Tischfield, J., Schwemberger, S., et al. (2010). *Mouse Embryonic Stem Cells, but Not Somatic Cells, Predominantly Use Homologous Recombination to Repair Double-Strand DNA Breaks* Stem Cells Dev., (19), S. 1699-1711.
Trujillo, K., Yuan, S., Lee, E., & Sung, P. (1998). *Nuclease activities in a complex of human recombination and DNA repair factors Rad50, Mre11, and p95.* J Biol Chem., (34), S. 21447-21450.

Truong, L., Li, Y., Shi, L., Hwang, P., He, J., Wang, H., et al. (2013). *Microhomology-mediated End Joining and Homologous Recombination share the initial end resection step to repair DNA double-strand breaks in mammalian cells.* Proc Natl Acad Sci USA., (9), S. 7720-7725.
UNSCEAR. (2000). United Nations Scientific Committee on the Effects of Atomic United Nations Scientific Committee on the Effects of Atomic Sources and Effects of Ionizing Radiation: Report to the General Assembly, with Scientific Annexes.
Valerie, K., & Povirk, L. (2003). *Regulation and mechanisms of mammalian double-strand break repair.* Oncogene, (37), S. 5792-5812.
van der Laan, S., Tsanov, N., Crozet, C., & Maiorano, D. (2013). *High Dub3 expression in mouse ESCs couples the G1/S checkpoint to pluripotency.* Mol Cell., (3), S. 366-379.
van Gent, D., Hoeijmakers, J., & Kanaar, R. (2001). *Chromosomal stability and the DNA double-stranded break connection.* Nat Rev Genet., (3), S. 196-206.
Wang, C., & Lees-Miller, S. (2013). *Detection and repair of ionizing radiation induced DNA double strand breaks: new developments in non-homologous end joining.* Int J Radiat Oncol Biol Phys., (3), S. 440-449.
Wang, H., & Xu, X. (2017). *Microhomology-mediated end joining: new players join the team.* Cell Biosci., (7), S. 6.
Wang, M., Wu, W., Wu, W., Rosidi, B., Zhang, L., Wang, H., et al. (2006). *PARP-1 and Ku compete for repair of DNA double strand breaks by distinct NHEJ pathways.* Nucleic Acids Res., (21), S. 6170-6182.
Wang, Q., & Goldstein, M. (2016). *Small RNAs Recruit Chromatin-Modifying Enzymes MMSET and Tip60 to Reconfigure Damaged DNA upon Double-Strand Break and Facilitate Repair.* Cancer Res., (7), S. 1904-1915.
Wei, W., Ba, Z., Gao, M., Wu, Y., Ma, Y., Amiard, S., et al. (2012). *A role for small RNAs in DNA double-strand break repair.* Cell, (1), S. 101-112.
White, J., & Dalton, S. (2005). *Cell cycle control of embryonic stem cells.* Stem Cell Rev., (2), S. 131-138.
Williams, D., Lee, K., Shi, J., Chen, D., & Stewart, P. (2008). *Cryo-EM structure of the DNA-dependent protein kinase catalytic subunit at subnanometer resolution reveals alpha helices and insight into DNA binding.* Structure, (16), S. 468-477.
Yajima, H., Fujisawa, H., Nakajima, N., Hirakawa, H., Jeggo, P., Okayasu, R., et al. (2013). *The complexity of DNA double strand breaks is a critical factor enhancing end-resection.* DDNA Repair (Amst), (11), S. 936-946.
Yang, W. (2008). *An equivalent metal ion in one- and two-metal-ion catalysis.* Nat Struct Mol Biol., (11), S. 1228-1231.
Yang, W., Lee, J., & Nowotny, M. (2006). *Making and breaking nucleic acids: two-Mg2+-ion catalysis and substrate specificity.* Mol Cell., (1), S. 5-13.
Yang, Y., Cortes, U., Patnaik, S., Jasin, M., & Wang, Z. (2004). *Ablation of PARP-1 does not interfere with the repair of DNA double-strand breaks, but compromises the reactivation of stalled replication forks.* Oncogene, (21), S. 3872-3882.
Yao, B., Fu, J., Hu, E., Qi, Y., & Zhou, Z. (2008). *The effects of over-expression and suppression of Cdc25A on the S-phase checkpoint induced by benzo(a)pyrene.* Toxicology, (3), S. 180-187.
Yoo, S., & Dynan, W. (1999). *Geometry of a complex formed by double strand break repair proteins at a single DNA end: recruitment of DNA-PKcs induces inward translocation of Ku protein.* Nucleic Acids Res., (24), S. 4679-4686.
Zhang, F., Shi, J., Bian, C., & Yu, X. (2015). *Poly(ADP-Ribose) Mediates the BRCA2-Dependent Early DNA Damage Response.* Cell Rep., (4), S. 678-689.
Zhao, D., Gish, G., Braunschweig, U., Li, Y., Ni, Z., Schmitges, F., et al. (2016). *SMN and symmetric arginine dimethylation of RNA polymerase II C-terminal domain control termination.* Nature, (7584), S. 48-53.
Zhou, B., & Elledge, S. (2000). *The DNA damage response: putting checkpoints in perspective.* Nature, (408), S. 433-439.

7 Appendix

7.1 Curriculum vital

Name: Amir Mofidi
Date of birth: 04.07.1984
Place of birth: Tehran, Iran
Nationality Iranian

Education

04.2014 - 11.2017	Technical University of Darmstadt, Department of Radiation Biology and DNA Repair, Darmstadt, Germany. PhD Thesis
07.2006 - 05.2008	Jamia Hamdard University, Department of Biotechnology, New Delhi, India. Master of Science Biotechnology
09.2003 - 06.2006	Azad University, Qom, Iran. Bachelor of Science Biology
09.1991 - 06.2003	Schlool and High school, Tehran Iran.

Research and Job Experiences

07.2010 - 02.2014	Center for Biotechnology and Biomedicine, University of Leipzig, Germany. Research Assistant
10.2008 - 06.2010	Center for Science and Technology, Tehran University of Medical Science, Iran. Research Assistant

Oral Presentation

2017	RISK-IR european project meeting. Oxford, UK.
2016	RISK-IR european project meeting. Munich, Germany.

Poster Presentations

2017 **15th International Wolfsberg meeting on Molecular Radiation Biology/Oncology, Ermatigen, Switzerland.**
DNA double strand break repair in murine embryonic stem cells: similarities and distinctions to repair in neural stem cells. Amir Mofidi, Dorothee Deckbar, Markus Löbrich.

2016 **DNA Repair 2016. Essen, Germany.**
DNA double strand break repair in murine embryonic and neuronal stem cells: similarities and distinctions to repair in somatic cells. Amir Mofidi, Markus Löbrich, Dorothee Deckbar.

Response to DNA damage: from molecule to disease. Egmond aan Zee, The Netherland.
2016 DNA double strand break repair and cell cycle control of murine stem cells after exposure to ionizing radiation. Amir Mofidi, Markus Löbrich, Dorothee Deckbar.

2014 **Radiation Biology and Cancer from molecular response to the clinic. Essen, Germany**.
DNA double strand break repair and cell cycle control of murine stem cells after exposure to ionizing radiation. Amir Mofidi, Markus Löbrich, Dorothee Deckbar.

2014 **2nd International Annual Conference of the German Stem Cell Network. Heidelberg, Germany**.
DNA double strand break repair and cell cycle control of murine neuronal stem cells after exposure to ionizing radiation. Amir Mofidi, Markus Löbrich, Dorothee Deckbar.

Honors and Awards

2016 Travel grant for participation in DNA Repair 2016 symposium.

2014 DFG-founded, Graduate School 1657 at Technical University of Dramstadt.

7.2 Acknowledgement

Foremost, I would like to express my sincere gratitude to my principle reviewer Prof. Dr. Markus Löbrich for giving me the opportunity to work in his research group and also for his continuous encouragement, support, advice and insight over the last four years.

My sincere thanks also goes to Dr. Dorothee Deckbar to provide me the chance to work on this interesting project and for her excellent supervision during the initial phase of my PhD project.

I am very thankful to Prof. Bodo Laube, Prof. Ulrike Nuber and Dr. Silvia Ritter for their insightful scientific comments and encouragement during my Grk-PhD committee meetings.

I would like to express my sincere gratitude and appreciation to all the staff of the department of Radiation Biology and DNA repair (AG Löbrich) who helped me with this research project. My special thanks goes to Christel Braun for her kind help and support during the entire period of my PhD project.

I would like to thank Dr. Marta Llorens Agost, Daniel Pfeffel and Holly Thomas for the proofreading and editing my thesis.

I thank my fellow labmate Anugrah Gawai for the scientific discussions and also for all the fun we have had during these years.

I also warmly appreciate Elham Abdollahi for her help and support during the moments when there was no one to answer my queries.

Last but not least, my special appreciation goes to my family: my lovely mom, my sister Ashraf, my brother in law Ahmad and my beautiful nieces Nadia and Neda for their encouragement and for supporting me spiritually in whatever I pursue. Without you, it would all be pointless.